AD-A035 940 BOSTON UNIV MASS DEPT OF ASTRONOMY F/G 4/1
THE IONOSPHERIC F-REGION NEAR 60 DEG MAGNETIC LATITUDE: MONTHLY--ETC(U)
SEP 76 M MENDILLO, M BUONSANTO F19628-75-C-0044
UNCLASSIFIED SER-II-NO-61 AFGL-TR-76-0233 NL

1 OF 2
AD A035940

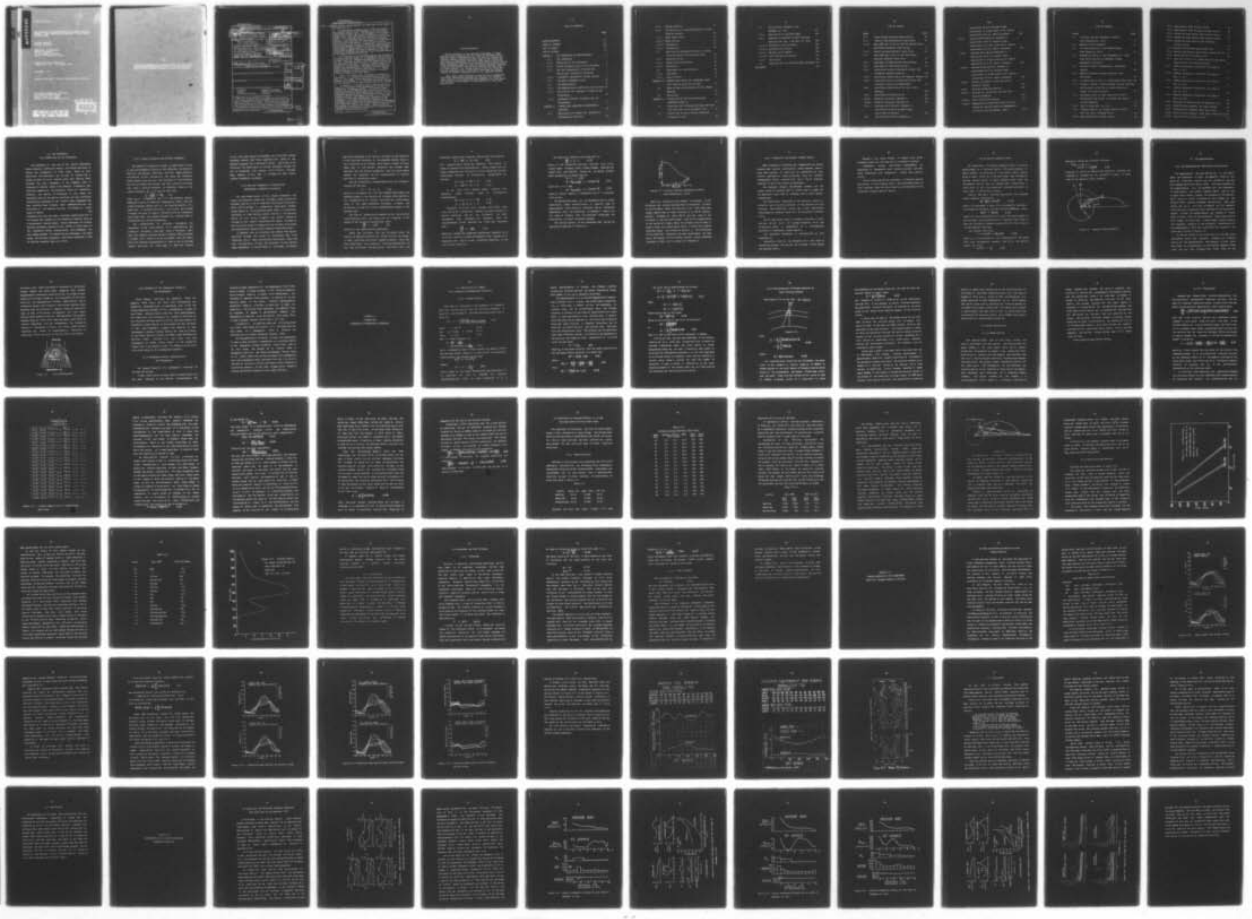

AFGL-TR-76-0233

THE IONOSPHERIC F-REGION NEAR 60° MAGNETIC LATITUDE: MONTHLY MEAN BEHAVIOR AND SUBSTORM EFFECTS DURING WINTER NIGHTS

Michael Mendillo
Michael Buonsanto

Department of Astronomy
Boston University
725 Commonwealth Avenue
Boston, Massachusetts 02215

Annual Scientific Report No. 2
1 September, 1975 - 31 August, 1976

September, 1976

AIR FORCE GEOPHYSICS LABORATORY
AIR FORCE SYSTEMS COMMAND
UNITED STATES AIR FORCE
HANSCOM AFB, MASSACHUSETTS 01730

Unclassified

SECURITY CLASSIFICATION OF THIS PAGE (When Data Entered)

REPORT DOCUMENTATION PAGE

READ INSTRUCTIONS BEFORE COMPLETING FORM

1. REPORT NUMBER: AFGL-TR-76-0233	2. GOVT ACCESSION NO.
3. RECIPIENT'S CATALOG NUMBER	
4. TITLE (and Subtitle): The Ionospheric F-Region Near 60° Magnetic Latitude: Monthly Mean Behavior and Substorm Effects During Winter Nights.	5. TYPE OF REPORT & PERIOD COVERED: Scientific Annual 1 Sept 75-31 Aug 76.
	6. PERFORMING ORG. REPORT NUMBER: A.C.B.U., Ser II. No.61
7. AUTHOR(s): Michael Mendillo, Michael Buonsanto	8. CONTRACT OR GRANT NUMBER(s): F19628-75-C-0044
9. PERFORMING ORGANIZATION NAME AND ADDRESS: Astronomy Department, Boston University, 725 Commonwealth Ave., Boston, MA 02215	10. PROGRAM ELEMENT, PROJECT, TASK AREA & WORK UNIT NUMBERS: 62101F 46430107 01
11. CONTROLLING OFFICE NAME AND ADDRESS: Air Force Geophysics Laboratory, Hanscom AFB, Bedford, MA 01731, CONTRL. MON: J.A. KLOBUCHAR/LIR.	12. REPORT DATE: September 1976
	13. NUMBER OF PAGES: 167. 169p.
14. MONITORING AGENCY NAME & ADDRESS (if different from Controlling Office): Ser-II-No-61, Scientific 2	15. SECURITY CLASS. (of this report): Unclassified
	15a. DECLASSIFICATION/DOWNGRADING SCHEDULE

16. DISTRIBUTION STATEMENT (of this Report)

Approved for public release; distribution unlimited

17. DISTRIBUTION STATEMENT (of the abstract entered in Block 20, if different from Report)

18. SUPPLEMENTARY NOTES

ACCESSION for
NTIS White Section
DDC Buff Section
UNANNOUNCED
JUSTIFICATION
BY
DISTRIBUTION/AVAILABILITY CODES
Dist. AVAIL. and/or SPECIAL
A

19. KEY WORDS (Continue on reverse side if necessary and identify by block number)

Ionosphere
F-Region
Total Electron Content
F-Region Peak Density
F-Region Slab Thickness
Substorms

20. ABSTRACT (Continue on reverse side if necessary and identify by block number)

The aim of this study is to provide the first detailed look at the morphology of the ionospheric F-region near a geomagnetic latitude of 60 degrees. This region is of considerable interest because it lies at the base of the geomagnetic field line which forms the average boundary of the plasmasphere, the geomagnetic field-aligned envelope of co-rotating plasma → next page

DD FORM 1 JAN 73 1473 EDITION OF 1 NOV 65 IS OBSOLETE

Unclassified

SECURITY CLASSIFICATION OF THIS PAGE (When Data Entered)

406 311

bpg

cont. →

which extends to approximately four earth radii in the equatorial plane (L = 4).

The observational parameters used in this study monitor two different aspects of the ionosphere's vertical electron concentration profile, $N_e(h)$. The ionospheric total electron content (TEC) is the total number of electrons in a vertical column of unit cross sectional area extending through the ionosphere. It is obtained by measuring the amount of Faraday rotation a plane polarized wave experiences in traveling from a satellite-borne radio beacon to a ground receiving station. The peak value of the electron concentration's vertical profile, denoted Nmax, ~~or NmF2,~~ is obtained from ground-based ionosonde measurements of the ionosphere's critical (or vertical penetration) frequency, ~~foF2.~~ The ratio of TEC/Nmax is called the ionospheric equivalent slab thickness, τ, a first-order measure of the shape of the Ne(h) profile.

An introduction to the relevant parameters and the physical principles involved (Chapter 1) is followed by a description of a computer model for ionospheric-plasmaspheric structure (Chapter II). This model is used to show that Faraday rotation can be meaningfully converted to TEC at L = 4 except under the conditions of a severe trough, a condition which is primarily a winter storm-time phenomenon. This model also shows that generally during winter nighttime conditions at L = 4, Faraday rotation measures the total electron content of a vertical column to heights greater than 2000 km.

Chapter III follows with a presentation of average conditions at L = 4, obtained from over three years of Goose Bay TEC, St. John's Nmax, and the equivalent slab thickness obtained via τ = TEC/Nmax. It is found that the general features of the ionosphere are the same as those found at mid latitudes.

In Chapter IV, a particular winter nighttime phenomenon near L = 4, increases in Nmax accompanied by constant or declining TEC, is examined in detail. A statistical survey covering 24 years of December foF2 data and two October to March periods reveals that nighttime Nmax increases occur very frequently during the winter, particularly in December. Comparable increases in TEC appear to be rare, i.e., these Nmax increases are most often accompanied by decreases in slab thickness. It is shown that vertical distortions of the ionospheric Ne(h) profile are the major cause of this phenomenon, but latitudinal motions of the electron density trough may also be important in producing this effect. These vertical and latitudinal drift motions are attributed to an enhanced magnetospheric convection electric field.

Acknowledgements

We are grateful to the Canadian Department of Communications for providing the many years of ionosonde data from St. Johns, Newfoundland, and the ISIS-II interpolated electron density topside profiles, used in this study. We also wish to acknowledge the World Data Center-A For Solar Solar Terrestrial Physics which provided multi-station ground-based ionosonde values and the true-height analysis necessary to derive the bottom-side electron density profiles used in our case studies. Dr. Jurgen Buchau of the Air Force Geophysics Laboratory most graciously performed the tedious scaling of several ionograms used in our substorm studies.

Once again, John Klobuchar of the Air Force Geophysics Laboratory contributed insight and guidance to virtually every aspect of the investigations summarized in this report. His continued encouragment in these matters is very much appreciated.

TABLE OF CONTENTS

		PAGE
ACKNOWLEDGEMENTS		iii
TABLE OF CONTENTS		iv
LIST OF TABLES		vii
LIST OF FIGURES		ix
CHAPTER I	THE IONOSPHERE AND MAGNETOSPHERE	1
1.1	The Ionosphere	2
1.1.1	Definition of the Ionosphere	2
1.1.2	Plasma Frequency and Critical Frequency	3
1.1.3	How the Ionosphere is Produced and Maintained; Ionospheric Structure	4
1.1.4	Ionospheric Variations: Trough, Aurora	9
1.2	The Earth's Magnetic Field	11
1.3	The Magnetosphere	13
1.3.1	The Magnetosphere: Definition and Structure	13
1.3.2	Relation of the Ionospheric Trough to the Plasmapause	17
1.3.3	Geomagnetic Storms, Substorms and the Plasmapause	17
CHAPTER II	A MODEL FOR IONOSPHERIC-PLASMASPHERIC STRUCTURE	19
2.1	Description of a Model for Ionospheric-Plasmaspheric Structure	20

2.1.1	Faraday Rotation	20
2.1.2	The Conversion of Faraday Rotation to Total Electron Content	23
2.1.3	Model Description	25
2.1.3.1	Model Outline	25
2.1.3.2	"Exosphere"	27
2.1.3.3	"Ionosphere"	29
2.2	Usefulness of Constant $\bar{M}$-factor at a High Latitude Station during Winter Night	35
2.2.1	Idealized Arrays	35
2.2.2	Severe Latitude Gradient	40
2.2.3	Conclusions	47
2.3	Ionosondes and Slab Thickness	48
2.3.1	Ionosondes	48
2.3.2	Slab Thickness	50
CHAPTER III	AVERAGE BEHAVIOR OF THE IONOSPHERE NEAR SIXTY DEGREES MAGNETIC LATITUDE	52
3.1	Mean and Normalized Monthly Curves; Median Behavior	53
3.2	Discussion	67
CHAPTER IV	DISTORTIONS OF THE WINTER NIGHTTIME IONOSPHERE NEAR L=4	73
4.1	Nighttime Slab Thickness Decreases Observed from Goose Bay during December, 1971	74
4.2	Statistical Survey of Winter Nighttime Increases in foF2	84

4.3	Case Studies: December 9 and December 15, 1971	102
4.3.1	Description of Available Data	102
4.3.2	Computer Simulations of Slab Thickness Decreases for Dec. 9 and Dec. 15, 1971	107
4.3.2.1	Preliminary Considerations	107
4.3.2.2	Latitude Shift Method	112
4.3.2.3	Vertical Drift Method	123
4.3.2.4	Shift and Distort Results	141
4.3.3	Conclusions	145
4.4	Mechanism for the Slab Thickness Decreases	147
REFERENCES		152

LIST OF TABLES

TABLE		PAGE
II-I	Three Faraday Rotation Observatories	35
II-II	Uniform Latitude Gradient Input Array	36
II-III	Best h(M) and "% dif at 420" for Uniform Data and Uniform Gradient Input Arrays	37
II-IV	Severe Latitude Gradient Input Array	42
II-V	Best h(M) and "% dif at 420" for Severe Latitude Gradient Input Array	45
III-I	Data Base for Mean Monthly Calculations	54
IV-I	Data Used in Statistical Survey	85
IV-II	Statistical Survey of Nocturnal Winter foF2 Increases: Seasonal Analysis	93
IV-III	Correlation Coefficients for Seasonal Analysis	95
IV-IV	Statistical Survey of Nocturnal Winter foF2 Increases: Solar Cycle Dependence	97
IV-V	Correlation Coefficients for Solar Cycle Analysis	100
IV-VI	Calculated and Observed TEC	110
IV-VII	Observed Increases- December 9	113
IV-VIII	Observed Increases- December 15	113
IV-IX	Latitude Shift Results- December 9 yzero=165km north of poleward edge, yzero=215km elesewhere	115
IV-X	Latitude Shift Results-December 9	

	yzero=230km north of poleward edge, yzero=120km in trough south to St. John's, yzero=215km from St. John's southward	115
IV-XI	Latitude Shift Results- December 1 yzero=203km north of poleward edge, yzero=153km in trough south to St. John's, yzero=222km from St. John's southward	118
IV-XII	Latitude Shift Results-December 15 yzero=203km north of poleward edge, yzero=120km in trough south of St. John's, yzero=222km from St. John's southward	118
IV-XIII	Latitude Shift Results- December 15 yzero=230km north of poleward edge, yzero=120km in trough south to St. John's, yzero=222km from St. John's southward	119
IV-XIV	Summary of Changes in Nmax and Ω for Different yzeros	119
IV-XV	Vertical Distortion Results	133
IV-XVI	Vertical vs. Equivalent Vertical TEC-Distortion Method	140
IV-XVII	Shift and Distort Results	142
IV-XVIII	Magnetospheric Dawn-Dusk Electric Field Values for Varying Levels of Geomagnetic Activity, from (Carpenter, 1970)	150

LIST OF FIGURES

FIGURE		PAGE
I-1	A typical daytime ionospheric profile from (Papagiannis, 1972)	8
I-2	Magnetic dipole geometry	12
I-3	Principal features of the magnetosphere from (Heikkila, 1973)	14
I-4	Equatorial radius of the plasmapause vs. local time during periods of moderate, steady geomagnetic agitation	15
I-5	Nishida's (1966) magnetospheric convection pattern	16
II-1	Relation between distance along ray path and height	23
II-2	A sample page of Isis II Interpolated Ne(h) data	30
II-3	Geometry showing relation between station latitude and height at which the ray path crosses the lowest invariant latitude	39
II-4	Distances along ray path where 80% of Ω is accumulated (10% above, 10% below) for case of uniform gradient	41
II-5	Isis II pass, Dec. 18, 1971	43
II-6	Electron density vs. height along ray path; Dec. 18, 1971; +8° degree shift	46
III-1	Mean monthly TEC diurnal curves	55

III-2	Mean monthly Nmax diurnal curves	56
III-3	Mean monthly Slab Thickness diurnal curves	57
III-4	Normalized mean monthly TEC diurnal curves	60
III-5	Normalized mean monthly Nmax diurnal curves	61
III-6	Normalized mean monthly slab thickness diurnal curves	62
III-7	Maximum and minimum mean monthly TEC	64
III-8	Maximum and Minimum mean monthly normalized TEC	65
III-9	Median monthly TEC contour plot	66
IV-1	Nmax and TEC for five nights when the increasing Nmax-constant TEC effect occurred	75
IV-2	Several parameters plotted for the night of Dec. 8, 1971	77
IV-3	Several parameters plotted for the night of Dec. 9, 1971	78
IV-4	Several parameters plotted for the night of Dec. 10, 1971	79
IV-5	Several parameters plotted for the night of Dec. 12, 1971	80
IV-6	Several parameters plotted for the night of Dec. 15, 1971	81
IV-7	Overplots of Nmax and TEC for December, 1971	82
IV-8	Classification example: Low bump, plateau	88
IV-9	Classification example: bump, short bump	89
IV-10	Classification example: large bump, irregular bump	90
IV-11	Classification example: no bump	91

IV-12	Classification example: insufficient data	92
IV-13	Statistical survey, seasonal analysis, fractional occurrence of all foF2 increases	94
IV-14	Statistical survey, solar cycle dependence, fractional occurrence of all foF2 increases	99
IV-15	Ionograms taken during the Dec. 15 event	104
IV-16	Ne(h) vs. latitude: Isis II pass 4:20UT, Dec. 9	106
IV-17	Ne(h) vs. latitude: Isis II pass 2:25UT, Dec. 15	108
IV-18	Model Nmax and Ω for Dec. 15 using various yzeros for a wide range of latitude shifts.	120
IV-19	Ne(h) vs. latitude contours for Dec. 15, 0 and -6 degree shifts, using yzeros shown in Table IV-XIII	121
IV-20	Ne(h) vs. latitude: Isis II pass 6:15UT, Dec. 9	124
IV-21	Ne(h) vs. latitude: Isis II pass 4:20UT, Dec. 15	125
IV-22	Typical nighttime Ne(h) profile showing that $N(hmax-\Delta h) < N(hmax+\Delta h)$	130
IV-23	Ne(h) vs. latitude: Dec. 9 distorted array	135
IV-24	Ne(h) vs. latitude: Dec. 15 distorted array	136
IV-25	Ne(h) along ray path: Dec. 9 original and distorted array	138
IV-26	Ne(h) along ray path: Dec. 15 original and distorted array	139
IV-27	Hypothetical response of Nmax to a vertical distortion at two different times during the night	147

CHAPTER I

THE IONOSPHERE AND MAGNETOSPHERE

1.1 The Ionosphere

1.1.1 Definition of the Ionosphere

The ionosphere is that part of the Earth's atmosphere which contains a sufficient density of ionized particles to affect the propagation of radio waves. Based on this definition the ionosphere can be said to extend from a height of about 40 km to several earth radii (Davies, 1965) although the term ionosphere is not commonly used in reference to heights above a few thousand kilometers. This definition emphasizes the practical nature of ionospheric research. The density of ionization is only about one thousandth that of the neutral particles yet this relatively insignificant component of the Earth's upper atmosphere has made possible long distance radio communication and the variations in its behavior are thus of interest to a wide range of people. The ionosphere not only has great practical significance but is of interest also because of its scientific research value as a conveniently located cosmic plasma laboratory for diverse physical processes. Because of the effect on radio waves of the ionospheric medium through which they propagate, the most common methods for observing the ionosphere use radio waves, and the most frequently used radio technique is that of vertical sounding (see sec. 2.3.1).

1.1.2 Plasma Frequency and Critical Frequency

The effect of ionospheric plasma on radio waves is due to the electromagnetic nature of the radiation. The electric field of the passing radio wave sets the light electrons oscillating at the frequency of the wave. The electrons absorb energy from the wave and reradiate it. The electrons thus act as forced oscillators, and like a block on a spring they have a natural frequency of vibration known as the plasma frequency, f_N. It is easy to show that:

$$f_N = \sqrt{\frac{e^2 N}{\pi m}} \cong 9\sqrt{N} \qquad (1.1)$$

where f_N is in megahertz and N is the electron density measured in units of $10^6 el/cm^3$ (Papagiannis, 1972). Thus the plasma frequency depends only on the electron density. If a radio wave is incident vertically at or below this plasma frequency the wave is totally reflected while at frequencies much larger than the plasma frequency the incident wave is transmitted with little attenuation.

The concentration of electrons throughout the ionosphere is far from uniform. It is negligible at the surface of the earth, also very small a few earth radii away, and reaches a maximum normally between 200km and 500km in height. This height is given the symbol hmax (or hmF2), while the electron concentration at hmax is called the peak density and given the symbol Nmax or NmF2 (see section

1.1.3). This peak density corresponds to a "critical" plasma frequency denoted foF2 (from equation 1.1), which is the maximum frequency for a vertically incident radio wave to be reflected. The measurement of critical frequency through the use of ionosondes (see section 2.3.1) directly provides Nmax. Because of this foF2 is perhaps the most widely studied ionospheric parameter.

1.1.3 How the Ionosphere is Produced and Maintained; Ionospheric Structure

The main constituents of the neutral atmosphere are atomic and molecular oxygen and nitrogen, atomic helium and hydrogen. Helium is not an important constituent below about 500km while hydrogen is unimportant below about 1000km. Oxygen begins to be dissociated above 100km by ultraviolet radiation. It then diffuses upward making it the dominant source of ions in the F-region (see below). Molecular nitrogen is not readily dissociated but atomic nitrogen as well as nitric oxide is produced by the ion-atom interchange and dissociative recombination reactions described below.

In general, ions and electrons are created from neutral particles through the action of ultraviolet and x-ray radiation, with a small contribution from cosmic rays. The rate of production of ions and electrons in the Earth's upper atmosphere is proportional to the number of neutral

particles available to be ionized and also to the intensity of the ionizing radiation. At the greatest heights there is very little gas to be ionized while below a height of about 100km most of the incident radiation has already been absorbed. Thus the maximum production rate will occur where neither the radiation nor the concentration of neutral particles is vanishingly small.

Loss of ionization by recombination with ions through a reaction of the form:

$$e^- + A^+ \longrightarrow A \qquad (1.2)$$

where A+ is an atomic ion, will not conserve both energy and momentum except in the presence of a neutral third particle. The concentrations of neutral particles are sufficiently large in the lower ionosphere (D-region, E-region, and F1-regions) so that this direct recombination process is the dominant one.

The rate of recombination depends on ion and electron concentrations, which are equal, and so it depends on the square of the electron concentration. Thus:

$$\frac{dN}{dt} = -\alpha N^2 \qquad (1.3)$$

where α is the recombination coefficient.

Above the F1-region lies the F2-region where the density of neutral particles has fallen to very low levels, so that three body collisions become extremely rare. Then more complicated loss processes involving combinations of two body collisions between neutral particles, ions, and

electrons, become most important. Notice that the reaction:

$$e^- + AB^+ \rightarrow A + B \qquad (1.4)$$

will conserve both energy and momentum. This process is known as dissociative recombination. Atomic oxygen ions are often recombined with electrons by first undergoing ion-atom interchange followed by dissociative recombination as follows:

$$O^+ + N_2 \rightarrow NO^+ + N \qquad (1.5)$$

$$e^- + NO^+ \rightarrow N + O \qquad (1.6)$$

It can also first undergo charge transfer with molecular oxygen followed again by dissociative recombination:

$$O^+ + O_2 \rightarrow O + O_2^+ \qquad (1.7)$$

$$e^- + O_2^+ \rightarrow O + O \qquad (1.8)$$

Equations (1.5) and (1.7) proceed more slowly than (1.6) and (1.8), respectively, because the concentrations of neutral particles are so low. Therefore, the upper ionospheric loss processes are dependent upon the concentrations of the neutrals. For these loss processes then:

$$\frac{dN}{dt} = -\beta N \qquad (1.9)$$

where β is called the attachment coefficient. Equation (1.9) is in the form of a simple "attachment-like" process as if electrons were lost by simply attaching themselves to the rare neutral particles.

The continuity equation describing N(t) is:

$$\frac{dN}{dt} = q - L \qquad (1.10)$$

where q is the production rate and L the loss rate. In his classic paper (Chapman, 1931), Sidney Chapman examined the steady state case dN/dt=0, whence q=L. By making several other assumptions he showed that for

$$q = L = -\alpha N^2$$

$$N = N_{max} \exp\tfrac{1}{2}[1 - z - \sec\chi \exp(-z)] \qquad (1.11)$$

while for $q = L = -\beta N$:

$$N = N_{max} \exp[1 - z - \sec\chi \exp(-z)] \qquad (1.12)$$

where χ = zenith angle, z = (h-hmax)/H with H = a constant scale height.

The assumptions made, viz., an atmosphere with a single constituent, plane stratification, a parallel beam of monochromatic solar ionizing radiation and an isothermal atmosphere, limit the usefulness of Chapman's theory, but its value is evident from its continued widespread use particularly in simple ionospheric models.

The various regions of the ionosphere seen during the daytime are depicted in figure 1-1.

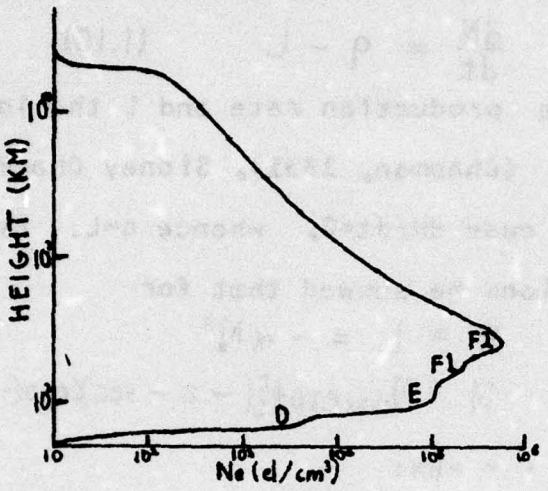

figure 1-1 A typical daytime ionospheric profile from (Papagiannis, 1972).

While the production rate reaches its maximum in the F1-region, the maximum concentration of electrons is found in the F2-region where the loss rate is so small that some plasma remains even at night. Distinct D, E, and F1 regions, however, disappear at night. While the loss rate in the F2-region is low one would expect from (1.9) a steady decay in the course of a night. While the minimum value of Nmax is usually found just before dawn, there is often not a smooth nighttime decay. The problem of explaining the maintenance of the nighttime ionosphere has been investigated for many years. One aspect of the problem- certain winter nighttime increases in foF2- will be taken up in Chapter 4.

1.1.4 Ionospheric variations: Trough, Aurora

Many ionospheric variations and "anomalies" (so called because they are not predicted by simple Chapman theory) have been studied. It would not be appropriate to even briefly describe all these variations (see, for instance (Papagiannis, 1972), section 2.6), but a few of greatest interest to this study should be mentioned.

The seasonal anomaly and December anomaly are the higher values of noontime foF2 in winter than in summer and the generally higher foF2 in December than in other months, respectively.

The latitudinal dependence of the electron density is primarily due to varying elevation of the noontime sun with latitude. The midlatitude trough has a more complicated interpretation, however, which will be discussed in section 1.3.2.

The 11 year solar cycle is a regular variation in solar activity as well as in the average intensity of UV and x-radiation which is accompanied by a corresponding variation in ionospheric plasma density.

The disturbed ionosphere is characterized by such phenomena as:

Sporadic-E, which is the formation of a thin layer of ionization between 100 and 140 km in height (Pike, Wagner and Akasofu, 1975).

Spread-F, the large spread in height from which ionosonde echoes are returned due to a "blobby" F-region.

Ionospheric storms, significant enhancements or depletions in ionospheric total electron content and foF2 often associated with geomagnetic storms (see section 1.3.3).

Aurora cause significant increases in electron density particulary in the E-region. While these phenomena occur at high latitudes, they are often found at mid-latitudes during occasional intense magnetic storms.

1.2 The Earth's Magnetic Field

For simplicity, the Earth's magnetic field is usually approximated by a centered dipole. This approximation is nearly perfect at distances of a few Earth radii, usually gives a value within 1% of the real field near the Earth's surface (except during a great magnetic storm when the discrepency may be 3%), but becomes poor beyond about 8 earth radii or L=8 (the equatorial distance expressed in Earth radii is called the L-value).

Some of the basic equations describing this centered dipole magnetic field follow.

$$B = \frac{M}{r^3}(1 + 3\sin^2\theta)^{\frac{1}{2}} \qquad (1.13)$$

where B is expressed in gauss, θ is the magnetic latitude, r the equatorial distance, and $M=8.05(\pm.002)\times10^{25}$ gauss. Also:

$$\tan I = 2\tan\theta \qquad (1.14)$$

where I is the inclination of the field line with respect to the vertical. One characteristic of magnetic field lines is that the inclination remains constant for all field lines at a given magnetic latitude.

For a given field line:

$$r = r_o\cos^2\theta = LR_e\cos^2\theta \qquad (1.15)$$

where r_o is the distance to the intersection of the field line with the magnetic equator, and Re is the Earth's radius. For r=Re:

$$\cos^2\Lambda = \frac{1}{L} \qquad (1.16)$$

where Λ is called the invariant latitude.

Since r = Re + h :

$$\cos^2\Lambda' = \frac{1 + h/Re}{L} \qquad (1.17)$$

where Λ' is called the generalized invariant latitude. For example, at h=1000km and L=4, $\Lambda' = 57^\circ 28'$. Figure 1-2 shows some of the magnetic dipole geometry.

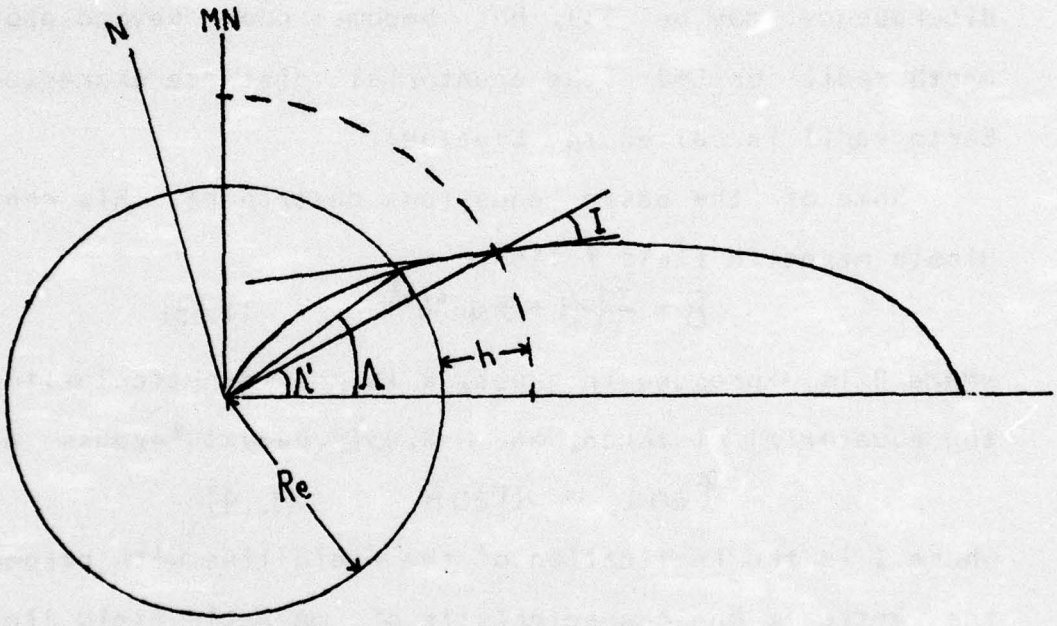

figure 1-2 Magnetic dipole geometry.

1.3 The Magnetosphere

1.3.1 The Magnetosphere: Definition and Structure

The magnetosphere has been defined as: "...the region above the ionosphere in which the magnetic field of the earth has a dominant control over the motions of gas and fast charged particles" (Gold, 1959). The lower boundary of the magnetosphere, i.e., its boundary with the ionosphere, is traditionally near 1000km (Parker, 1968). Even in the F-region (near 300km), however, the presence of the magnetic field exerts a strong influence on the plasma, re: the "frozen field" concept (Rishbeth and Garriott, 1969, page 244-5), and as we shall see in Chapter IV, the magnetic field can cause substantial drift motions of the ionospheric plasma. In 1959 the magnetosphere was thought to extend about 10 Earth radii in the equatorial plane symmetrically with respect to local time. A more recent diagram showing the remarkable progress in the scientific investigation of the magnetosphere which has paralleled the advent of the space age is given in figure I-3.

It was the effect of the solar wind on the near earth environment which most radically altered the original picture of the magnetosphere. The pressure of this solar wind leads to a compression of the dayside magnetic field lines and the long streaming open field lines of the

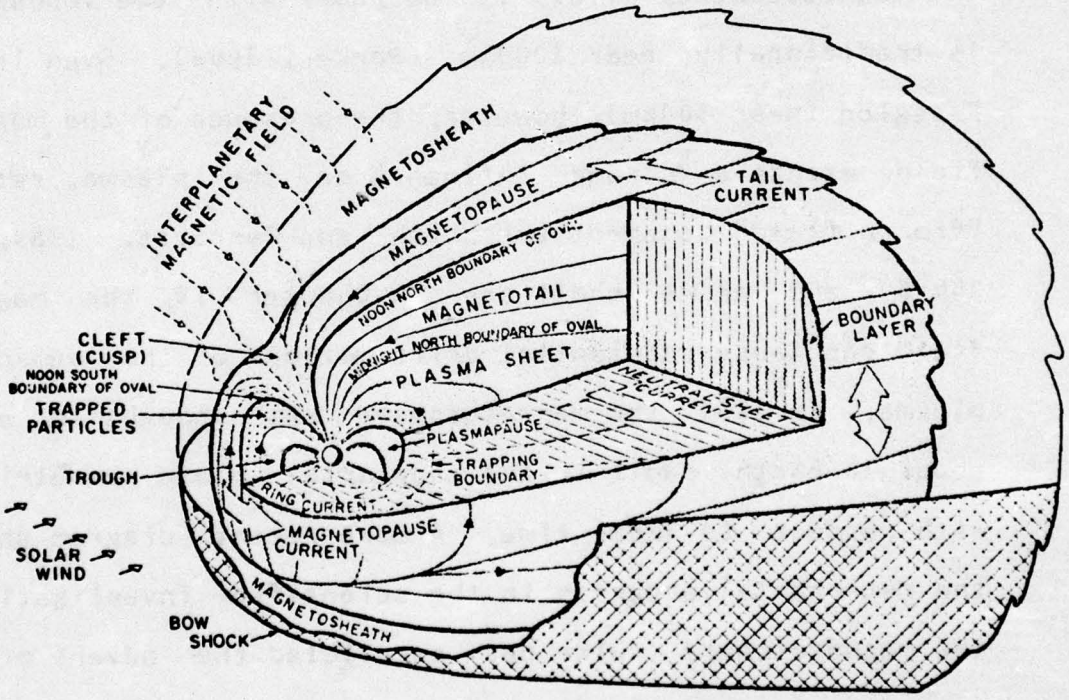

Figure 1-3 Principal features of the magnetosphere, from (Heikkila, 1973)

geomagnetic tail.

The boundary on the nightside between field lines which are always closed and those which are sometimes open has been associated with the equatorial plasmapause, discovered in 1963 (Carpenter, 1963). Using whistler data, Carpenter found a sudden decrease from about 1000el/cm^3 to only about 1el/cm^3 at this plasma knee or plasmapause. Carpenter studied the temporal dependence of plasmapause position and found that near midnight it is located at L=4 (Carpenter, 1966). In the course of a day the plasmapause position was seen to vary from a little over L=3 to over L=5 (see figure I-4).

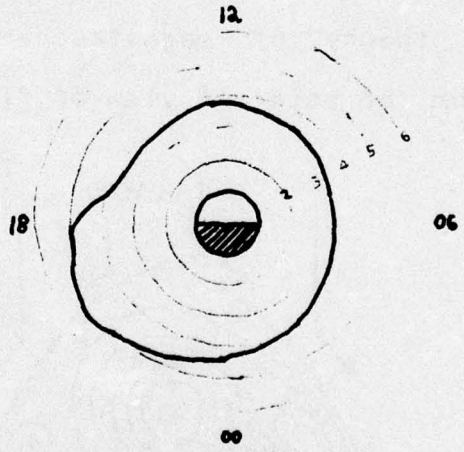

figure I-4 Equatorial radius of the plasmapause vs. local time during periods of moderate steady geomagnetic agitation; (Carpenter, 1966).

The variations in the position of the plasmapause have been dealt with in the context of theories of magnetospheric

structure. Even before Carpenter's discovery of the plasma "knee", Axford and Hines (1961) suggested that sunward magnetospheric convection would be driven by a dawn to dusk electric field (E_{DD}) caused by the interaction of the solar wind with the magnetosphere. Nishida (1966) showed that a convection pattern would develop with outward moving plasma obtained from the draining of magnetic tubes of force which open as they drift across the magnetic tail, and inward moving plasma obtained from the $\vec{E}x\vec{B}$ mechanism. The boundary between tubes of force which open and those which never do Nishida identified with the plasmapause. His convection pattern is reproduced in figure 1-5. Brice (1967) further developed the theory of magnetospheric convection by examining it from the point of view of field line merging.

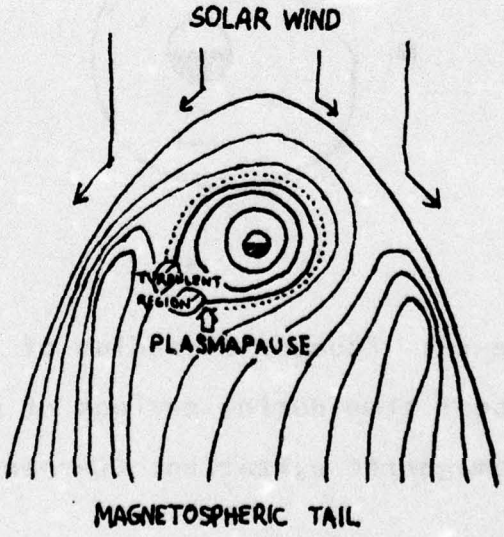

figure 1-5 from (Nishida, 1966)

1.3.2 Relation of the Ionospheric Trough to the Plasmapause

Since charged particles are generally "tied to" magnetic field lines, the field line intersecting the equatorial plasmapause may be considered also to be the three-dimensional boundary of the plasmasphere, a region of much higher electron density than the outer magnetosphere. This same field line intersects the surface of the Earth at the invariant latitude given by (1.16). One then expects the ionospheric plasma density to drop sharply at that latitude. In fact deep ionospheric troughs are found at or near plasmapause L-values. Electron density may drop by a factor of two within 10km at a height of 1000km. (see (Rishbeth and Garriott, 1969), sections 5.52 and 7.54). The term plasmapause no longer refers merely to the equatorial "knee," but is now generally used in reference to the field line which serves as the plasmasphere boundary.

1.3.3 Geomagnetic Storms, Substorms and the Plasmapause

The general features of a geomagnetic storm may be outlined as follows.

A solar flare ejects a large cloud of plasma which in a few days impinges on the Earth's magnetosphere. The

resultant sudden compression of the geomagnetic field lines usually causes a sudden increase in the observed magnetic field strength known as a sudden storm commencement. The increase in magnetic field strength is referred to as the positive phase of the storm. Enhanced magnetospheric convection leads to a buildup of particles at about L=4 known as a ring current which depresses the magnetic field by hundreds of gammas (1 gauss=100000 gammas). This depression is referred to as the storm's main phase. There is then a gradual recovery which lasts 2 to 3 days.

A substorm has no positive phase and is distinguished by a short main phase (1-3 hours). It is believed that the main phase of a geomagnetic storm is actually the superposition of several substorms (Akasofu, 1968).

During magnetically disturbed periods, the plasmapause is seen to move earthward accompanied by a southward motion of the ionospheric trough. Carpenter (1966) found about a six hour phase lag between Kp (a popular index of geomagnetic activity) and inward plasmapause motion. Brace et. al. (1974) noted that during the August 1972 geomagnetic storm the plasmapause moved earthward from L=4.5 to L=1.9 at the peak of the storm. Tulunay and Sayers (1971) completed a statistical analysis of over 1000 troughs which showed an inverse correlation between Kp and trough latitude.

CHAPTER II

A MODEL FOR

IONOSPHERIC-PLASMASPHERIC STRUCTURE

2.1 Description of a Model for Ionospheric-Plasmaspheric Structure

2.1.1 Faraday Rotation

The index of refraction in the presence of a magnetic field and ionized plasma with low collision frequency is found from the fundamental Appleton-Hartree equation and is given by:

$$\mu^2 = 1 - \frac{X(1-X)}{(1-X) - \frac{1}{2}Y_T^2 \pm \left[\frac{1}{4}Y_T^4 + (1-X)^2 Y_L^2\right]^{\frac{1}{2}}} \qquad (2.1)$$

where $X = f_N^2 / f^2$ (2.2)

and $Y_T = Y\sin\theta, \quad Y_L = Y\cos\theta$ (2.3)

where $Y = f_H / f$ (2.4)

Here f = wave frequency and

$$f_H = \frac{\omega}{2\pi} = \frac{eH}{2\pi mc}$$

$$= \text{gyrofrequency} \approx \frac{eB}{2\pi mc} \qquad (2.5)$$

and θ = propagation angle = angle between the magnetic field and the wave normal. Unless θ is close to 90°, a considerable simplification can be made. We can take

$$\frac{1}{4}Y_T^4 \ll (1-X)^2 Y_L^2$$

whence:

$$\mu^2 = 1 - \frac{X}{1 \pm Y_L} \qquad (2.6)$$

This is known as the "quasi-longitudinal approximation." It is excellent for $\theta < 86$ at $f = 100$MHz for instance (Hajeb-Hosseinieh, 1973). At lower frequencies it is a

poorer approximation, of course, but Faraday rotation studies are normally carried out using frequencies larger than 100MHz so its use is generally justified.

The magnetosphere is a so-called "magnetoionic" medium. Such a medium, like a crystal, has birefringent properties, i.e., a radio wave is broken up into two components, an ordinary wave, and an extraordinary wave. The Faraday rotation, a rotation of the plane of polarization of a radio wave, is best explained by using the fact that a linearly polarized wave can be regarded as the sum of two circularly polarized waves rotating in opposite directions, one of which may be identified with the ordinary wave, the other with the extraordinary wave. The ordinary and extraordinary waves have different indices of refraction corresponding to the positive and negative signs respectively in (2.1) and (2.6). We also have:

$$\mu = C/V_{ph} \qquad (2.7)$$

where V_{ph} is the phase velocity. Thus the phase velocities of the two modes differ resulting in a phase lag:

$$d\Omega = \tfrac{1}{2}(d\phi_o - d\phi_E) \qquad (2.8)$$

where:

$$d\phi_{o,E} = \frac{2\pi\, dl}{\lambda_{o,E}} = \frac{2\pi\, dl}{V_{ph}/f} = \frac{2\pi f dl}{c/\mu f} \qquad (2.9)$$

Thus:

$$d\Omega = \frac{\pi f\, dl}{c}(\mu_o - \mu_E) \qquad (2.10)$$

But (2.6) can be approximated as follows:

$$\mu^2 = 1 - \frac{X}{1 \pm Y_L} \simeq 1 - X(1 \mp Y_L)$$

$$\mu = [1 - X(1 \mp Y_L)]^{\frac{1}{2}} \simeq 1 - \tfrac{1}{2}X(1 \mp Y_L) \qquad (2.11)$$

Then:

$$\mu_o = 1 - \tfrac{1}{2}X(1 - Y_L)$$

$$\mu_e = 1 - \tfrac{1}{2}X(1 + Y_L)$$

Substitution into (2.10) gives:

$$d\Omega = \frac{\pi f\, dl}{c} X Y_L \qquad (2.12)$$

Using (2.2), (2.3), (2.5), and (1.1) we arrive at:

$$d\Omega = \frac{e^3 N B \cos\theta\, dl}{2\pi m^2 c^2 f^2}$$

or

$$\Omega = \frac{K}{f^2} \int_0^l N(l) B(l) \cos\theta\, dl \qquad (2.13)$$

here K = .236 in CGS units with B expressed in gammas.

From (2.13) one can see that knowledge of the Faraday rotation Ω of a radio wave transmitted from a satellite provides information about the total amount of plasma encountered along the ray path. It would be most useful to translate the information contained in (2.13) into knowledge of a vertical column of standard cross section located at a certain point along a slanted ray path. The number of electrons in such a column is referred to as the total electron content of the column (TEC). We will next outline the technique for deriving the TEC from Ω.

2.1.2 The Conversion of Faraday Rotation to Total Electron Content

From figure II-1 we see that: $dl = dh \sec\chi$

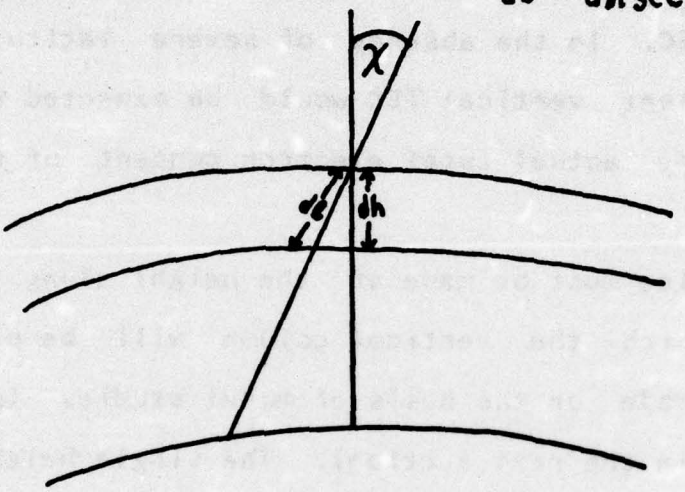

figure II-1

Thus:

$$\Omega = \frac{K}{f^2}\int_0^h N(h)\,B(h)\cos\theta\sec\chi\,dh = \frac{K}{f^2}\int_0^h MN(h)\,dh \qquad (2.14)$$

where:

$$M = B(h)\cos\theta\sec\chi \qquad (2.15)$$

For a geostationary satellite (at r=6.619Re), the upper limit of the integral is usually taken to be 1000km or 2000km because of the small amount of Faraday rotation which occurs in the plasmasphere and beyond (Titheridge, 1972). Over the small range from the surface of the earth to 1000 or 2000km, M changes slowly so a mean value is taken

corresponding to the height along the ray path at which the vertical column is taken. Then:

$$\Omega = \frac{K}{f^2} \bar{M} \int_0^h N(h)dh \qquad (2.16)$$

The integral in (2.16) is referred to as the equivalent vertical TEC. In the absence of severe latitude gradients the equivalent vertical TEC would be expected to be quite close to the actual total electron content of the vertical column.

A choice must be made of the height along the ray path $h(\bar{M})$ at which the vertical column will be placed This choice is made on the basis of model studies (such as that described in the next section). The single height is chosen at which the equivalent vertical TEC and the actual electron content of the vertical column are in best agreement for a wide variety of conditions, i.e., solar cycle, seasonal, diurnal and latitudinal variations, for instance, must be examined by such a model.

Using such a model Titheridge (1972) concluded that use of $h(\bar{M})$=420km with Faraday rotation measurements of geostationary satellite signals (satellite at r=6.619Re in the equatorial plane) would give the electron content up to 2000km of a vertical column to 5% accuracy for a wide variety of conditions. Little Faraday rotation is added above 2000km. If one wished to extend the vertical column to the height of the satellite, no single value of $h(\bar{M})$ would suffice. This results from the high variability in electron

density in these upper regions due to the wide variations in the height of the O+/H+ transition level. This can lead to changes in $\bar{M}$ by even a factor of four, corresponding to a 3000km variation in $h(\bar{M})$. Papagiannis et. al. (1975) showed that the $\bar{M}$ value used to calculate the electron content up to 1000km from signals transmitted by a satellite at 1000km is approximately the same (within 1-2%) as the $\bar{M}$ value used to calculate the electron content up to 2000km from signals transmitted by a geostationary satellite.

2.1.3 Model Description

2.1.3.1 Model Outline

The computer model used in this study divides the Earth's environment into two regions: the regions below and above 1000km. In the lower region which may be loosely called the "ionosphere" we create a two dimensional "real data" array by reading into the program data obtained from the Isis II topside sounder satellite, interpolating between the data points and adding a model bottomside profile. For the upper region (the "exosphere") we can calculate the electron density at any location by using one of two models, each dependent upon conditions at a reference height (1000km). The choice between the two models : a "collisionless" (r^{-4}) model or a diffusive equilibrium

model, depends upon whether the point in question lies within or is outside the plasmasphere. The Faraday rotation and TEC accumulated along a ray path down to 1000km in height is added up, and combined with that of the lower region. The Faraday rotation for the lower region is obtained by interpolating (or extrapolating) between the "real data array" points. So by matching the two sections one can follow the ray path from the satellite to the ground. The vertical TEC below 1000km at various points along the ray path is calculated by the creation of a 51 by 51 "interpolated" density array which divides the range of latitude the ray path covers below 1000km into 51 vertical segments, one vertical column through each of 51 height steps of 20km.

A more detailed description follows.

2.1.3.2 "Exosphere"

Angerami and Thomas (1964) studied theoretically the distribution of plasmaspheric electrons and ions. For the case of a constant temperature along a given field line and equal ion and electron temperatures, their results give:

$$\frac{N(s)}{Neo} = \left[\frac{\exp(-z/H1) + \eta_2 \exp(-z/4H1) + \eta_3 \exp(-z/16H1)}{\eta}\right]^{\frac{1}{2}} \qquad (2.17)$$

Here Neo = the electron density at a reference height (1000km in this study) along the field line. N(s) is the electron density at a given distance along the field line. H1 is a constant scale height. $\eta = \eta 1 + \eta 2 + \eta 3$ where the etas are the ratios of the ion densities hydrogen, helium and oxygen to that of oxygen. The parameter z, called the geopotential height, is given by:

$$z = R_o \left\{\left[1 - \frac{\cos^2\theta_o}{\cos^2\theta'}\right] + \frac{\omega^2 R_o}{2 g_o}\left[\cos^2\theta_o - \frac{\cos^6\theta'}{\cos^4\theta_o}\right]\right. \qquad (2.18)$$

where R_o is the distance from the center of the Earth to the reference height, θ_o is the generalized invariant latitude at the reference height, θ' is the magnetic latitude of the given point along the field line, ω is the Earth's angular velocity of rotation and g_o is the gravitational acceleration at the reference level.

In utilizing these equations, the temperature (needed for the scale height) and the reference level concentrations of electrons and relative ion concentrations must be

provided. The electron density at our chosen reference level (1000km) is obtained by interpolating linearly (or extrapolating) between the Isis II real data points. For the other four parameters the following distributions were assumed for the winter nighttime conditions we will be considering later (the ion concentrations are fractions):

$$\text{temp} = 1125.0 + 1050.0(\Lambda' - 30^{\circ}.0)/30^{\circ}.0 \qquad (2.19)$$

$$\text{oxygen} = 0.10 + 0.80(\Lambda' - 33^{\circ}.0)/22^{\circ}.0$$

$$\text{hydrogen} = 0.82 - 0.73(\Lambda' - 33^{\circ}.0)/22^{\circ}.0 \qquad (2.20)$$

$$\text{helium} = 1 - \text{oxygen} - \text{hydrogen}$$

except that for Λ'(which refers to 1000km) greater than 55°:

$$\text{oxygen} = 0.90$$

$$\text{hydrogen} = .09 \qquad (2.21)$$

$$\text{helium} = .01$$

The temperature relation was scaled from (Brace, Reddy, and Mayr, 1967), while the composition formulas (2.20) and (2.21) were obtained, following (Mendillo and Klobuchar, 1974), from Millstone Hill data and from the observations of Prasad (1970) at Arecibo. See also (Grebowsky et. al., 1975). Studies such as (Taylor et. al., 1968) have shown that nitrogen ions are also a significant constituent at high latitudes. The compositions, however, are only needed by the model computer program inside the plasmasphere (never at high latitudes) so that ignoring the presence of nitrogen is a justifiable simplification.

For field lines outside the plasmasphere, where simple

diffusive equilibrium does not hold, a convenient model suggested by Angerami and Carpenter (1966) is adopted. This model is expressed by (2.22) below:

$$N = N_{eo}\left(\frac{R_o}{r}\right)^4 \qquad (2.22)$$

Angerami and Carpenter (1966) pointed out that this simple r model closely approximates the more accurate "collisionless" model obtained from (Eviatar et. al., 1964), and has the advantage of extreme simplicity.

The collisionless model assumed a pure hydrogen plasma, while observations of a light ion trough show that for ionospheric heights hydrogen becomes a minor constituent at high latitudes (Grebowsky et. al., 1975). The error introduced should not significantly affect the conclusions of this analysis because the stations we will be concerned with are seldom poleward of the plasmapause. The ray paths more frequently encounter the collisionless model at great heights, beyond the plasmapause, where the contribution to Ω is negligible.

2.1.3.3 "Ionosphere"

The heart of the semiempirical model used in this study is N(h) data obtained from the Isis II topside sounder satellite launched April 1, 1971. A sample page of data is shown in figure II-2. As seen from the sample, the soundings were taken about every fifteen seconds, or about every

DEPARTMENT OF COMMUNICATIONS
COMMUNICATIONS RESEARCH CENTRE
OTTAWA, CANADA

ISIS II NEAL HEIGHT PROFILES
(EL/CC # 1?**, KM)

	YR DAY	GMT	LONG	LAT	CHI	DIP	FM	G		TOTALN	P				
ORT	71 344	651/ 1	-110.**	49.67	153	74	.880	7		.085E13	9				
	.13	1406.	.18	1194.	.27	977.		.53	743.	.92	598.	1.51	458.	2.44	407.
	3.28	341.	3.55	317.											
ORT	71 344	651/19	-110.**	48.72	154	74	.870	7		.055E13	7				
	.17	1406.	.23	1204.	.35	963.		.63	731.	1.04	601.	1.52	521.	2.16	458.
ORT	71 344	651/34	-110.**	47.93	154	73	.870	6		.085E13	9				
	.16	1405.	.21	1191.	.31	971.		.81	771.	.88	619.	1.32	524.	1.81	465.
	3.15	363.	3.63	328.											
ORT	71 344	651/49	-110.**	47.14	155	72	.870	7		.049E13	7				
	.19	1405.	.24	1220.	.32	1015.		.**	856.	.72	676.	1.18	552.	1.73	477.
ORT	71 344	652/ 3	-11?.**	46.**1	156	72	.860	6		.100E13	9				
	.20	1404.	.27	1172.	.35	991.		.50	821.	.83	647.	1.29	541.	1.89	472.
	3.17	346.	**.*0	316.											
ORT	71 344	652/17	-110.5	45.67	157	71	.860	7		.052E13	7				
	.21	1403.	.30	1157.	.42	947.		.56	796.	.89	641.	1.35	542.	1.79	491.
ORT	71 344	652/32	-110.5	44.88	158	71	.850	6		.099E13	9				
	.25	1403.	.31	1183.	.42	956.		.55	819.	.88	662.	1.33	572.	1.94	502.
	3.20	418.	**.33	356.											
ORT	71 344	652/45	-110.5	44.19	158	70	.850	8		.046E13	6				
	.28	1402.	.34	1202.	.46	956.		.41	809.	.94	646.	1.35	564.		
ORT	71 344	652/59	-110.5	43.**5	159	70	.840	6		.119E13	9				
	.32	1402.	.42	1137.	.57	907.		.72	785.	1.12	628.	1.69	542.	2.84	454.
	4.00	396.	5.07	345.											
ORT	71 344	653/15	-110.5	42.61	160	69	.840	7		.067E13	7				
	.33	1401.	.41	1174.	.56	924.		.68	808.	.99	656.	1.47	556.	2.27	478.
ORT	71 344	653/28	-110.5	41.72	160	68	.830	6		.134E13	10				
	.35	1401.	.45	1144.	.56	971.		.65	850.	.95	682.	1.37	592.	1.96	525.
	3.52	438.	5.10	381.	6.27	339.									
ORT	71 344	653/42	-110.5	41.19	161	68	.830	7		.138E13	10				
	.39	1400.	.50	1136.	.64	917.		.94	715.	1.36	609.	1.92	545.	3.68	457.
	5.33	415.	6.82	385.	7.43	366.									
ORT	71 344	653/57	-110.6	40.39	162	67	.820	6		.157E13	10				
	.40	1400.	.47	1214.	.58	1015.		.78	853.	1.08	717.	1.65	602.	2.66	513.
	4.43	430.	6.39	382.	7.50	348.									
ORT	71 344	654/11	-110.6	39.65	163	67	.820	6		.197E13	11				
	.40	1399.	.54	1150.	.66	983.		.88	814.	1.22	679.	1.69	594.	2.59	517.
	4.73	434.	7.51	375.	9.55	338.		10.39	317.						
ORT	71 344	654/25	-110.6	38.91	163	66	.810	6		.197E13	12				
	.44	1399.	.55	1156.	.69	961.		.85	830.	1.09	714.	1.50	621.	1.90	575.
	2.89	510.	**.87	440.	7.36	387.		9.26	349.	10.16	324.				
ORT	71 344	654/40	-110.6	38.12	164	65	.810	6		.192E13	11				
	.49	1398.	.57	1212.	.70	1020.		.91	849.	1.25	706.	1.74	620.	2.31	566.
	3.95	487.	6.43	427.	8.63	382.		9.80	353.						
ORT	71 344	654/54	-110.**	37.38	165	65	.800	5		.187E13	11				
	.50	1398.	.61	1185.	.75	990.		1.01	818.	1.30	704.	1.70	625.	2.13	580.
	3.55	500.	5.67	438.	7.56	398.		9.23	357.						
ORT	71 344	655/ 8	-110.7	36.64	166	64	.790	6		.215E13	11				
	.52	1397.	.64	1177.	.79	971.		.99	815.	1.29	682.	1.79	598.	2.50	541.
	4.52	460.	6.94	408.	9.62	356.		10.71	324.						
ORT	71 344	655/23	-110.7	35.85	166	63	.790	6		.179E13	11				
	.56	1396.	.67	1210.	.82	1020.		1.01	872.	1.22	759.	1.60	662.	2.04	601.
	2.91	536.	**.81	466.	6.97	418.		8.89	378.						
ORT	71 344	655/36	-110.7	35.16	167	63	.780	6		.238E13	11				
	.58	1396.	.69	1208.	.84	1016.		1.13	812.	1.49	690.	2.00	618.	3.38	533.
	5.77	463.	8.29	412.	10.10	376.		11.41	339.						
ORT	71 344	655/50	-110.7	34.42	168	62	.780	6		.215E13	9				
	.62	1395.	.76	1179.	1.02	917.		1.55	719.	2.21	640.	**.12	531.	6.76	458.
	9.14	415.	10.60	387.											

Figure II-2 A sample page of Isis II interpolated Ne(h) data

degree of geographic latitude. The quality (Q in figure II-2) varies considerably. Best quality ionograms are assigned Q values of 4 while the ionograms with the least information are assigned a Q value of 9. According to the introduction to the compilation of Isis II data (see Acknowledgements), for the best quality ionograms, the accuracy in the real height is probably better than 5%. Unfortunately, Ne(h) is not always given down to hmax. Furthermore, no indication in the data compilation is given where this occurs, so in some cases hmax is actually lower than the figure we are forced to take.

As noted earlier (section 2.1.3.1), a latitude vs. height "real density array" is constructed using this data. Linear interpolation is used between the data points to obtain the electron densities at 1000 and 700km heights: N(1000) and N(700), respectively. The other parameters read by the model program are: Nmax, hmax, and yzero, where yzero is the height at which the electron density of the model drops to zero on the bottomside. Ne(h) below 1000km in height is treated in three parts: (a), from 700km to 1000km an exponential of scale height HH is matched with (b), an exponential of scale height HL between hk and 700km; finally, (c), a bi-parabola of semithickness ym extends around the peak from yzero to hk, where hk=hmax+ym/4, and ym=hmax-yzero. The equation of the bi-parabola is:

$$N = N_{max}\left[1-\left(\frac{h-h_{max}}{y_m}\right)^2\right]^2 \qquad (2.23)$$

At the height hk:

$$N = \left(\frac{15}{16}\right)^2 N_{max} \cong N_k \qquad (2.24)$$

The scale height HL is obtained from (2.26) by rearranging the exponential equation (2.25) and substituting HL, Nk, hk, N(700) and 700 for H, No, ho, N, and h respectively:

$$N(h) = N_o \exp\left(\frac{h_o - h}{H}\right) \qquad (2.25)$$

$$HL = \frac{700 - hk}{\ln[Nk/N(700)]} \qquad (2.26)$$

Similarly for the upper exponential:

$$HH = \frac{300}{\ln[N(700)/N(1000)} \qquad (2.27)$$

Now that the scale heights have been obtained, the computer program can calculate N(h) at selected heights. A step size of 20km was chosen as it is small enough to prevent loss of important detail near the peak. It is now necessary to consider the range of latitudes over which the ray path passes below 1000km. This range is divided into 51 vertical sections, each section corresponding to one of the 51 heights along the ray path (again the step size is 20km) where the electron density is calculated. In order to fill in this second array which we call an "interpolated density array," it will be necessary to interpolate between the latitudes of the real density array and, occasionally, to extrapolate beyond the range of the real density array. The interpolation is linear, as is the extrapolation, but the number of points used to determine the extrapolated line depends on the position of any trough. In extrapolating

north or south of the real array at least the last two points are taken. Additional points are taken as long as each additional point differs from the preceding one by less than 25%. If the first point, on the other hand, differs by at least 25% from the second, a third point is taken. Additional points are taken if necessary until the needed extrapolated value is positive. A least squares subroutine is used to fit a line to the selected points, and this line provides the extrapolated values needed.

Once the interpolated density array has been constructed, the vertical TEC at 51 columns along the ray path is found simply from the vertical segments. The slant TEC is added up along the ray path by multiplying the electron density at each point along the ray path by the distance between points. The vertical TEC increment along the ray path is then obtained by multiplying each slant TEC increment by $\cos\chi$. The sum of these vertical increments will be called here the "vertical equivalent TEC." The M factor is then calculated at each point along the ray path by using (2.15) and the Faraday rotation is found by transforming (2.14) into a sum:

$$\Omega = \frac{K}{f^2} \sum_{i=1}^{51} N(i) M(i) \Delta h \qquad (2.28)$$

After the total Faraday rotation along the ray path is computed, it is combined with the M value at each height to give 51 values of equivalent vertical TEC. These may be

compared with the TEC of the vertical columns.

Titheridge's (1972) conclusion that for a wide variety of conditions the use of h(M)=420km converts the Faraday rotation to TEC up to 2000km leads us to extend our vertical columns up to 2000km so that we may compare them with the 51 equivalent vertical TEC values just mentioned. This cannot be done to great accuracy without quadrupling the computer printout, but for our purposes we simply integrate from 1000km to 2000km using the closed expression:

$$\int_{1000}^{2000} N(h)\,dh = \int_{1000}^{2000} N(1000)\exp\left(\frac{1000-h}{H}\right)dh = HN(1000)\left[1-\exp\left(-\frac{1000}{H}\right)\right] \qquad (229)$$

A scale height of H=1000km, for example, simplifies the result to:

$$\int_{1000}^{2000} N(h)\,dh = HN(1000)\left(1-\frac{1}{e}\right) = .63212\,N(1000) \qquad (230)$$

where N(1000) is in units of 10^4el/cm^3 and the TEC is in units of 10^{12}el/cm^2.

2.2 Usefulness of constant $\bar{M}$-factor at a high latitude station during winter night

The usefulness of equivalent vertical TEC below 1000km except in the presence of a steep trough, has already been shown at mid-latitudes by Hajeb-Hosseinieh (1973). We extend his work to high latitudes and also consider the region above 1000km for the particular case of winter nighttime conditions.

2.2.1 Idealized Arrays

Consider a uniform data array extending from 24° to 67° geographic latitude with the following input parameters: Nmax=2×10^{5}, N(700)=2.63×10^{4}, N(1000)=1×10^{4}, hmax=320km, and yzero=200km. The ray path travels from a geostationary satellite to each of three stations, the coordinates of which are found in Table II-I.

Table II-I

station	geog. lat.	geog. long.	mag. lat.
Hamilton	42.63	70.82W	54.34
Goose Bay	53.30	60.33W	64.82
Narssarssuaq	61.20	45.40W	71.38

Consider the input data shown in Table II-II (the

Table II-II

Uniform Latitude Gradient Input Array

geog. lat.	N(1000) (10^4 el/cm^3)	N(700)	Nmax	hmax (km.)	yzero (km.)
25	1.6	3.5	14.0	320	200
28	1.5	3.3	13.4	320	200
31	1.4	3.1	12.8	320	200
34	1.3	2.9	12.2	320	200
37	1.2	2.7	11.6	320	200
40	1.1	2.5	11.0	320	200
43	1.0	2.3	10.4	320	200
46	0.9	2.1	9.8	320	200
49	0.8	1.9	9.2	320	200
52	0.7	1.7	8.6	320	200
55	0.6	1.5	8.0	320	200
58	0.5	1.3	7.4	320	200
61	0.4	1.1	6.8	320	200
64	0.3	0.9	6.2	320	200
67	0.2	0.7	5.6	320	200
70	0.1	0.5	5.0	320	200

densities are in units of $10^4/cm^3$).

It represents a uniform latitude gradient. Examination of Brace et. al. (1967) will show that the data was chosen as a reasonable compromise between average winter nighttime conditions and the requirements of constructing a uniform density gradient over a large range of latitudes.

Examination of the "vertical equivalent" TEC accumulated for each of these two arrays exclusively using the diffusive equilibrium model for heights above 1000km leads to the the conclusion that a scale height H=1000km in (2.29) will reproduce the results to the required accuracy. Using (2.30) we now extend the 51 vertical columns to 2000km and compare with the equivalent vertical TEC computed for the 51 columns. The results are shown in Table II-III where "best h($\bar{M}$)" refers to the height at which the vertical columnar TEC matches the equivalent vertical TEC using the $\bar{M}$ factor for that height. "%dif at 420" gives the percentage difference between the vertical TEC at the 420-km point and the equivalent vertical TEC using the $\bar{M}$ factor at 420km.

Table II-III

station	best h($\bar{M}$)		%dif at 420	
	Unif data	Unif grad	Unif data	Unif grad
Hamilton	371km	220km	2.8	7.4
Goose Bay	400km	17km	1.2	9.1
Narssarssuaq	383km	4km	2.1	17.7

The results clearly show that the use of $h(\bar{M})$=420km gives good agreement for a uniform data array. For a gradient, however, there is decreasing agreement with increasing station latitude. Caution must be used in considering the results since both of these arrays are quite idealized.

It is the gradient, and not a uniform data array which more closely approximates typical winter nighttime conditions. Examination of the computer output shows that the Faraday rotation technique as far poleward as the trough minimum apparently measures total electron content not to 2000km, but to some greater height for these winter nighttime conditions. The effect is due to the fact that heights along the ray path in the range 2000km to 5000km coincide with field lines of the lowest invariant latitude, i.e., the the highest reference level (1000km) electron densities. This enhances the Faraday rotation accumulated in this upper region. Furthermore, the minimum invariant latitude corresponds to higher heights for higher latitude stations, enhancing the effect there. For the uniform gradient the minimum invariant latitude occurs at about 2500km observing from Hamilton, Mass. (42°.6N, 70°.8W), 3700km from Goose Bay, Labrador (53°.3N, 60°.3W), and 4200km from Narssarssuaq, Greenland (61°.2N, 45°.4W). The geometry is shown

in figure II-3.

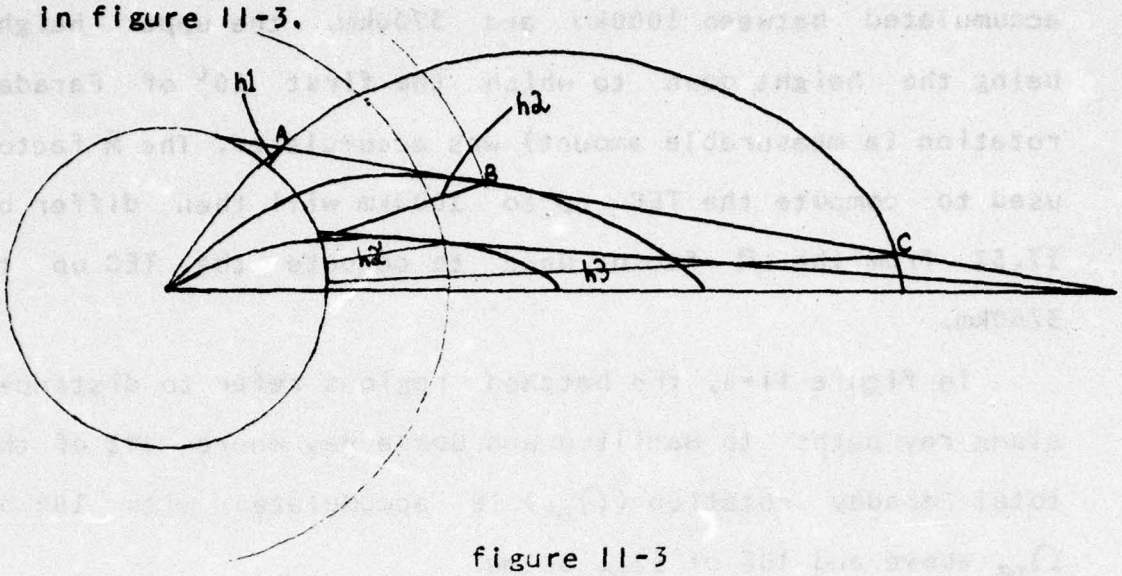

figure II-3

In figure II-3, the lowest invariant latitude the ray path crosses at one point (point B), corresponding to the height h2. Points A and C have the same invariant latitude and correspond to smaller and greater heights respectively. For a lower latitude station the lowest invariant latitude corresponds to a lower height h2'.

To check that this effect is real and not due to the use of an idealized gradient, a real gradient taken from Isis II topside data was used (December 15, 1971). The conclusions above were confirmed.

Clearly a non-negligible error is introduced in assuming that the $\bar{M}$ value used to calculate equivalent vertical TEC up to 1000km is little different from the $\bar{M}$ value used to calculate equivalent vertical TEC up to 2000km or higher. For the uniform gradient observed from Goose Bay, for instance, 17.5% of the "vertical equivalent TEC" is

accumulated between 1000km and 3700km, the upper height being the height down to which the first 10° of Faraday rotation (a measurable amount) was accumulated. The $\tilde{M}$ factor used to compute the TEC up to 1000km will then differ by 17.5% from the $\tilde{M}$ factor used to compute the TEC up to 3700km.

In figure II-4, the hatched regions refer to distances along ray paths to Hamilton and Goose Bay where 80% of the total Faraday rotation (Ω_{Tot}) is accumulated, with 10% of Ω_{Tot} above and 10% of Ω_{Tot} below.

2.2.2 Severe Latitude Gradient

Consider the data array shown in Table II-IV.

This data was obtained between 2:19 UT and 2:30 UT on December 18, 1971 when a severe magnetic storm was occurring. At the time the data was taken the Kp index stood at 4-. Six hours earlier it had reached 7+. The parameters Nmax, N(700), N(1000), and N(sat) are plotted in figure II-5. N(sat) is the measurement closest to the satellite, always near 1400km. One can clearly see the sharp equatorward edge of the trough near 40° which is identified with the plasmapause. The poleward edge of the trough is also steep and north of the trough the profile is erratic.

The yzeros were somewhat arbitrarily assigned but the presence of the auroral E layer near the trough poleward

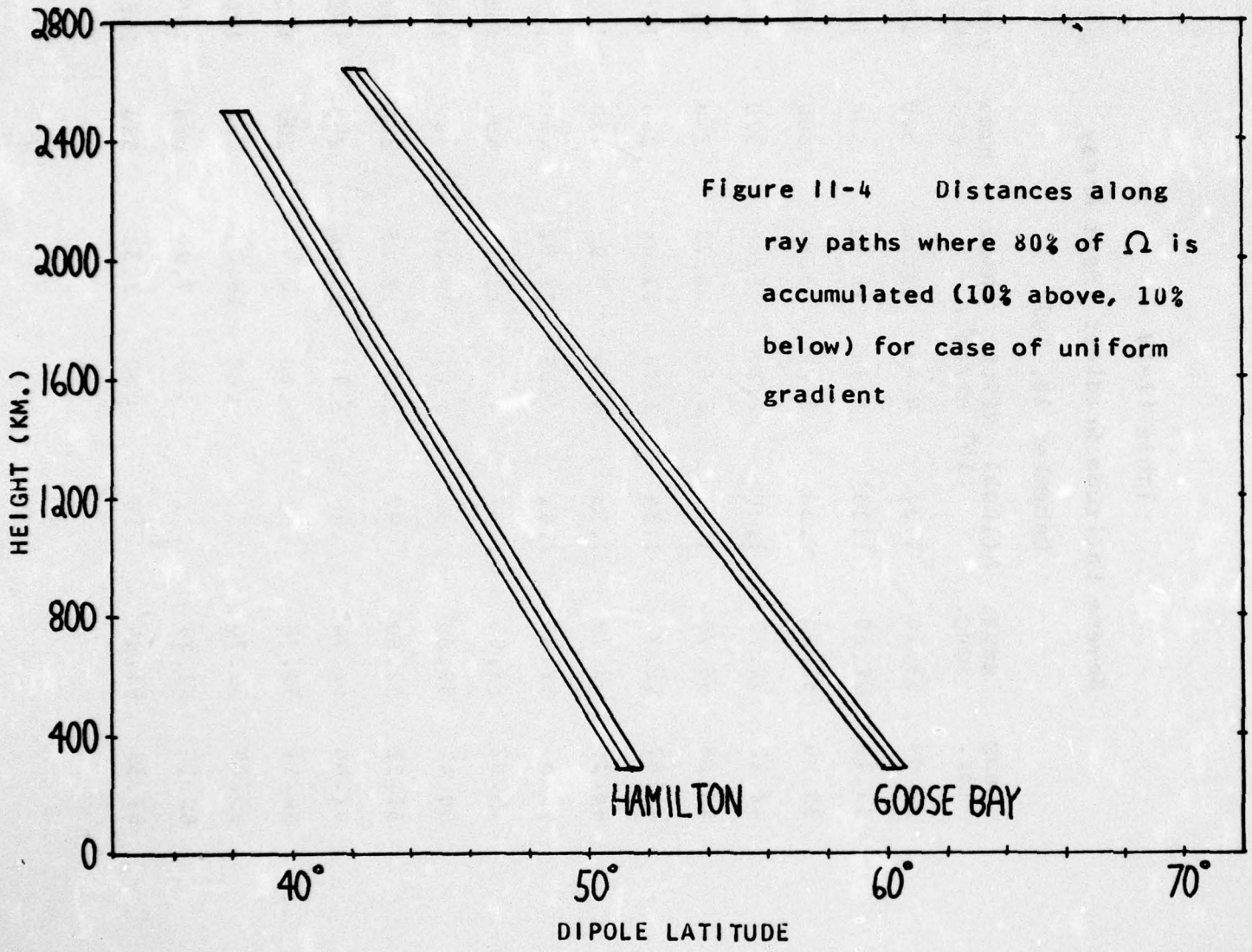

Figure II-4 Distances along ray paths where 80% of Ω is accumulated (10% above, 10% below) for case of uniform gradient

Table II-IV

Severe Latitude Gradient Input Array

December 18, 1971

geog. lat.	geog. long.	N(1000)	N(700) (10^4 el/cm^3)	Nmax	hmax (km.)	yzero (km.)
30.09	53.10	1.37	4.45	16.26	520	195
39.16	52.80	1.13	3.78	12.51	500	195
39.90	52.80	.59	1.24	3.94	300	195
42.12	52.70	1.00	2.26	8.80	320	195
43.65	53.70	1.05	2.65	8.77	340	195
46.67	52.70	1.34	3.76	11.04	360	195
48.15	52.70	1.53	4.24	9.92	420	195
48.88	52.60	2.81	7.85	17.51	480	165
49.62	52.60	1.67	4.87	12.25	400	165
50.41	52.60	2.50	6.01	19.00	340	165
51.21	52.60	.97	2.32	12.23	260	165
52.68	52.70	.48	1.11	15.66	200	120
54.21	52.70	.32	.80	6.57	200	120
55.68	52.70	.31	.80	16.01	200	120
60.16	52.80	.32	.78	7.90	260	165
67.35	53.50	.15	.60	2.35	360	165

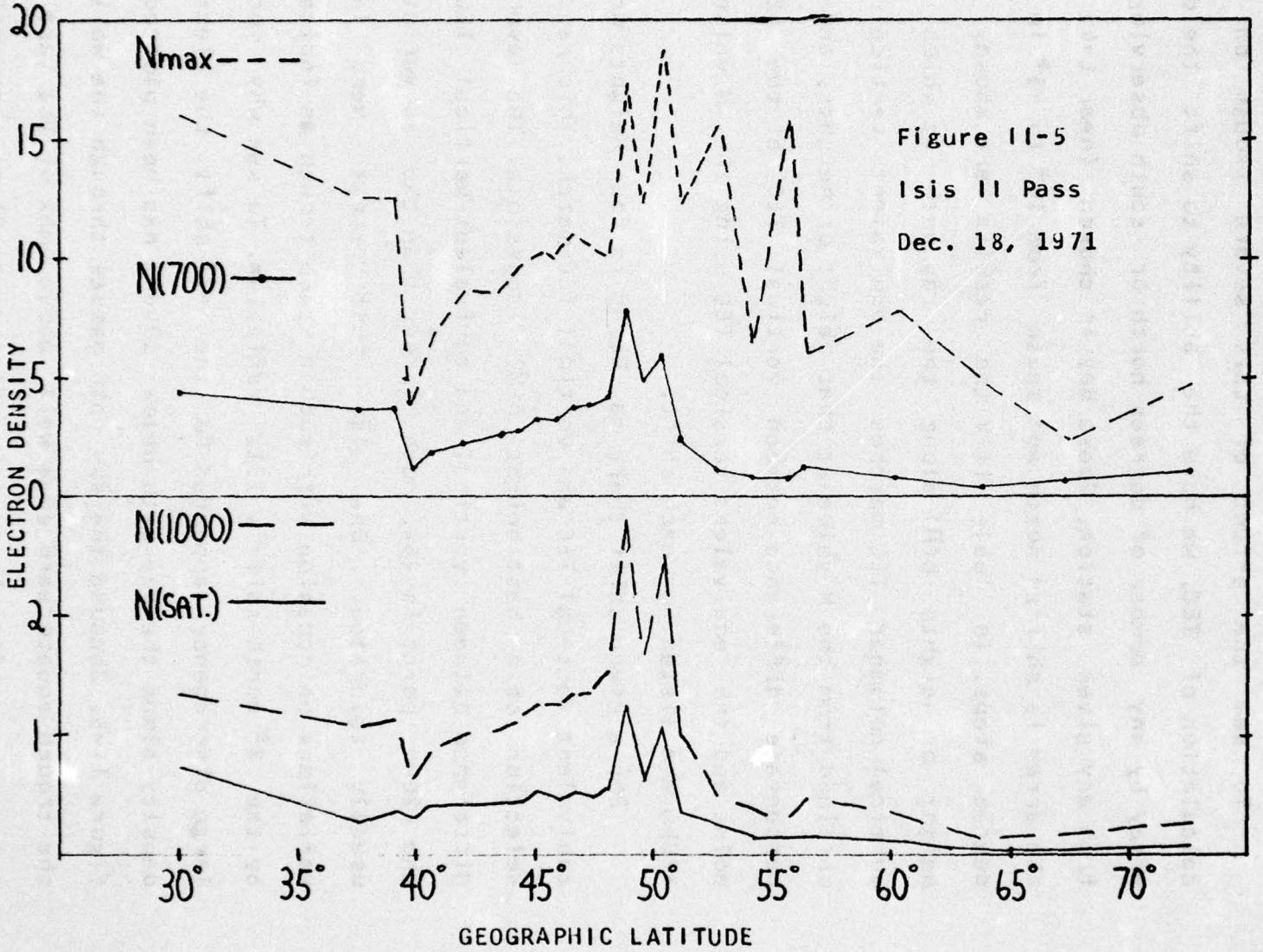

Figure II-5

Isis II Pass

Dec. 18, 1971

edge necessitates the low yzero values there.

To see the effect of this severe trough on the calculation of TEC, we have the ability to shift the data array by any number of degrees north or south observing it from any given station. Goose Bay is chosen (near L=4) and the array is shifted north and south from 10° to -5° in one degree steps. In Table II-V the results are shown. The height or heights h($\bar{M}$) along the ray path at which the vertical columnar TEC matches the equivalent vertical TEC obtained from the M value at that height or heights, and the percentage difference between vertical TEC at the 420km point and the equivalent vertical TEC using the $\bar{M}$ value at 420km are listed for each shift.

For a given shift there may be up to four heights where equivalent vertical TEC and vertical TEC match. This renders selection of a best height h($\bar{M}$) impossible. The average difference between vertical and equivalent vertical TEC at the 420km point is 26%, much larger than the 5% variation usually tolerated. One also must expect very large variations on occasion with such a steep trough as indicated by the 8° north shift's 151% variation. To see why such a large discrepency appeared for the +8° shift the electron density along the ray path below 1000km has been plotted in figure II-6. Because the ray path passes through the wall of the trough equatorward edge well above hmax of the vertical column the profile is greatly distorted. Since the vertical

Table II-V

shift	best h(M)	% dif at 420km.
+10	none	6.5
+9	9	4.8
+8	67,480	151.
+7	940,557,136	73.
+6	331,641	15.
+5	397,740	2.2
+4	426,850	1.1
+3	462	6.7
+2	508	13.
+1	539	15.
0	161,403	1.0
-1	267,360,456	25.
-2	359,412,497,527	5.1
-3	429,515,548,630	9.3
-4	504,620,735	41.
-5	596,720,834	49.

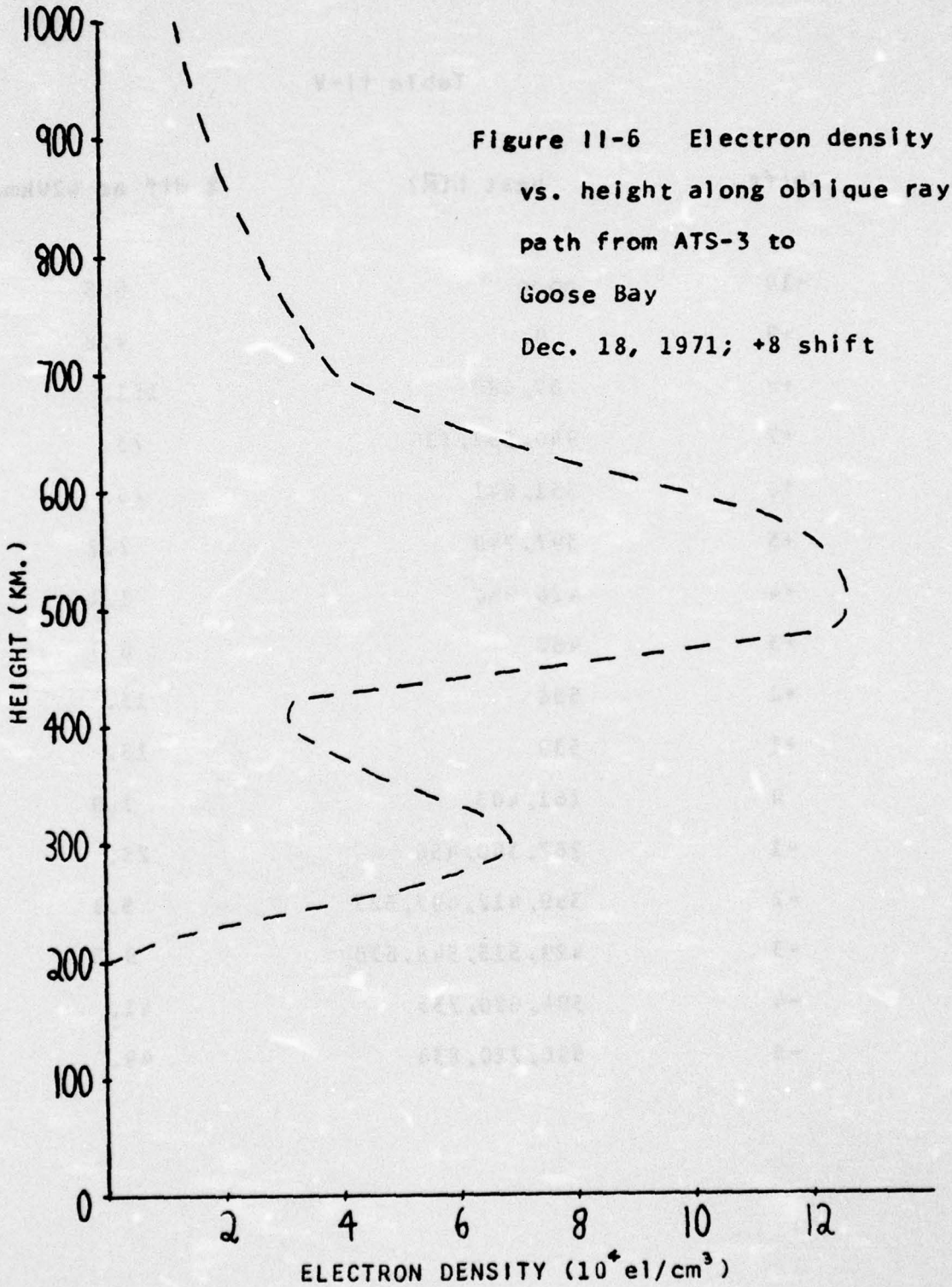

Figure II-6 Electron density vs. height along oblique ray path from ATS-3 to Goose Bay Dec. 18, 1971; +8 shift

column is inside the trough the vertical total content is far less than the "vertical equivalent" TEC.

It appears that for a severe trough one cannot legitimately convert Faraday rotation into the total electron content of a vertical column, confirming Hajeb-Hosseinieh (1973).

2.2.3 Conclusions

For the winter nighttime conditions we have examined at high latitudes, Faraday rotation apparently is a measurement of equivalent vertical TEC up to some height higher than 2000km. A more refined model is needed to fix the actual height. Under conditions of a severe trough Faraday rotation cannot be meaningfully converted to total electron content using any mean $h(\bar{M})$. In attempting to understand such conditions it is best to study the variations in Faraday rotation without attempting to convert it into the total content of a vertical column. Further study is needed to determine the dependence of the best $h(\bar{M})$ on seasonal, solar cycle, diurnal variations, and differences in station latitude in the absence of a severe trough.

2.3 Ionosondes and Slab Thickness

2.3.1 Ionosondes

The Isis II satellite observations described earlier were taken by an ionosonde. Ionosondes collect huge quantities of data from the ground as well, and in fact are the most widely used means of monitoring ionospheric electron density in addition to many other ionospheric parameters. Ionosonde observations taken from the surface of the Earth probe the "bottomside" ionosphere, i.e., the ionosphere below hmax, where the last reflection occurs. Similarly, satellite sounders such as that on Isis II probe the "topside" ionosphere.

The ionosonde makes use of pulsed radio signals, each pulse sweeping over a range of frequencies from 1-2 MHz to perhaps 25 MHz. The receiver displays on an oscilloscope a trace showing the frequency of the returned signal vs. time. The virtual height h' at which the signal was reflected is then given by:

$$h' = \tfrac{1}{2}ct \qquad (2.31)$$

In order to see why the virtual height and the true height of the reflection differ it is necessary to review the process of reflection. For this simple argument we ignore the presence of the magnetic field and of collisions. Then the transmitted radio wave passes through a medium with

an index of refraction given by (2.6) with $Y_L=0$, i.e.,

$$\mu = \sqrt{1 - \frac{f_N^2}{f^2}} \qquad (2.32)$$

The phase velocity of the wave is then related to the index of refraction and the group velocity by the next two relations:

$$v_{ph} = c/\mu \qquad (2.33)$$

$$v_{ph} v_{gr} = c^2 \qquad (2.34)$$

As the radio wave goes into regions of higher electron density the plasma frequency increases by (1.1) which decreases μ, increases v_{ph} and decreases v_{gr} thus slowing the wave packet down. When $f_N = f$ the group velocity becomes zero and the wave is reflected. Thus we see that the reflection is not instantaneous but rather gradual so that the virtual height is always greater than the true height of the reflection. The relation between the two is given by the process of true height analysis, too complicated to be even outlined here. For a brief description see (Rishbeth and Garriott, 1969).

True height analysis is costly and not often necessary. The peak density NmF2 can be easily obtained from (1.1) by reading foF2 right off the ionogram trace. foF2 is always obtained from a vertical reflection. The maximum frequency reflected to a 3000km distance is known as MUF(3000)F2. An empirical formula known as the Shimazaki relation gives a good approximation to the true height of the reflection, especially at night (Shimazaki, 1955) using MUF(3000)F2 (or

M(3000)F2). It is:

$$hmF2 = \frac{1490}{M(3000)F2} - 176km \qquad (2.35)$$

While refinements have been proposed by Wright and McDuffie (1960) and by Bradley and Dudeney (1973), (2.35) remains fairly accurate for nighttime conditions.

2.3.2 Slab Thickness

Slab thickness τ is defined as the ratio:

$$\tau = TEC/Nmax \qquad (2.36)$$

and thus represents the thickness the ionosphere would have if the electron density throughout was the constant peak value. Here Nmax must be the peak density of the vertical TEC column unless there are very shallow horizontal gradients in TEC and Nmax.

Slab thickness is an important ionospheric parameter since monitoring it gives an indication of the shape of the vertical profile of N(h) without the need to resort to true height analysis. If the total content of a vertical column remains constant while the peak density changes, for example, one must conclude that a redistribution of plasma has taken place, i.e., the shape of the profile of electron density vs. height has changed. Alternately, if TEC changes and Nmax does not, one concludes that an influx of plasma has occurred probably bringing electrons down from the exosphere into the vertical column. As seen in section 2.2

one must be cautious about making such conclusions using Faraday rotation measurements in the presence of troughs since the equivalent TEC and not the actual TEC of the column is known.

In chapter four we will see examples in which slab thickness decreases significantly in the presence of troughs on the basis of Faraday rotation measurements. We will investigate the possible roles of both trough motions and vertical distortions in producing this phenomenon.

CHAPTER III

AVERAGE BEHAVIOR OF THE IONOSPHERE NEAR SIXTY DEGREES MAGNETIC LATITUDE

3.1 Mean and Normalized Monthly Curves

Median Behavior

In the previous chapter we discussed the importance of three ionospheric parameters: total electron content (TEC), peak density of the F-2 layer (Nmax), and the ratio of these two quantities, the equivalent slab thickness (t=TEC/Nmax). The purpose of this chapter is to briefly discuss the average seasonal and diurnal behavior of these three parameters at 60 degrees magnetic latitude.

In this chapter, the term "TEC," will refer to the *equivalent vertical TEC* through the 420-km point, i.e., in order to obtain the TEC, Faraday rotation measurements are combined with a constant $\bar{M}$ value at 420km height along the ray path. With TEC defined in this manner, the terms total electron content (TEC) and Faraday rotation (Ω) may be used interchangeably.

38 months of TEC data collected at Goose Bay, Labrador (53°.3geog.N, 60°.3geog.W) will be combined to calculate the mean monthly behavior of TEC. A vertical column intersecting the ray path to the geostationary satellite (ATS-3) at 420km height is located at geographic coordinates 47°.5N, 62°.2W, and *generalized invariant* latitude 59°.9 (L=3.98). Fortunately, we have available many years of Nmax data taken by the ionosonde at St. John's, Newfoundland (47°.6geog.N, 52°.7geog.W), located at nearly the identical latitude as the

420-km point and only thirty minutes of local time to the east. 41 months of St. John's Nmax data spanning the same period as the TEC measurements will give us the mean monthly Nmax behavior. Then we will combine the TEC and Nmax data into mean monthly slab thickness results based on 37 months. The months from which the mean monthly behavior of the three parameters are derived are listed in Table III-1.

Table III-1

Data Base for Mean Monthly Calculations

Parameter	
TEC	Nov., 1971-Nov., 1973; April, 1974-April, 1975
Nmax	Nov., 1971-March, 1975
τ	Nov., 1971-Nov., 1973; April, 1974-March, 1975

The monthly mean diurnal behavior, which for TEC we call MTEC(Y,M,H), is found by first calculating the mean values at each hour of local time for the 3 parameters during each month. This gives 24 numbers for each month. All the Januarys, Februarys, etc., are then combined by taking the mean of the mean values for each local time. This gives mean monthly diurnal curves which for TEC we call MMTEC(M,H), and also curves for Nmax and τ. These curves are presented in figures III-1, III-2, and III-3.

In calculating these mean monthly diurnal curves, we have followed (Hawkins and Klobuchar, 1974). In that study, seven years of TEC data collected at Hamilton, Mass. (42°.6 geog.N, 70°.8geog.W) were presented. We will be interested in

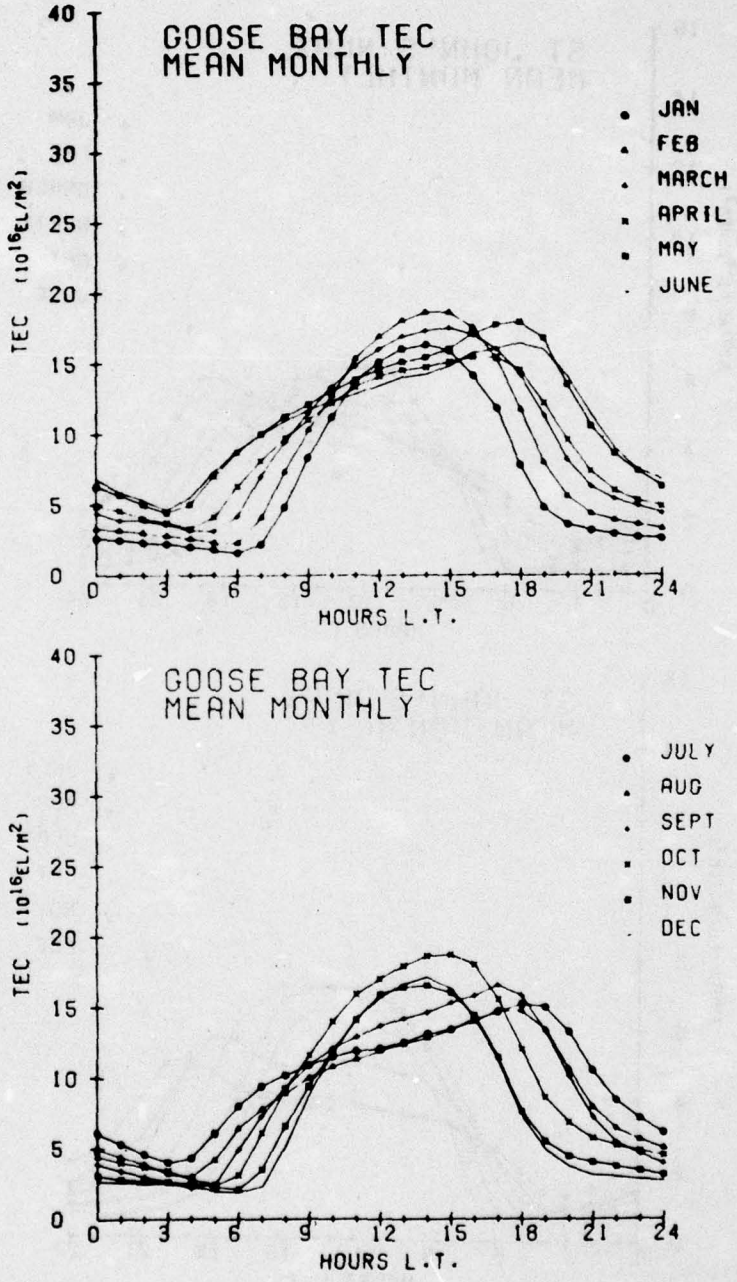

Figure III-1 Mean monthly TEC diurnal curves

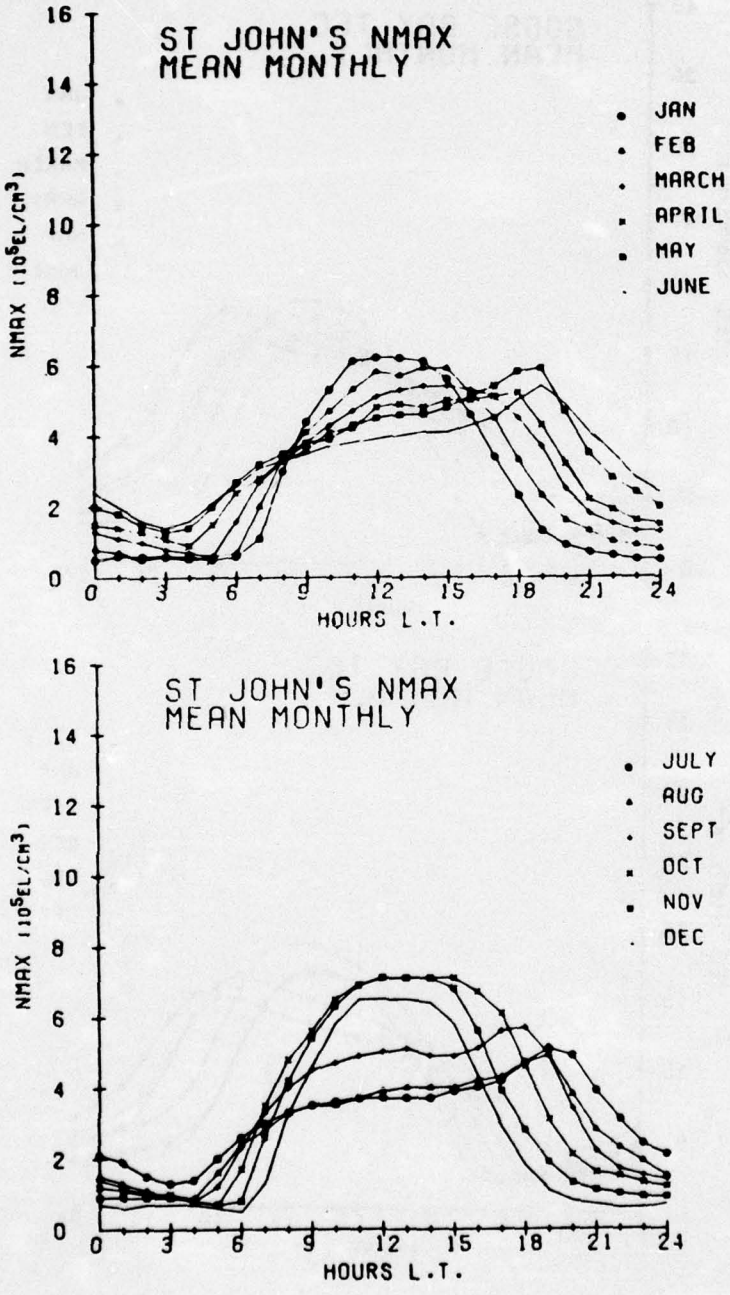

Figure III-2 Mean monthly Nmax diurnal curves

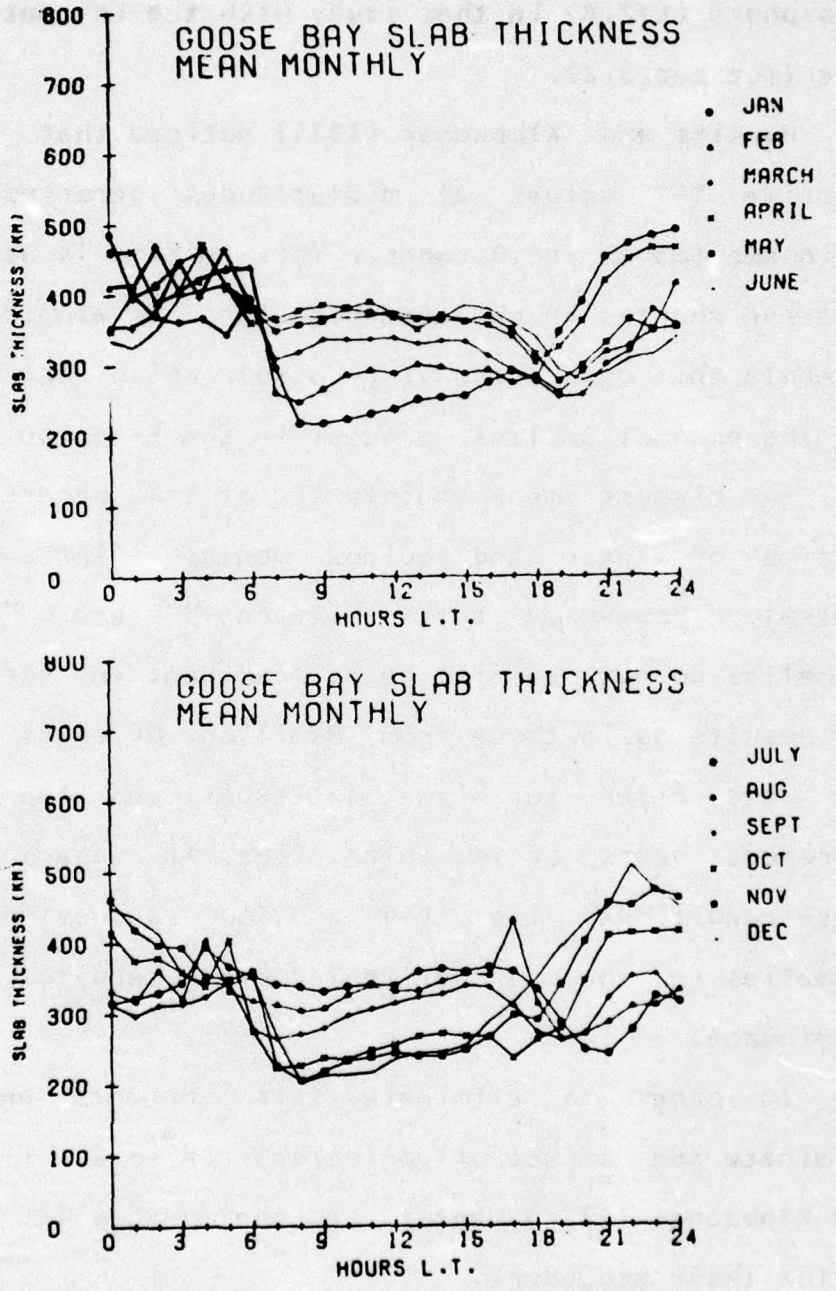

Figure III-3 Mean monthly slab thickness diurnal curves

comparing the average behavior found for the mid-latitude ionosphere (L=2.8) in that study with the L=4 data presented here (see sec.3.2).

Hawkins and Klobuchar (1974) noticed that the highest noontime TEC values at midlatitudes occurred near the equinoxes (March and October). This effect is attributed to relative changes in the concentrations of atomic oxygen and molecular nitrogen (the O/N_2 ratio), which are responsible for the production/loss process in the F-region. We notice that the highest mean monthly TEC at L=4 occurs during the daytime of winter and equinox months (figure III-1). In general, however, these "seasonal" and "equinoctal" anomalies do not seem to be as prominent in the mean Goose Bay results as in those from Hamilton. Of course, the Goose Bay data refer to higher latitudes and the data base represents years of low solar flux. It appears that under these conditions, i.e., L=4 and low sunspot number, such anomalies in the mean diurnal curves tend to decrease in prominence.

In order to eliminate this effect, and also to eliminate the effect of variations in solar flux, Hawkins and Klobuchar (1974) normalized the monthly TEC values. We follow their procedure.

First the monthly mean TEC values (MMTEC) for a period of 24 hours are averaged together:

$$ATEC(Y,M) = \frac{1}{24} \sum_{H=1}^{24} MTEC(Y,M,H) \qquad (3.1)$$

Then normalized monthly mean curves are obtained via:

$$NTEC(Y,M,H) = MTEC(Y,M,H)/ATEC(Y,M) \qquad (3.2)$$

The normalized curves were averaged over the years of the study by calculating:

$$NMTEC(M,H) = \frac{1}{n} \sum_{Y=1}^{Y'} NTEC(Y,M,H)$$

These mean normalized monthly TEC curves remove any variation due to the solar flux and the "equinoctal anomaly," large effects from which would tend to increase ATEC(Y,M). What remains is the seasonal variation in the diurnal curves. The results of this analysis for TEC appear in figure III-4. The same procedure has been followed for Nmax and τ, and the normalized curves for these parameters are found in figures III-5, and III-6.

Note the smooth progression in noon-time normalized TEC (figure III-4), with highest values in winter, and lowest in summer. These curves show that the winter ionosphere is solar production dominated, responding primarily to changes in solar zenith angle. The seasonal anomaly is strikingly shown, with the lower summer daytime values due to enhanced loss processes which result from the high summer neutral temperature. The maximum and minimum MMTEC and NMTEC are

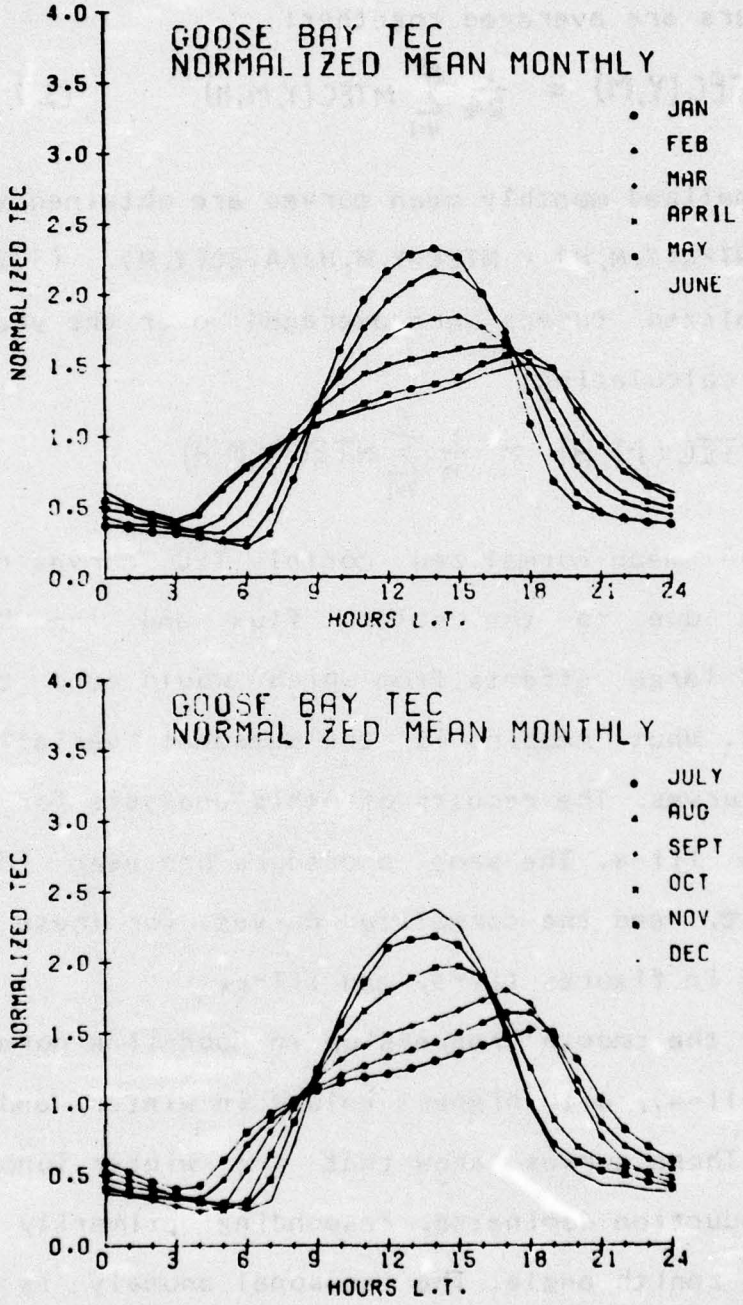

Figure III-4 Normalized mean monthly TEC diurnal curves

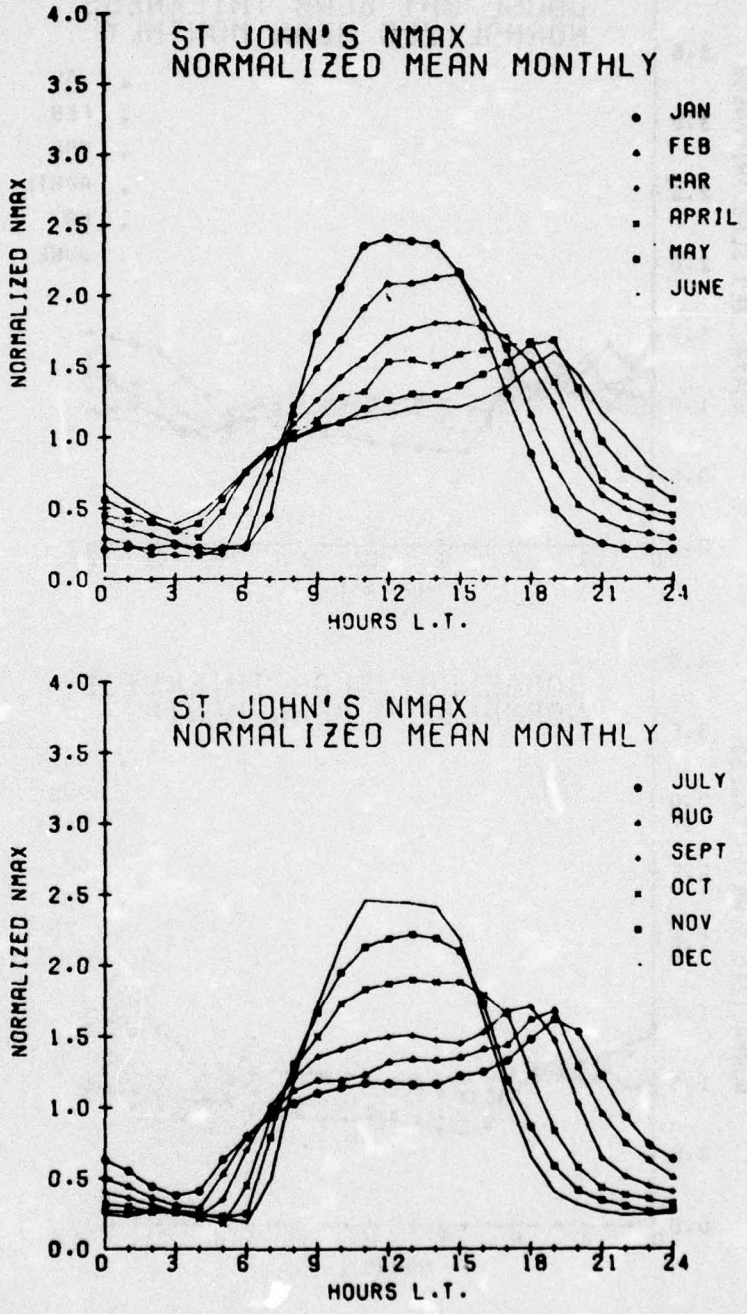

Figure III-5 Normalized mean monthly Nmax diurnal curves

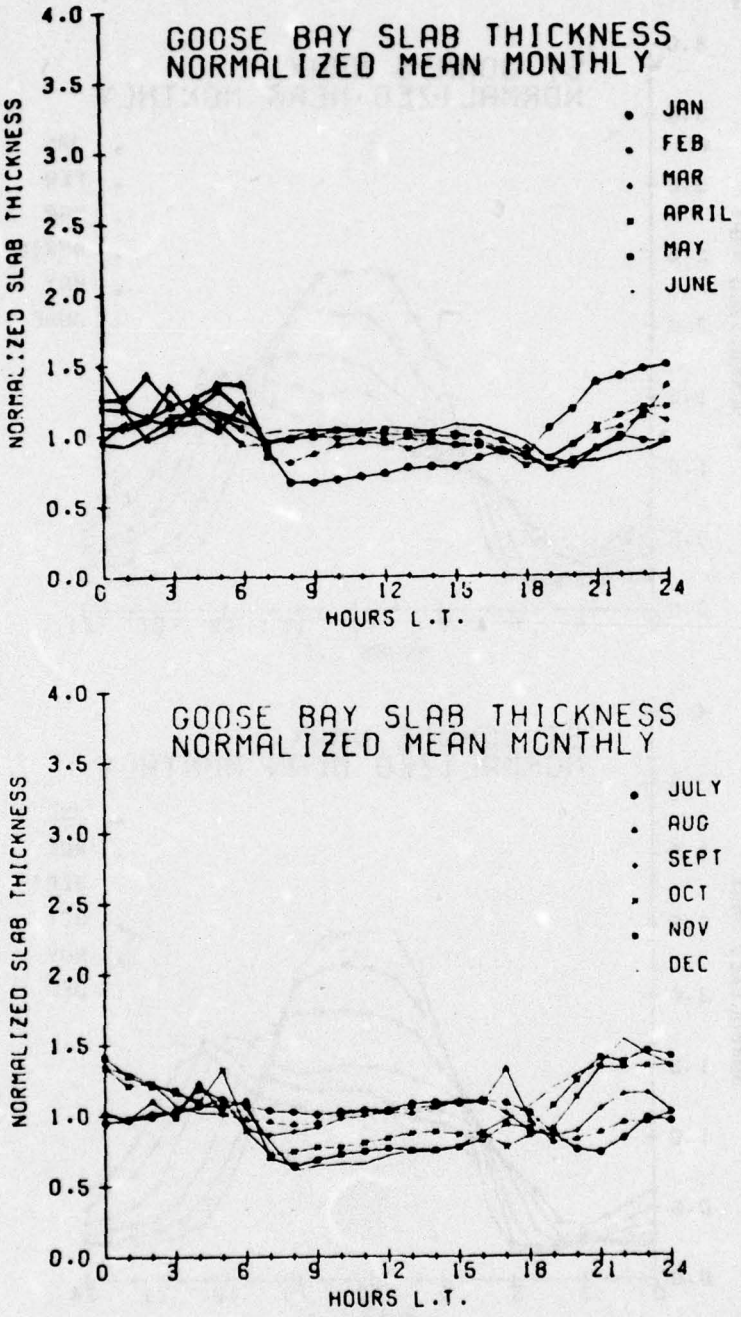

Figure III-6 Normalized mean monthly slab thickness diurnal curves

plotted in figures III-7 and III-8, respectively.

In figure III-8, curves for both Hamilton (from the Hawkins and Klobuchar study) and Goose Bay are provided. Notice how the smooth seasonal progression apparent for the maximum values in figure III-8 is not found in figure III-7. The minimum values follow a fairly regular progression in both figures. One thing of interest is the close correlation between the curves for Hamilton and Goose Bay in figure III-8.

Monthly conditions for the TEC observed from Goose Bay are presented in the form of a contour plot in figure III-9. This plot covers all 38 months of TEC data. Times of sunrise and sunset at the 420-km point are indicated by tics.

We will discuss the general features of ionospheric behavior at L=4 in the next section with reference to the curves already presented.

MAXIMUM AND MINIMUM MEAN MONTHLY TEC

GOOSE BAY (1971-1975)

MONTH	JAN	FEB	MAR	APR	MAY	JUN	JUL	AUG	SEP	OCT	NOV	DEC
DAY NO.	15	45	74	105	135	166	196	227	258	288	319	349
HIGHEST	16.3	18.6	17.5	15.4	17.9	16.4	15.2	14.7	16.5	18.7	16.5	17.1
LOWEST	1.6	2.3	3.1	3.3	4.4	4.6	4.0	3.0	2.2	2.4	2.1	1.9

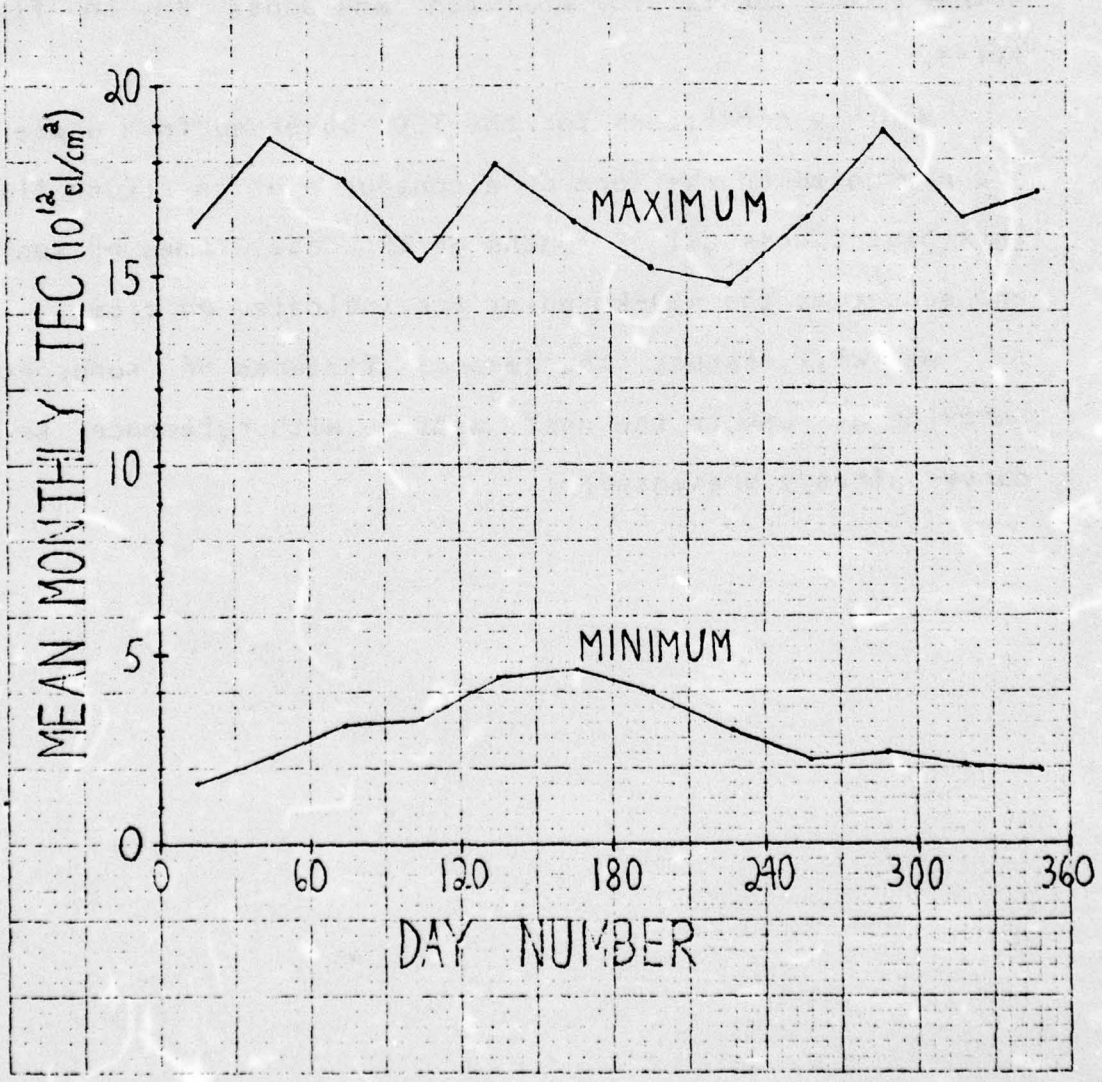

MAXIMUM AND MINIMUM MEAN MONTHLY NORMALIZED TEC

HAMILTON (1967-1973)*

MONTH	JAN	FEB	MAR	APR	MAY	JUN	JUL	AUG	SEP	OCT	NOV	DEC
DAY NO.	15	45	74	105	135	166	196	227	258	288	319	349
HIGHEST	2.10	1.96	1.77	1.56	1.50	1.42	1.44	1.49	1.62	1.92	2.05	2.10
LOWEST	.28	.30	.29	.35	.39	.42	.39	.32	.29	.25	.31	.33

GOOSE BAY (1971-1975)

HIGHEST	2.32	2.15	1.84	1.63	1.58	1.50	1.52	1.64	1.80	1.97	2.18	2.37
LOWEST	.22	.27	.32	.34	.39	.41	.40	.33	.29	.25	.28	.25

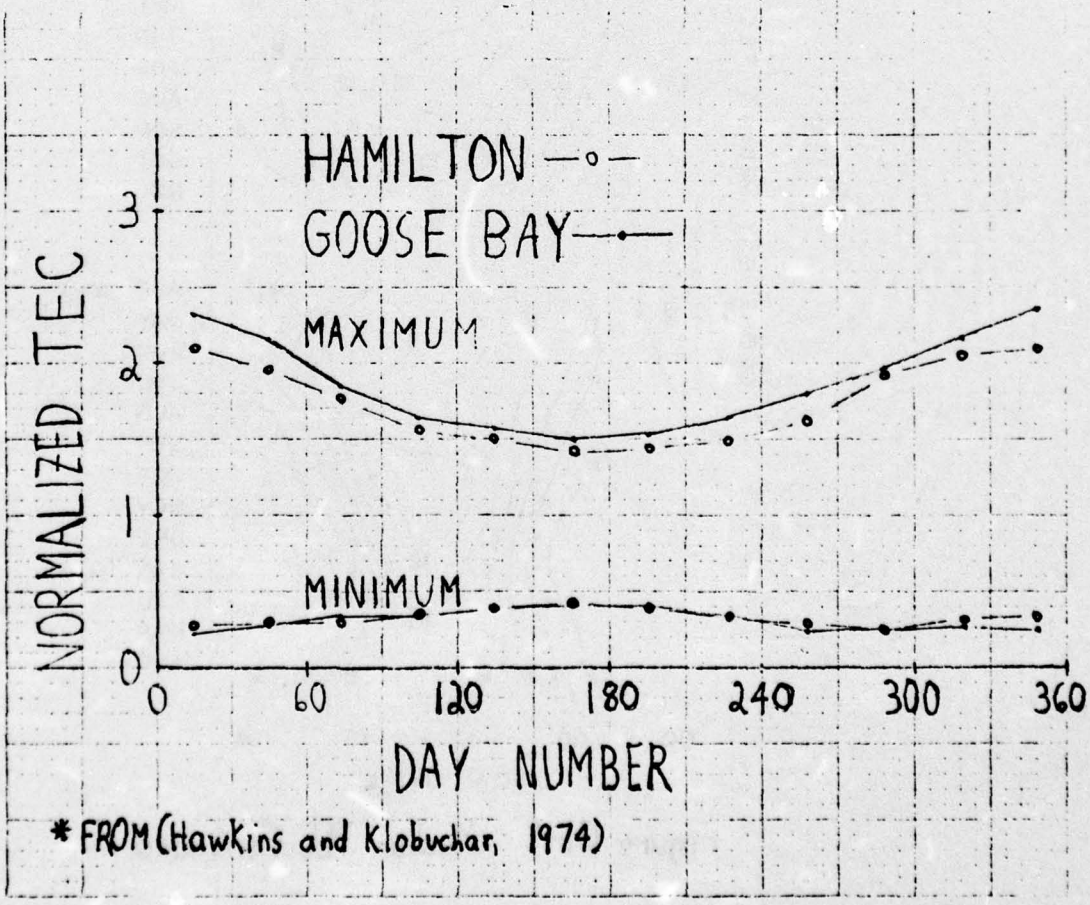

* FROM (Hawkins and Klobuchar, 1974)

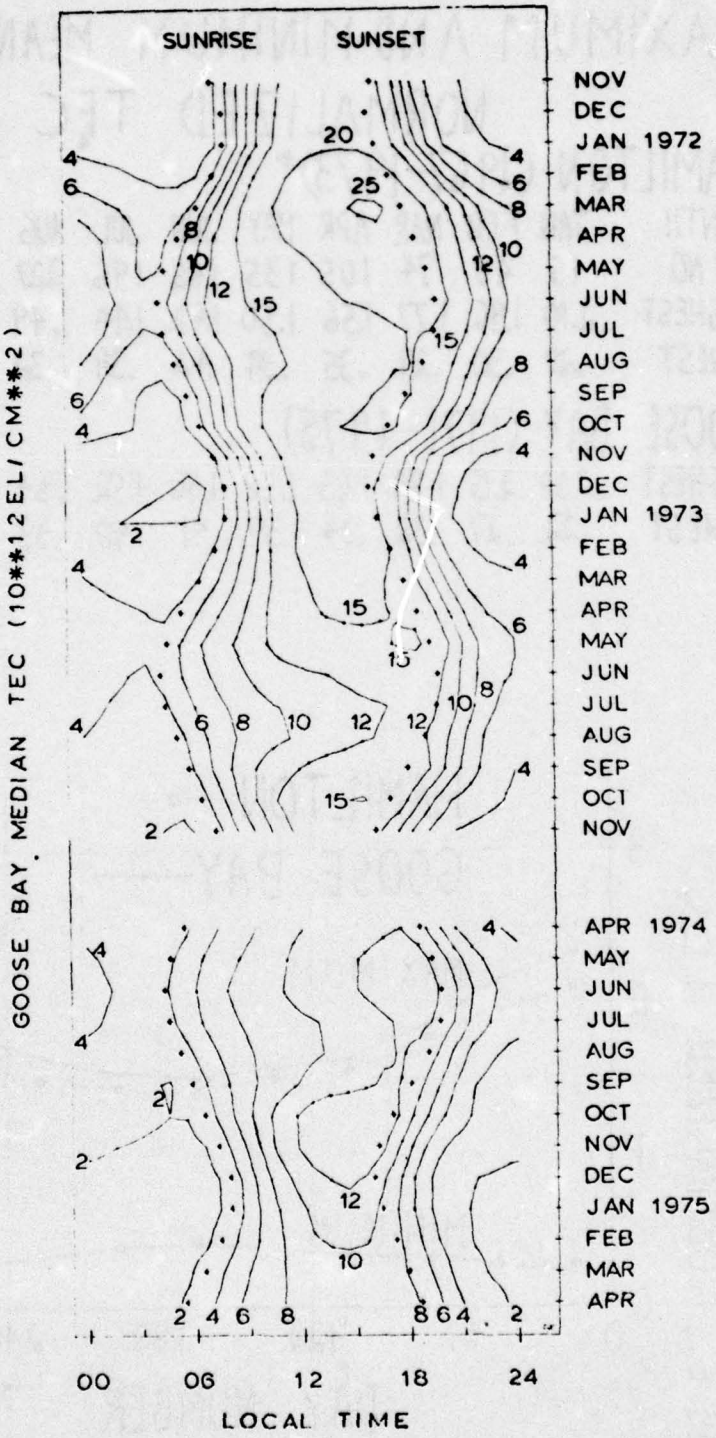

Figure III-9 Median TEC Contours

3.2 Discussion

We now wish to briefly discuss the general characteristics of the ionosphere as observed from Goose Bay (TEC measurements) and St. John's (Nmax results), and to compare these features with available midlatitude results.

Figure III-1 has shown that the general features of the mean monthly TEC at Goose Bay are the same as those at Hamilton, which Hawkins and Klobuchar (1974) described as follows:

> "a. A decay during the hours of darkness, prolonged and linear in summer months, more abrupt in winter with a low-level steady component in the latter part of the night.
> "b. An abrupt rise at dawn at approximately 0900UT, and
> "c. A daytime maximum in the p.m. hours with a growth and decay that approximates to a sinusoid in winter and a saw-tooth in summer."

Comparison of the mean curves at Goose Bay and Hamilton (figure III-1 here and figure 2 in Hawkins and Klobuchar's (1974) study), shows that for each month and each hour, mean monthly TEC observed at Goose Bay is less than that observed at Hamilton. This is to be expected from the greater solar zenith angle at all hours at the Goose Bay 420-km point compared to the Hamilton 420-km point, and from the higher sunspot number during the midlatitude study.

One also notices that the seasonal variation in maximum TEC seems to be less at Goose Bay than at Hamilton. Since the normalized curves (see especially figure III-8) show a

nearly identical seasonal variation, this effect must be due to the factors mentioned in the last section, viz., higher latitude and low sunspot number.

The evening anomaly, i.e., maximum values of TEC in summer months occurring during the early evening hours, is certainly present both in the Goose Bay and in the Hamilton data. In the Goose Bay results, maximum daily TEC occurred from May through August at 1800LT.

Since the (Hawkins and Klobuchar, 1974) study did not present Nmax and τ curves, we are unable to compare our results for St. John's Nmax with comparable results for Wallop's Island (or Ft. Belvoir), near the Hamilton 420-km point. We can notice, however, that the mean monthly Nmax curves seem to be similar in over-all shape to the mean monthly TEC curves. The seasonal anomaly (see sec. 1.1.4) is present, as is an evening anomaly. For the evening anomaly, we notice that maximum daily Nmax occurs at 1900LT from May through August.

While mean monthly mean τ curves, i.e., curves representing several years of data, are not available for mid-latitudes, Klobuchar and Allen (1970), presented monthly mean slab thickness diurnal curves for several months in 1968. From these curves it appears that, at midlatitudes, τ is lower at night except in winter. These curves also show that the highest noontime τ values occur in the summer months, with a steady progression from high values in summer

to low values in winter. This latter variation is also apparent in the mean monthly τ curves for Goose Bay and St. John's (figure III-3).

As in the case of midlatitudes, there is no clear monthly progression at night, although nighttime τ seems to be higher in winter than in summer. It appears that τ is higher at night for most of the year, contrary to the midlatitude results.

These results are in accord with our generalization that the electron density trough is more prominent in winter and at higher latitudes, because while Nmax will decrease to very low values in the trough, the Faraday rotation, which is accumulated along a long ray path passing through higher density regions to the south, will not decrease as much. Therefore, τ=TEC/Nmax will increase under trough conditions. Since electron densities increase along the ray path south of the vertical column, the Faraday rotation measures the total electron content of the vertical column to heights greater than 2000km during trough conditions. This is the same conclusion we reached in Chapter II through analysis of a model density gradient.

Let us now turn our attention to the normalized curves (figures III-4 to III-6). Figure III-4 for TEC should be compared with figure 8 in (Hawkins and Klobuchar, 1974). These sets of curves are remarkably similar. The seasonal progression of the curves is identical, showing a strong

seasonal anomaly for both sets. The close correlation between these two sets of curves has already been pointed out by reference to figure III-8, where the only significant difference seems to be a slightly greater maximum normalized TEC for all seasons at L=4 than at midlatitudes. This means there is a greater difference between daytime and nighttime TEC, which is apparently due to very low values at night associated with the electron density trough in the Goose Bay data.

The normalized Nmax curves (figure III-5) show a very striking seasonal anomaly, more prominent than that found for the mean monthly Nmax (figure III-2).

The normalized slab thickness curves (figure III-6) show less variation from month to month than the mean monthly τ curves, but otherwise show basically the same seasonal progression, with lowest daytime τ in the winter and greatest nighttime τ in that season.

In the contour plot of monthly median TEC (figure III-9), which covers all 38 months of data, we can clearly note several of the effects previously mentioned. An "equinoctal anomaly" is present, as seen by the high daytime values in March and October, 1972, October, 1973, and October, 1974. There is unquestionably a strong variation from year to year. Compare, for example, March, 1972, 1973, and 1975. The maximum daytime value in March, 1972 is over 26×10^{12} el/cm^2. In March, 1973, it falls to about 17×10^{12},

and in March, 1975, it has reached as low as 9×10^{12}. The unfortunate four month gap in the data prevents us from comparing a March, 1974 value with the values for the other three years. This yearly variation is clearly due to changes in solar flux. The mean value of the observed solar flux at 2800MHz prepared by Ottawa is 128.5 in March, 1972, but only 72.4 in March, 1975. As 1975 is near the low point of the solar cycle, the rate of production of electrons is very low at that time. Other things to notice are the higher nighttime values of TEC in summer, and the presence of the evening anomaly in that season (maximum values in the early evening).

3.3 Conclusions

The ionosphere at L=4 shows many similarities with the midlatitude ionosphere. Comparison of Goose Bay TEC (refering to L=4) for the period 1971-1975 with Hamilton TEC (refering to L=2.8) for the period 1967-1973 revealed that the Goose Bay data showed lower TEC on the average for all seasons and times of day. This is due to two factors: the larger solar zenith angle at all times at L=4 in comparison with L=2.8, and the fact that the years of the Hamilton study were years of higher sunspot number than the years of the Goose Bay data. The other differences between the two data sets are not as striking and can all, it seems, be traced to the presence of the electron density trough at L=4, most prominent during winter nights.

CHAPTER IV

DISTORTIONS OF THE WINTER NIGHTTIME IONOSPHERE NEAR L=4

4.1 Nighttime Slab Thickness Decreases Observed from Goose Bay during December, 1971

As discussed in the previous chapter, total electron content obtained at Goose Bay, Labrador may be combined with simultaneous peak density observations at St. John's, Newfoundland to measure the "equivalent slab thickness" of the ionosphere above St. John's. Many nights during December, 1971 exhibited appreciable decreases in slab thickness (τ=TEC/Nmax). Specifically, there were increases in Nmax on these nights accompanied by constant or decreasing TEC.

As in the previous chapter, the term "TEC," will refer to the equivalent vertical TEC through the 420-km point, i.e., TEC obtained from Ω and the constant $\bar{M}$ value at 420km height along the ray path. Thus the terms "TEC" and "Faraday rotation" (or "Ω"), may be used interchangeably.

In figure IV-1 Nmax and TEC have been plotted vs. Universal Time for five nights during which the increasing Nmax-constant TEC effect mentioned above occurred. Note that local midnight occurs at St. John's at 3:31 UT, and at 4:01 UT at Goose Bay. The Kp index also has been plotted. Note that with the exception of December 9, the increase in Nmax is not associated with an increase in magnetic activity according to the Kp index. The AE index and H at Narssarssuaq ($61^{\circ}.2$N, $45^{\circ}.4$W) are plotted in addition to the

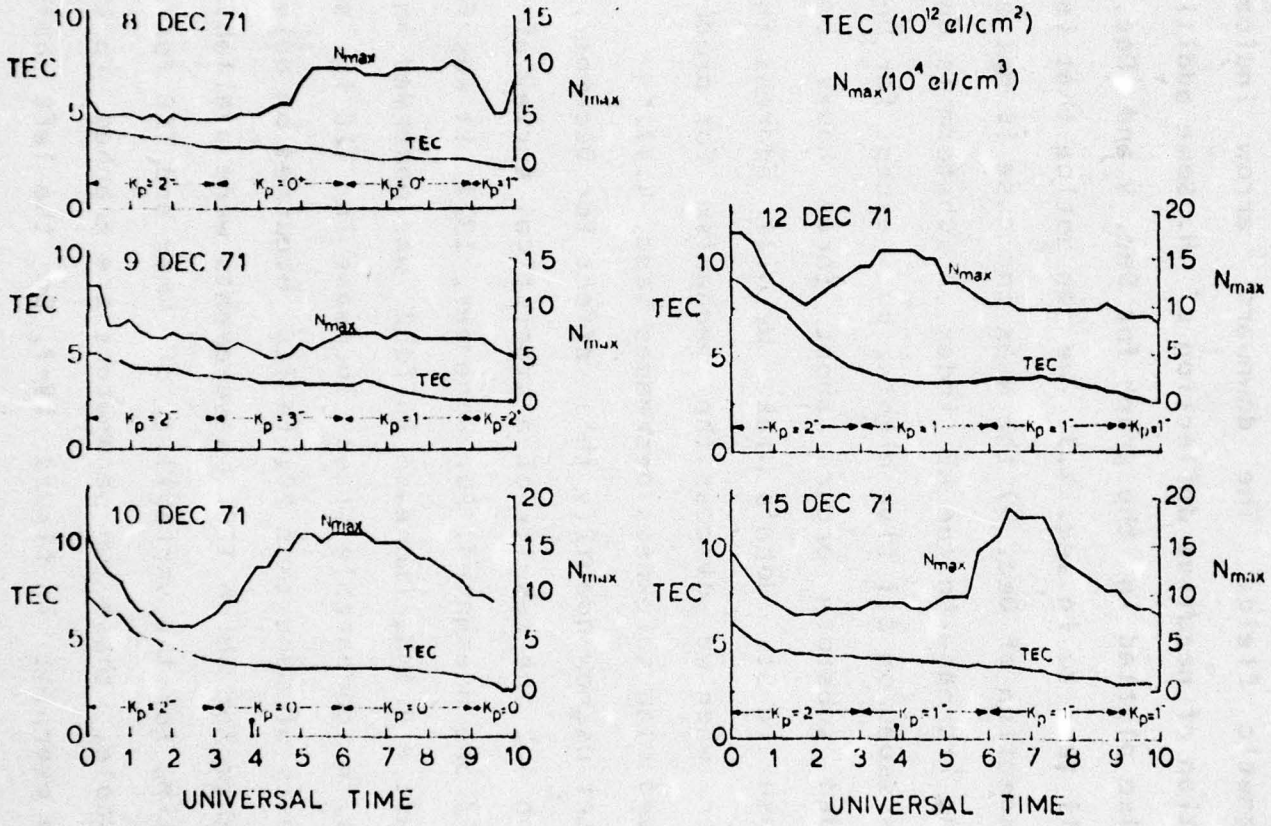

Figure IV-1 Nmax and TEC for five nights when the increasing Nmax-constant TEC effect occurred

above three parameters for the same five days in figures IV-2 to IV-6. H is the horizontal component of the geomagnetic field. The downward arrow indicates the direction of negative deflection of H. Some additional data are also plotted in the graph for Dec. 9 and Dec. 15 which we will turn to in sec. 4.3. We can notice that (again with the exception of Dec. 9) the Nmax increase is not associated with an increase in the AE index. A substorm is observed at Narssarssuaq on all five nights, but except for Dec. 9, the recorded substorm occurs about three hours before the increase in St. John's Nmax. We will address this topic further when we discuss the mechanism for producing the observed slab thickness decreases (sec. 4.4).

Let us now quantify this effect for December, 1971. In section 4.2 the results of a statistical survey of increases in foF2 are presented. For December, 1971, it was found that at least a 0.3MHz increase in foF2 was observed on 21 of 25 nights. A comparable sized increase in TEC is about 20%. Increases of more than 20% in TEC occurred on only 8 out of 27 nights for which TEC measurements were available. To get a feeling for the variability of Nmax and TEC for the month as a whole, these two parameters are graphed in the format of an overplot in figure IV-7. On the left half of the figure, the two parameters are plotted for all of the days for which data were available. To the right, ten of the days on which substantial increases in Nmax were observed are

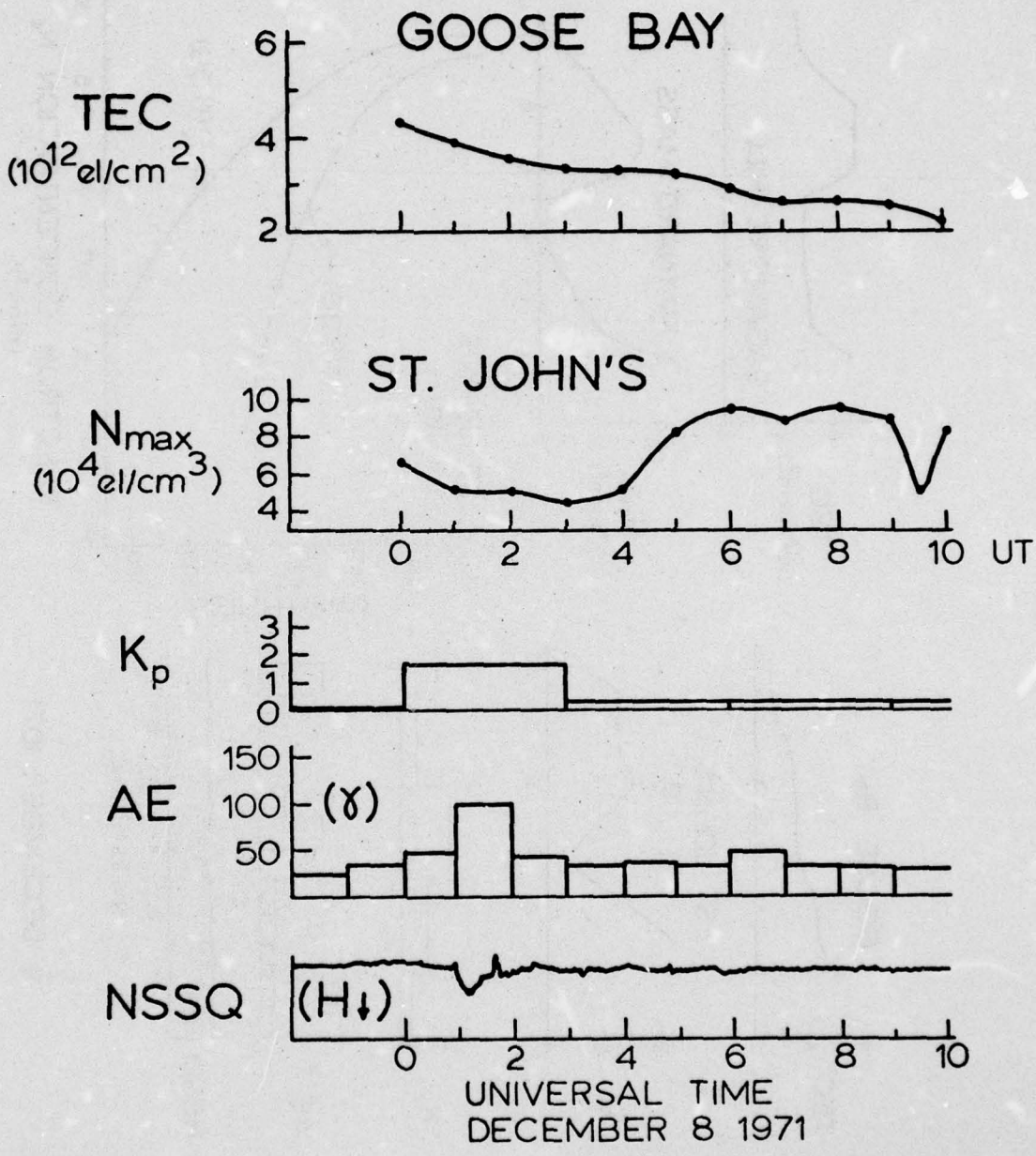

Figure IV-2 Several parameters plotted for the night of December 8, 1971

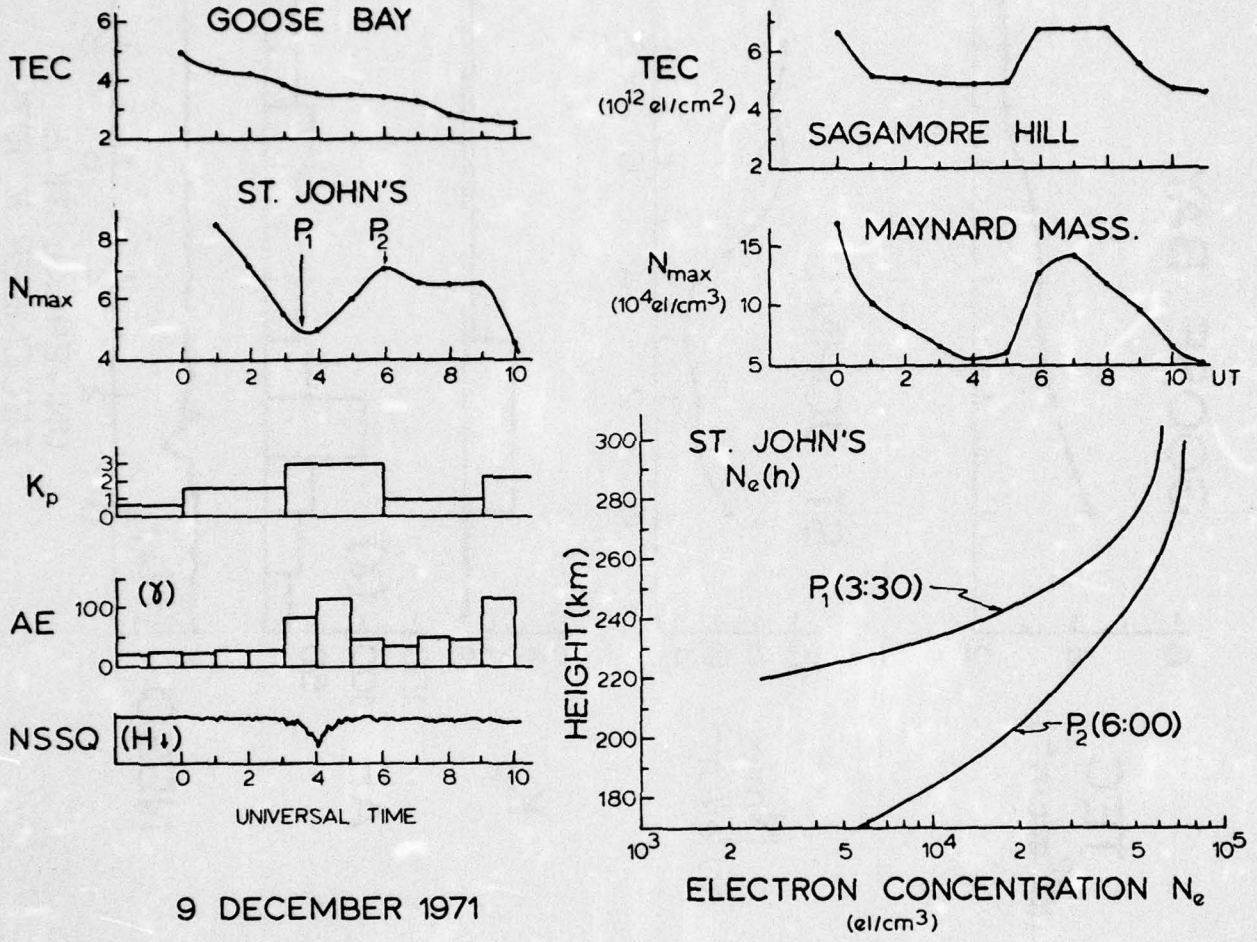

Figure IV-3 Several parameters plotted for the night of December 9, 1971

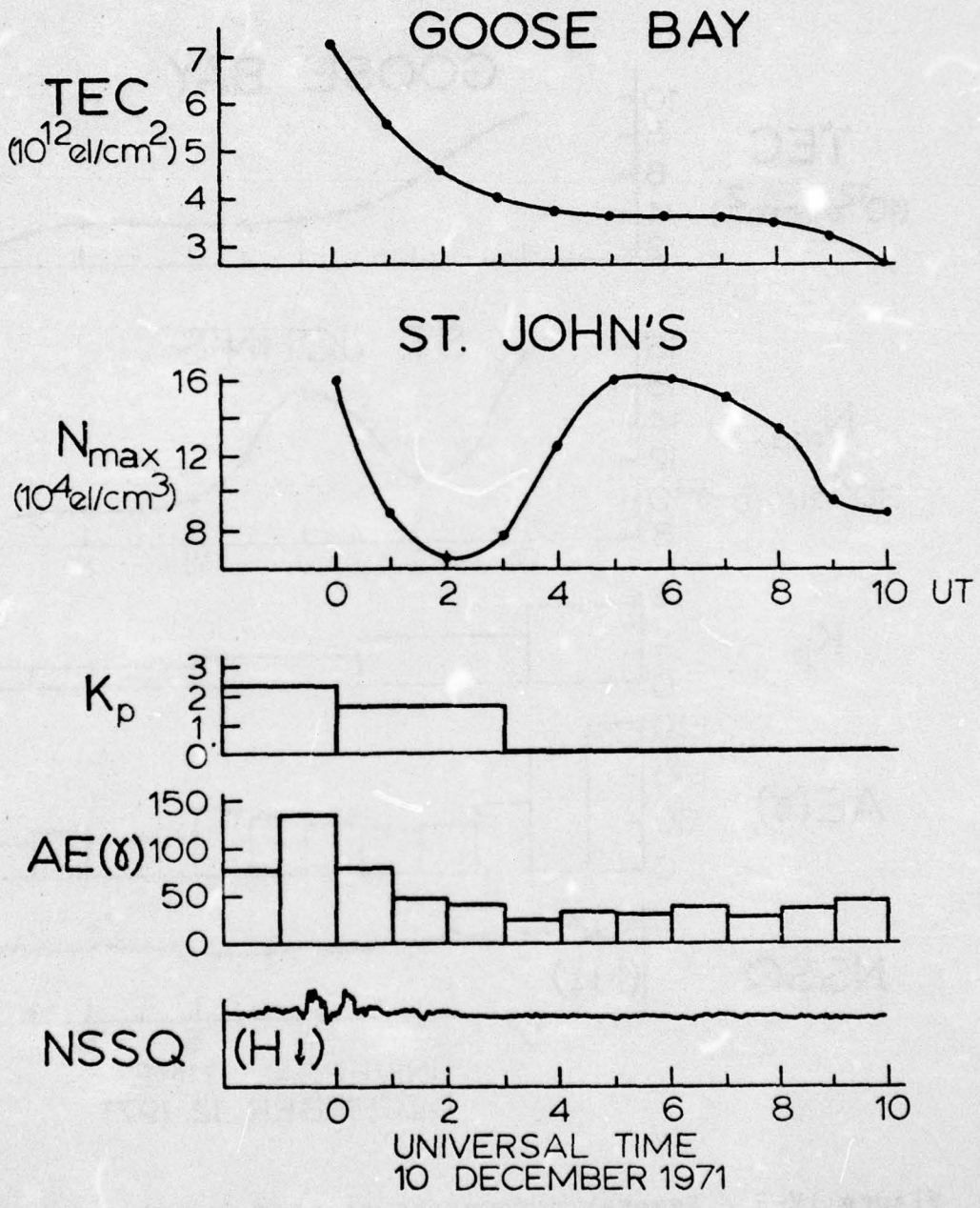

Figure IV-4 Several parameters plotted for the night of December 10, 1971

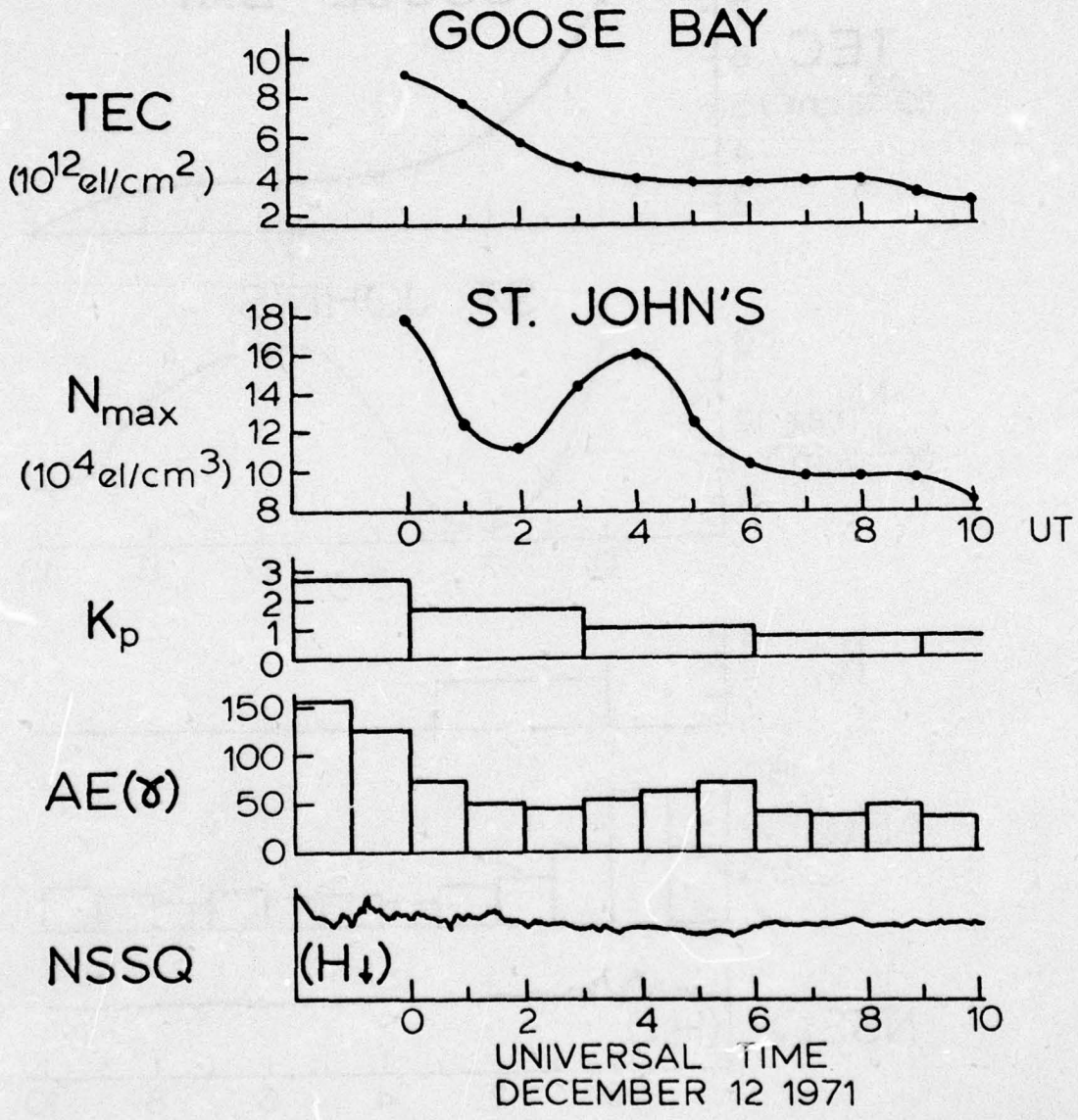

Figure IV-5 Several parameters plotted for the night of December 12, 1971

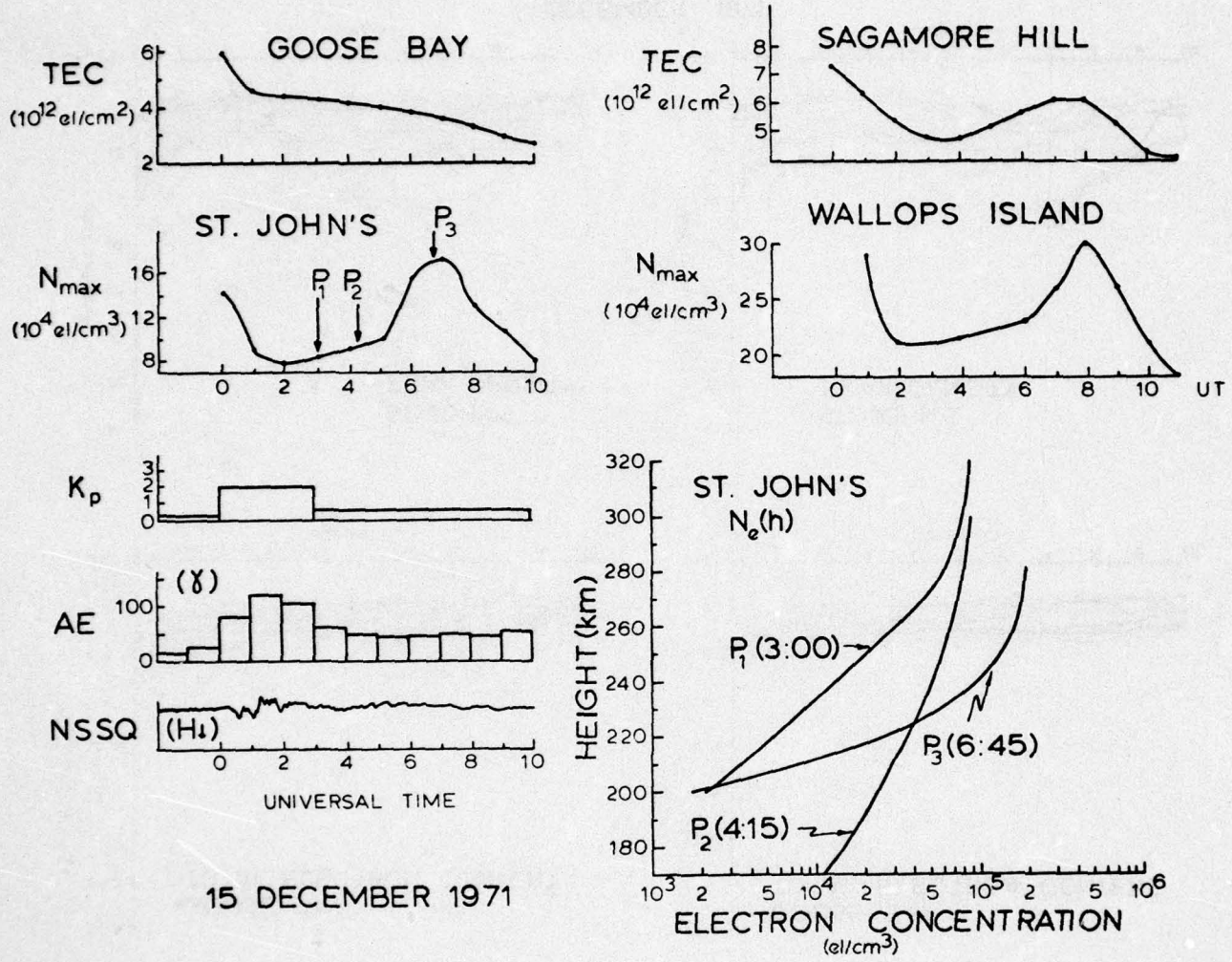

Figure IV-6 Several parameters plotted for the night of December 15, 1971

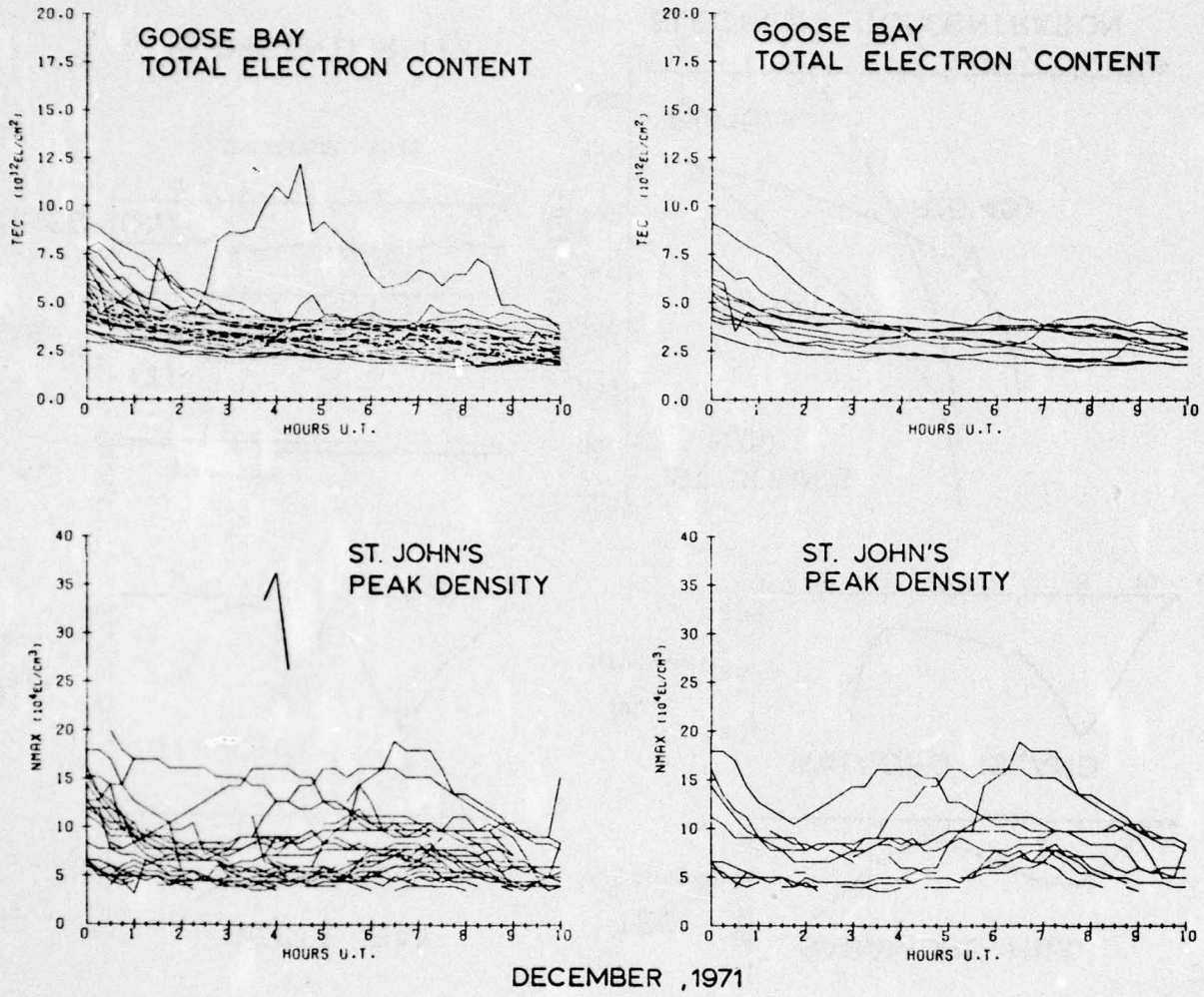

Figure IV-7 Overplots of Nmax and TEC for December, 1971

plotted. For the monthly overplot, the data collected during the great magnetic storm of Dec. 17 stand out sharply from the other data as the only night on which TEC rose above 10^{13} el/cm^2 and Nmax rose above 3×10^5 el/cm^3. With the exception of this day, an "envelope" drawn around the plots would extend from about 2.5 to 5.0 for TEC and from about 5 to 15 for Nmax (in the units shown). This demonstrates the significantly greater variability of peak density compared with TEC at L=4 during winter nighttime conditions.

AD-A035 940 BOSTON UNIV MASS DEPT OF ASTRONOMY F/G 4/1
THE IONOSPHERIC F-REGION NEAR 60 DEG MAGNETIC LATITUDE: MONTHLY--ETC(U)
SEP 76 M MENDILLO, M BUONSANTO F19628-75-C-0044
UNCLASSIFIED SER-II-NO-61 AFGL-TR-76-0233 NL

2 OF 2
AD
A035940

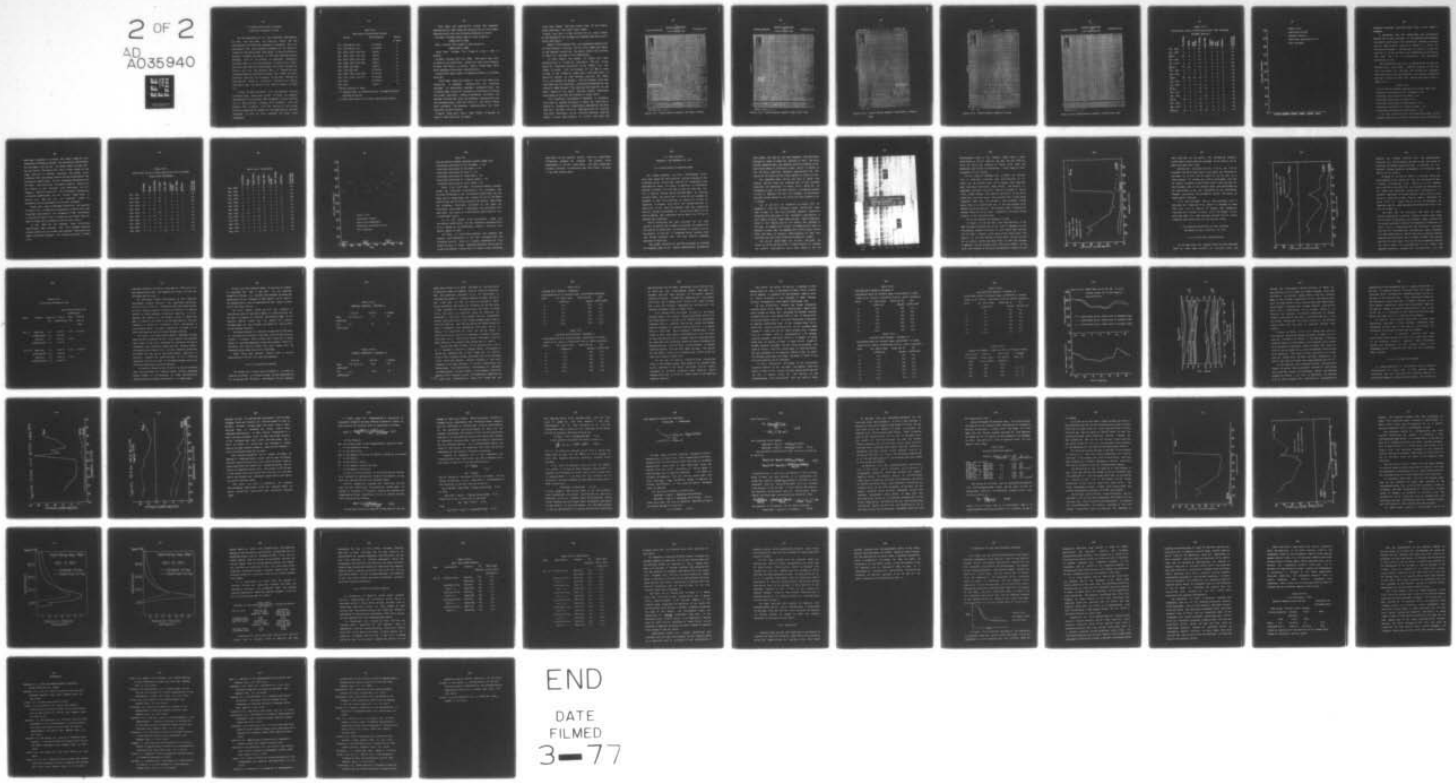

END

DATE
FILMED
3-77

4.2 Statistical Survey of Winter Nighttime Increases in foF2

For the determination of slab thickness, measurements of both TEC and Nmax are required. Since the TEC observations from Goose Bay commenced in November, 1971, our knowiedge of the slab thickness parameter at St. John's is limited to the period after that month. It would be foolish, however, to ignore the wealth of foF2 data available before November, 1971, in our attempt to understand ionospheric processes near L=4. We have gathered 24 years of St. John's foF2 data from the *World Data Center A for Solar Terrestrial* Physics and from the Canadian Dept. of Communications, Telecommunications Engineering Branch. The months for which data were analyzed, the frequency of the data (whether we obtained foF2 values at 15 minute, half-hourly or hourly intervals), and the source of the data are given in Table IV-1.

As can be seen from Table IV-1, the December data we collected spans three solar cycles. To check the seasonal dependence of the nocturnal foF2 increases, we also examined two six month periods, October, 1971 to March, 1972, and October, 1972 to March, 1973. The results of this survey provide a quantitative summary of the magnitude of the foF2 increases, as well as their seasonal and solar cycle dependence.

Table IV-1

Data Used in Statistical Survey

Period	Data Interval	Source of Data
Oct. 1971-March, 1972	15 minute	C
Oct. 1972-March, 1973	15 minute	C
Dec. 1945, 1947, and 1948	hourly	W
Dec. 1950, 1951, and 1953	hourly	W
Dec. 1957, 1958, and 1959	hourly	W
Dec. 1960, 1961, and 1962	hourly	W
Dec. 1963, and 1964	hourly	W
Dec. 1965 and 1966	30 minute	C
Dec. 1967, 1968, and 1969	15 minute	C
Dec. 1970, 1971, and 1972	15 minute	C
Dec. 1973	15 minute	C
Dec. 1974	hourly	C

Code for sources of data:

C = Canadian Dept. of Communications, Telecommunications Engineering Branch

W = World Data Center A for Solar Terrestrial Physics

Each night was examined for primary and secondary characteristics. Each night was assigned one of five primary characteristics with the following selection criteria:

low bump: increase from trough to crest given by:

$$.3\text{MHz} \leq \Delta\text{foF2} \leq .5\text{MHz}$$

bump: increase from trough to crest given by:

$$.6\text{MHz} \leq \Delta\text{foF2} \leq .9\text{MHz}$$

large bump: increase from trough to crest 1 MHz or greater.

no bump: increase less than .3MHz, less than 1 hour long or based on one data point, except for cases with frequency of data half hourly or hourly, when a single data point could determine the primary characteristic.

Insufficient data: unable to determine whether an increase occurred.

After each night was placed in one of the above five categories, a secondary characteristic was sometimes assigned. In determining secondary characteristics, the criterion that it must be possible to judiciously eliminate any single data point without eliminating the effect was applied. Failing this test, the secondary characteristic was not assigned except when only hourly or half hourly values were available. The secondary characteristics and their selection criteria follow:

Irregular bump: more than 1 peak. Trough in between at least 0.3 MHz below the two peaks.

short bump: "bump" less than 3 hours long (if only hourly values available, less than 4 hours long).

plateau: less than 0.1 MHz variation for at least 3 hours at the maximum of the increase (no plateaus when only hourly values available).

Pages of the Canadian data are reproduced showing each of these effects in figures IV-8 to IV-12. Numerical Tables of the seasonal results and the yearly results are provided as Table IV-II and Table IV-IV respectively.

In both tables, the number of nights with each characteristic is listed for each month. The last column gives the fractional occurrence of the effect, i.e., the number of nights with an increase of 0.3 MHz or more divided by the number of nights with sufficient data to determine whether an foF2 increase occurred. For Table IV-II, the numbers for October, 1971 and October, 1972 have been added and the fractional occurrence determined for the composite "mean October." The same has been done for all the other months in the table. The mean monthly fractional occurrences of the foF2 are plotted in figure IV-13.

The fractional occurrence in December is greatest, while that in October and March is least. The sharp dip in January is probably not significant, considering the fact that only two years' worth of data were used. In spite of this small data base, we can initially conclude that the effect we have been studying is a winter one, with the

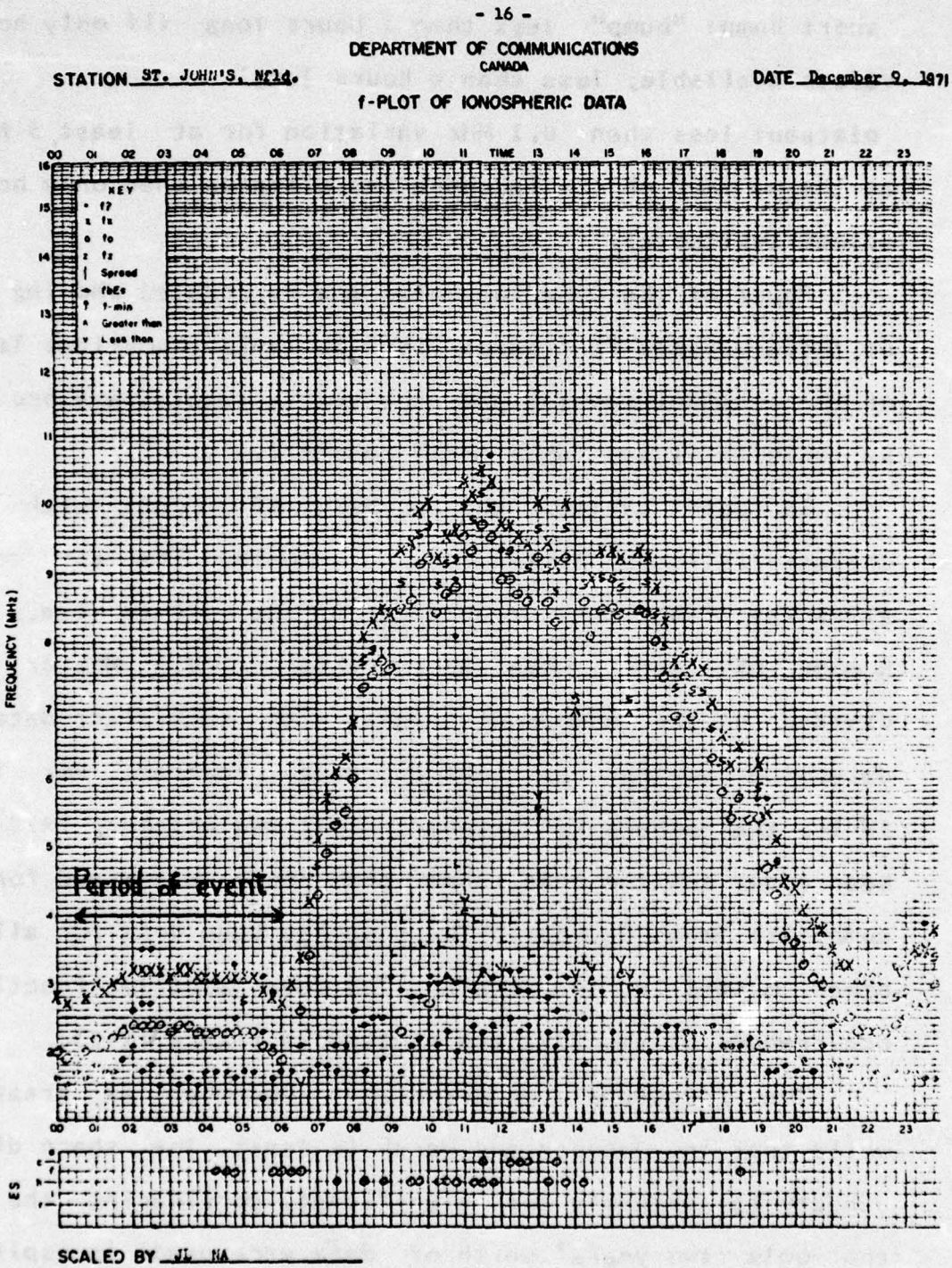

Figure IV-8 Classification example: low bump, plateau

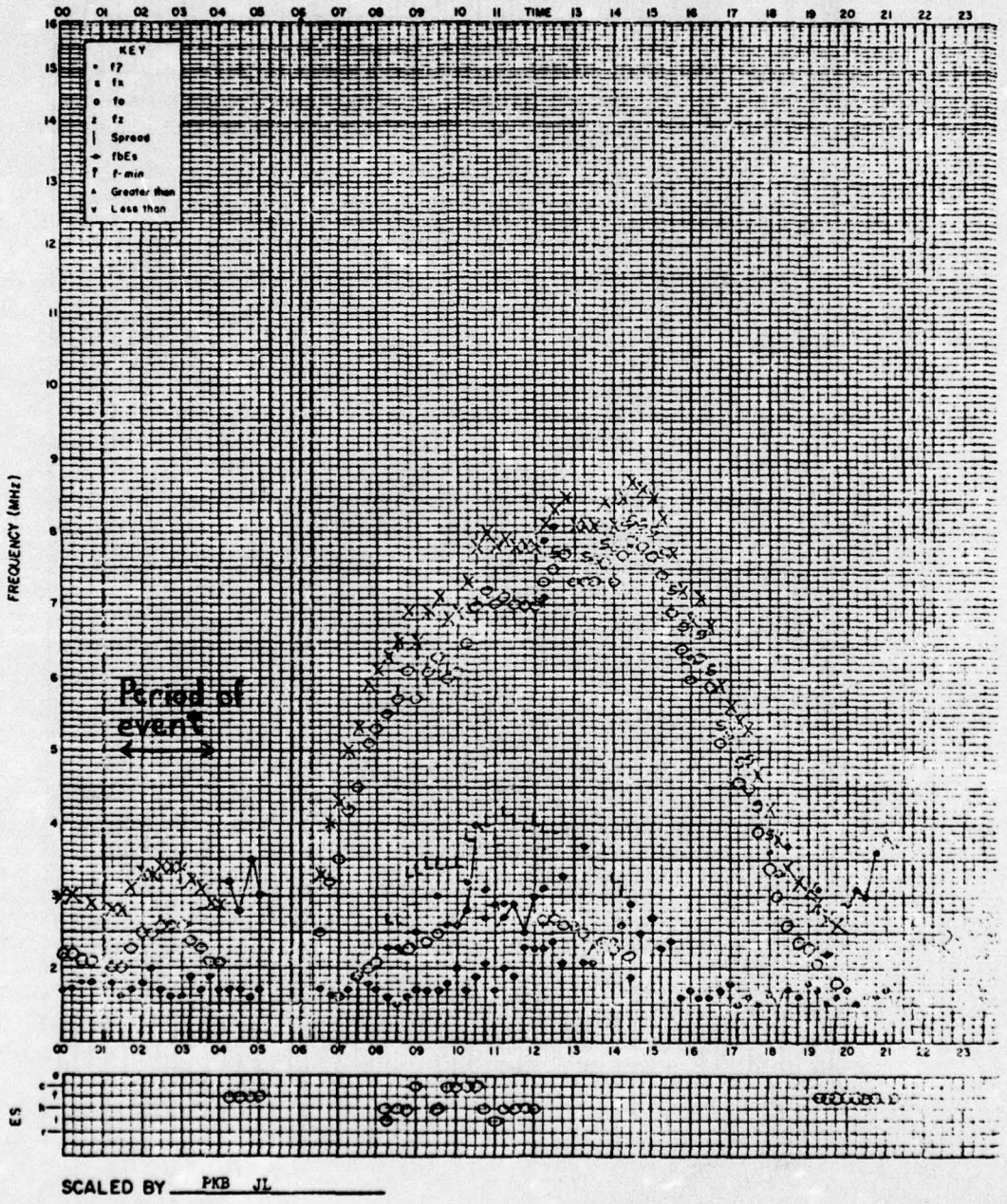

Figure IV-9 Classification example: bump, short bump

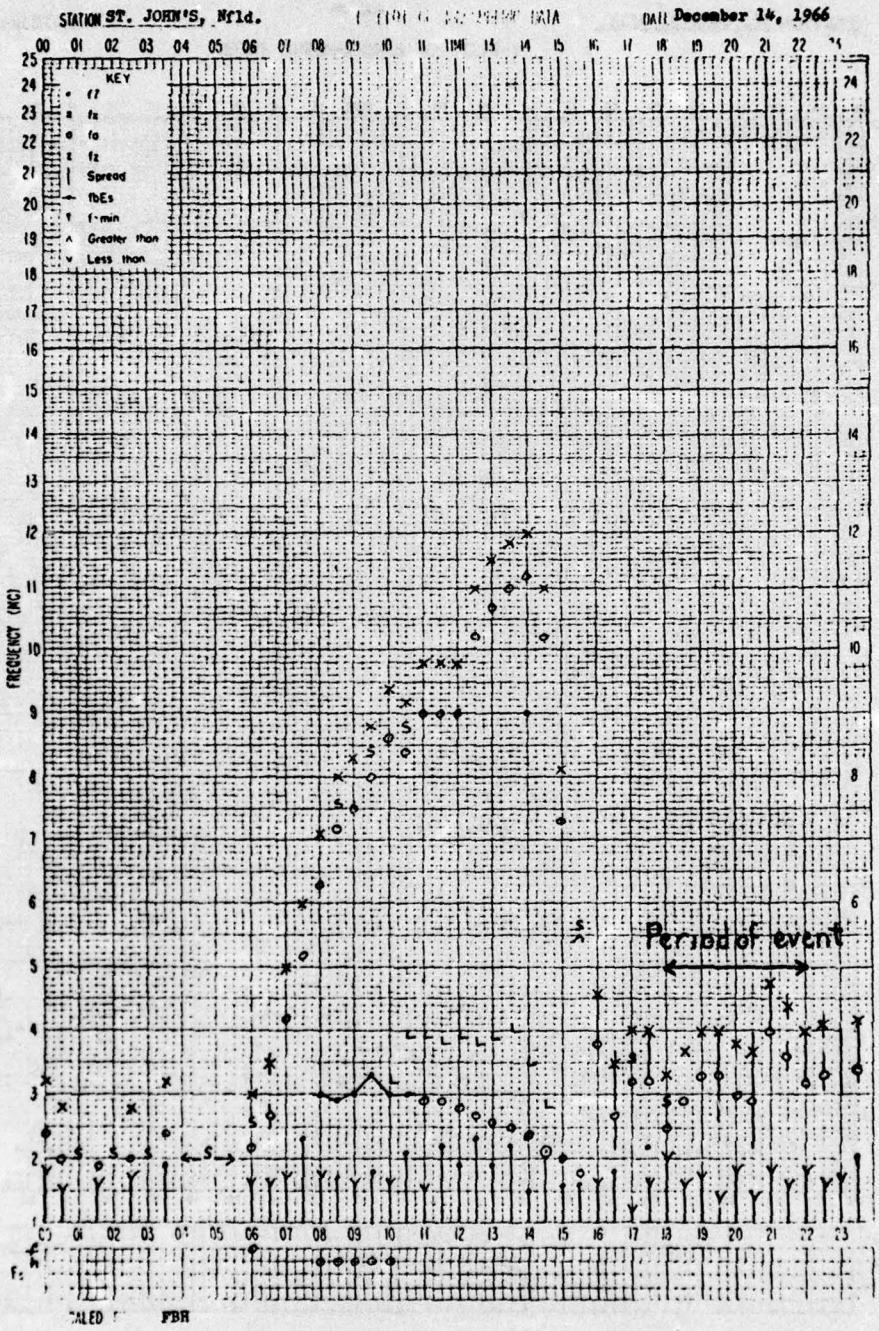

Figure IV-10 Classification example: large bump, irregular bump

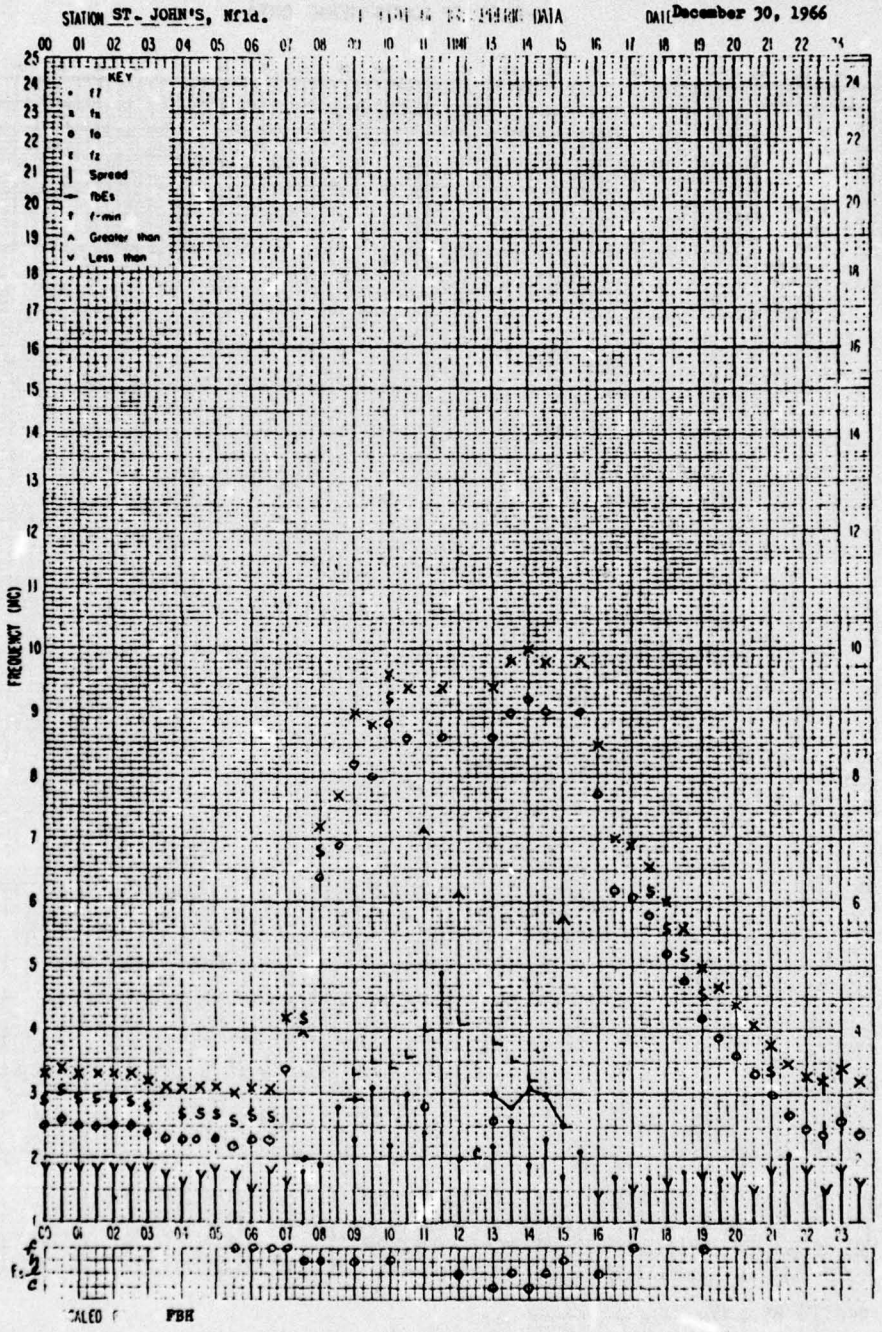

Figure IV-11 Classification example: no bump

DEPARTMENT OF COMMUNICATIONS
CANADA

STATION ST. JOHN'S, Nfld

DATE December 26, 1971

f-PLOT OF IONOSPHERIC DATA

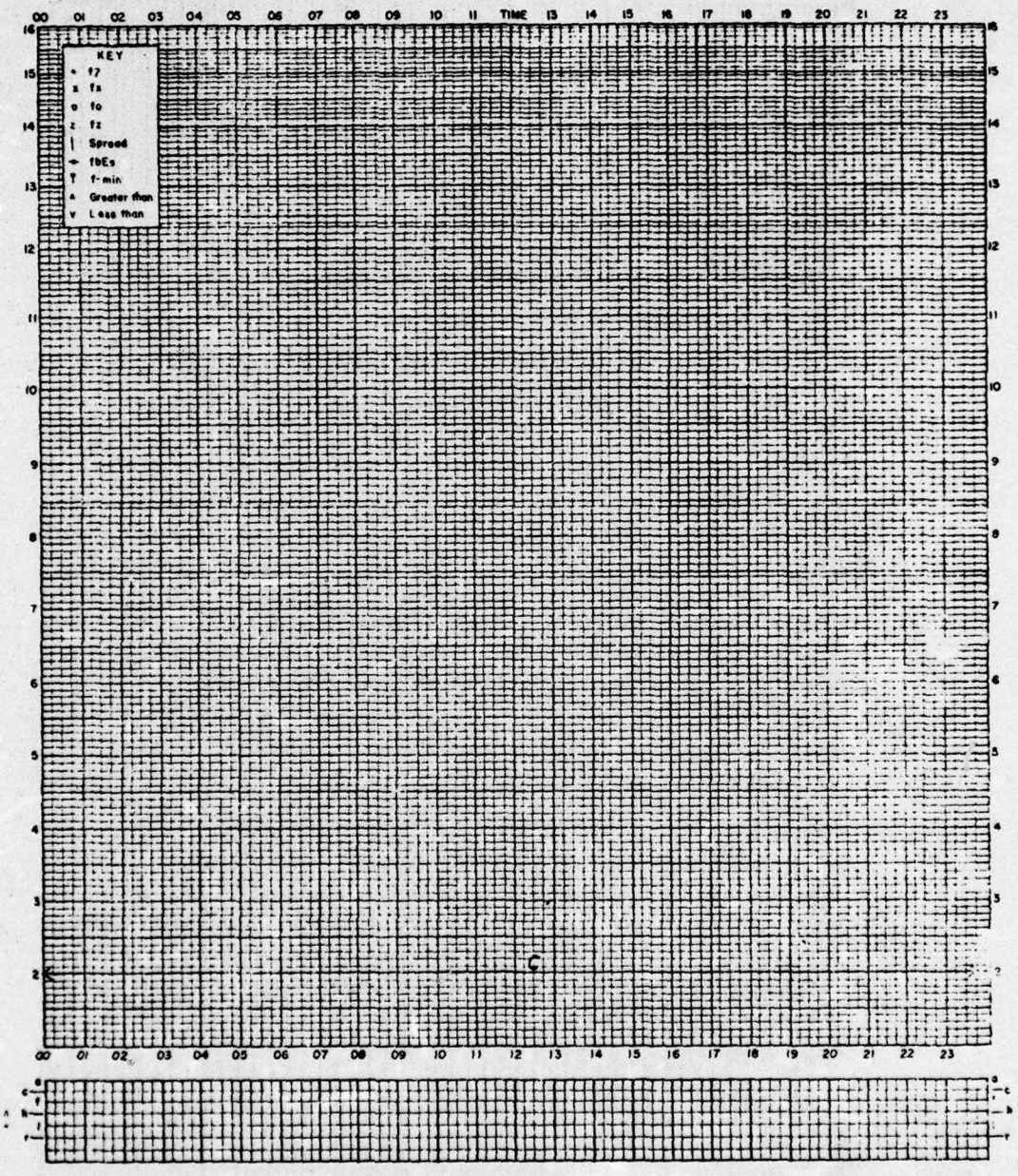

SCALED BY JL

Figure IV-12 Classification example: insufficient data

Table IV-II

Statistical Survey of Nocturnal Winter foF2 Increases

SEASONAL ANALYSIS

	low bumps	bumps	large bumps	no bumps	insuf. data	irregular bumps	short bumps	plateaus	fractional occurrence
Oct. 1971	7	2	2	20	0	2	2	0	.35
Oct. 1972	6	4	2	17	2	1	1	0	.41
$\sum$ Oct.	13	6	4	37	2	3	3	0	.38
Nov. 1971	7	8	1	10	4	5	1	0	.62
Nov. 1972	6	8	3	8	5	4	1	0	.68
$\sum$ Nov.	13	16	4	18	9	9	2	0	.65
Dec. 1971	8	7	6	4	6	3	3	1	.84
Dec. 1972	7	7	5	6	6	2	1	0	.76
$\sum$ Dec.	15	14	11	10	12	5	4	1	.80
Jan. 1972	3	8	4	8	8	0	1	0	.65
Jan. 1973	5	1	0	12	13	1	1	0	.33
$\sum$ Jan.	8	9	4	20	21	1	2	0	.51
Feb. 1972	7	5	1	11	4	1	1	0	.51
Feb. 1973	6	4	2	6	10	2	1	0	.67
$\sum$ Feb.	13	9	3	17	14	3	2	0	.60
Mar. 1972	5	2	0	20	4	2	2	0	.26
Mar. 1973	5	0	0	20	6	1	2	0	.20
$\sum$ March	10	2	0	40	10	3	4	0	.23

Figure IV-13
Statistical Survey
Seasonal Analysis
Fractional occurrence of all
foF2 increases

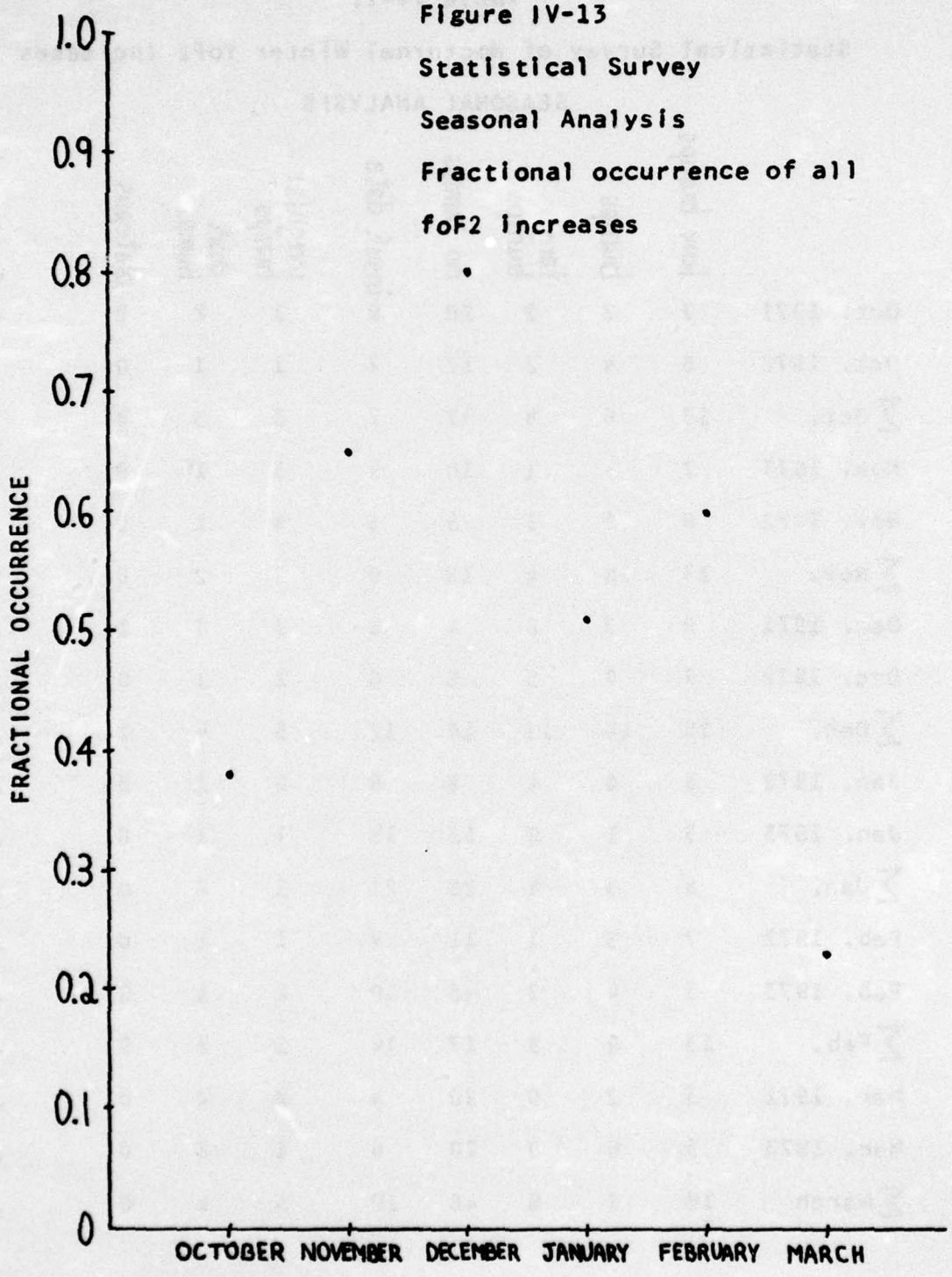

greatest fractional occurrence most likely to be found in December.

A convenient tool for quantifying the correlation between two or more variables is the Pearson Product-Moment correlation coefficient. The correlation between a variable and the same variable using this method is 1, while the correlation between a variable and its inverse (x and 1/x) would be -1. If two variables are independent of one another such that there is no correlation, the correlation coefficient is zero.

This method has been used to determine the correlation between solar zenith angle (angular distance of the Sun from the zenith) at noon and the primary and secondary characteristics (with the exception of plateaus, because of the small number of them). The results are given below in Table IV-III.

Table IV-III

The correlation between noontime solar zenith angle and:

fractional occurrence of all increases = .88

fractional occurrence of low bumps = .46

fractional occurrence of bumps = .91

fractional occurrence of large bumps = .83

fractional occurrence of irregular bumps = .27

fractional occurrence of short bumps = -.21

The high correlation for fractional occurrence of all increases confirms our initial conclusion that the effect we

have been studying is a winter one. There seems to be a significant difference between the correlation coefficients for low bumps (.46) and for the larger bumps (.91 and .83). One can notice from Table IV-II that a large number of low bumps occurred in October, February, and March, while relatively few large bumps occurred during those months. The correlation coefficients for the secondary characteristics are small, and since they represent a smaller fraction of the nights, we must discount their importance. We will suggest a possible reason for this difference between the correlation coefficients for the low and larger bumps in section 4.4, when we turn our attention toward an explanation of the mechanism for the foF2 increases.

Twenty four years of December statistics are compiled in Table IV-IV. In addition to appearing in Table IV-IV, the fractional occurrence of all increases 0.3 MHz and greater is plotted in figure IV-14. A glance at this figure does not seem to reveal any correlation with the solar cycle.

As was done for the seasonal case, correlation coefficients were computed, this time between observed sunspot number and the primary and secondary characteristics (again excluding plateaus). The results are given in Table IV-V.

Table IV-IV

Statistical Survey of Nocturnal Winter foF2 Increases

SOLAR CYCLE DEPENDENCE

	low bumps	bumps	large bumps	no bumps	insuf. data	irregular bumps	short bumps	plateaus	fractional occurrence
Dec. 1945	7	4	9	4	7	1	3	-	.83
Dec. 1947	8	6	5	11	1	1	7	-	.63
Dec. 1948	9	4	6	10	2	1	2	-	.66
Dec. 1950	12	6	0	6	7	2	5	-	.75
Dec. 1951	8	3	10	7	3	7	2	-	.75
Dec. 1953	13	3	1	10	4	0	1	-	.63
Dec. 1957	4	5	15	5	2	2	3	-	.83
Dec. 1958	9	6	6	8	2	22	5	-	.72
Dec. 1959	3	7	9	11	1	3	0	-	.63
Dec. 1960	9	1	6	9	6	2	4	-	.64
Dec. 1961	6	6	2	4	13	0	0	-	.78

Table IV-IV (continued)

	low bumps	bumps	large bumps	no bumps	insuf. data	irregular bumps	short bumps	plateaus	fractional occurrence
Dec. 1962	5	2	0	7	17	0	0	-	.50
Dec. 1963	2	1	1	2	25	1	0	-	.67
Dec. 1964	9	7	1	8	6	0	2	-	.68
Dec. 1965	8	9	1	3	10	2	2	0	.86
Dec. 1966	8	7	4	7	5	2	0	0	.73
Dec. 1967	5	7	7	7	5	1	2	1	.73
Dec. 1968	9	4	4	13	1	1	0	3	.57
Dec. 1969	5	10	7	9	0	2	0	0	.71
Dec. 1970	15	1	4	10	1	5	0	0	.67
Dec. 1971	8	7	6	4	6	3	3	1	.84
Dec. 1972	7	7	5	6	6	2	1	0	.76
Dec. 1973	6	7	4	2	12	7	1	2	.89
Dec. 1974	4	4	2	3	18	0	1	0	.77

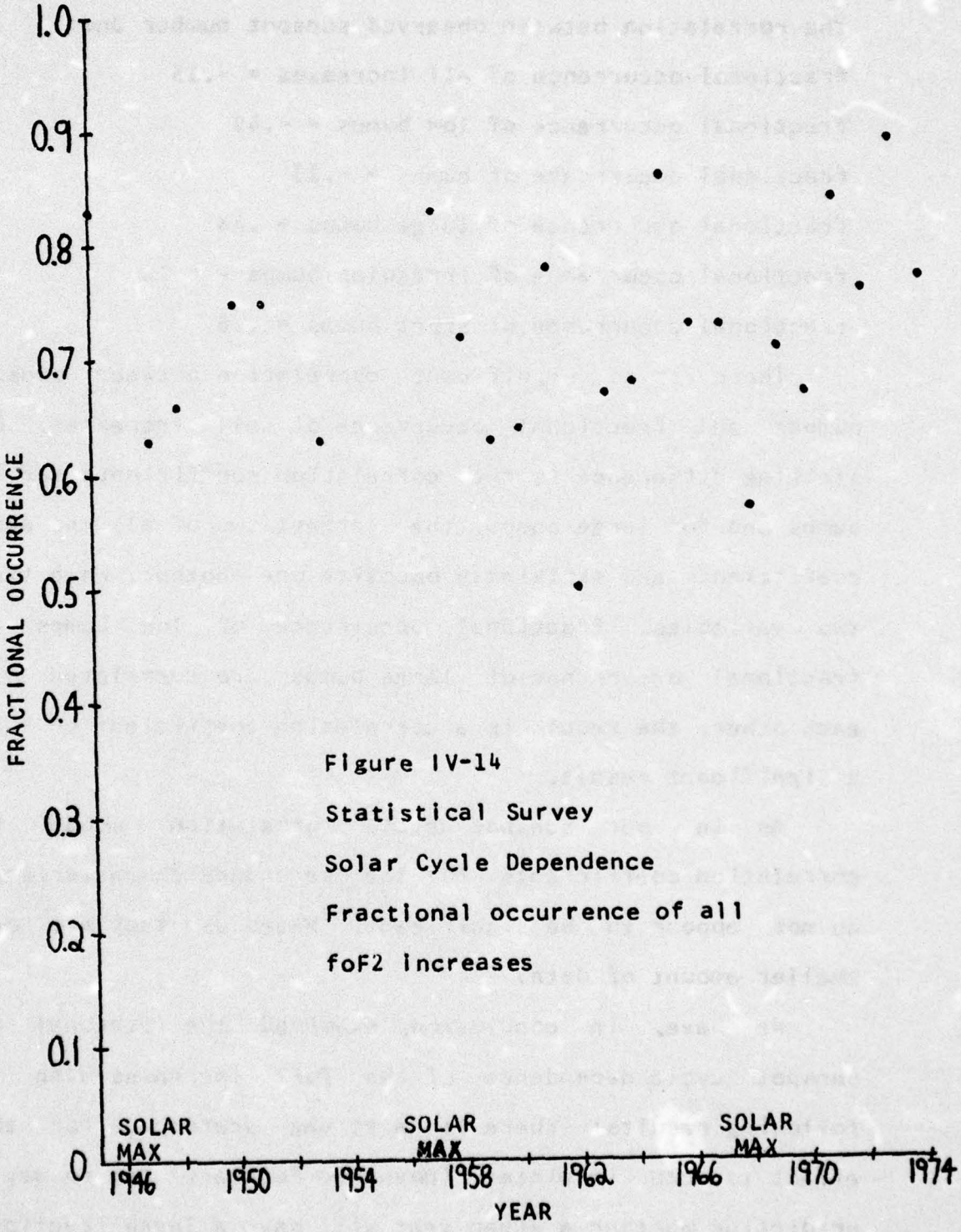

Figure IV-14

Statistical Survey

Solar Cycle Dependence

Fractional occurrence of all foF2 increases

Table IV-V

The correlation between observed sunspot number and:

fractional occurrence of all increases = -.13

fractional occurrence of low bumps = -.49

fractional occurrence of bumps = -.23

fractional occurrence of large bumps = .48

fractional occurrence of irregular bumps = -.12

fractional occurrence of short bumps = .26

There is no significant correlation between sunspot number and fractional occurrence of all increases. One striking difference is the correlation coefficients for low bumps and for large bumps, the largest two of all the above coefficients and strikingly opposite one another. When these two variables, fractional occurrence of low bumps and fractional occurrence of large bumps are correlated with each other, the result is a correlation coefficient of -.70, a significant result.

As in our sunspot cycle correlation study, the correlation coefficients for the secondary characteristics do not appear to be significant, based as they are on a smaller amount of data.

We have, in conclusion, examined the seasonal and sunspot cycle dependence of the foF2 increases with the following results: there is a strong preference for this effect to occur in winter (November-February) but no way of predicting whether a given year will have a large fractional

occurrence of the overall effect; there are significant differences between the seasonal and sunspot cycle dependences of low and large bumps, the large bumps more strongly clustered in mid-winter and more likely to occur during high sunspot years.

4.3 Case Studies: December 9 and December 15, 1971

4.3.1 Description of Available Data

Two nights, December 8-9, 1971, and December 14-15, 1971, were chosen for more detailed analysis because of the relatively large variety and quantity of geophysical data available for these two nights. In addition to information plotted in figures IV-3 (for Dec. 9) and IV-6 (for Dec. 15), Isis II topside sounder passes recorded Ne(h) vs. latitude on both nights. Two passes are of value for our purposes on December 9. The first occurred at about 4:20 UT and at longitude 71 degrees west, while the second occurred at about 6:15 UT and about 100 degrees west. Two passes are also of interest on December 15, occurring at about 2:25 UT and 49 degrees west longitude, and at about 4:20 UT and 78 degrees west longitude.

While discussing the data available for our case studies, we should take a moment to consider the question of the quality of these data. As mentioned in section 2.1.3.3, the quality of the Isis II ionograms varied greatly, with real height obtained from the best quality ionograms accurate to about $\pm 5\%$.

The primary evidence for the foF2 increases is provided by ionograms taken at St. John's, Newfoundland. We obtained

foF2 values for many of the same ionograms from different sources in order to check the accuracy in foF2. The three sources compared were: the Canadian source previously cited, World Data Center A, previously cited, and Dr. J. Buchau at the Air Force Cambridge Research Laboratories. The foF2 scaled by the three sources always agreed to within 0.2 MHz.

Two ionograms taken during the Dec. 15 event (one before, and one after the greatest part of the increase occurred) are reproduced in figure IV-15. While the two ionograms are not of the best quality, a sizeable increase in foF2 is apparent from the first ionogram to the second. The foF2 values marked on the figure are those scaled by Dr. J. Buchau.

Let us now turn our attention to figure IV-3 for December 9, 1971. As previously noted, figure IV-3 shows that on Dec. 9, the most disturbed magnetic conditions coincided with the onset of the increase in peak density. A much larger increase began about an hour later at Maynard, which is 18.8 degrees west of St. John's. The increase in TEC seen at Sagamore Hill should be compared with Nmax at Wallop's Island, near the Sagamore Hill 420-km point, rather than with Nmax at Maynard. Unfortunately, no data were available for the time in question at Wallop's Island.

On the St. John's Nmax vs. UT plot, two times are marked P_1 (3:30) and P_2 (6:00). A least squares fit between the profile calculated by World Data Center A and the

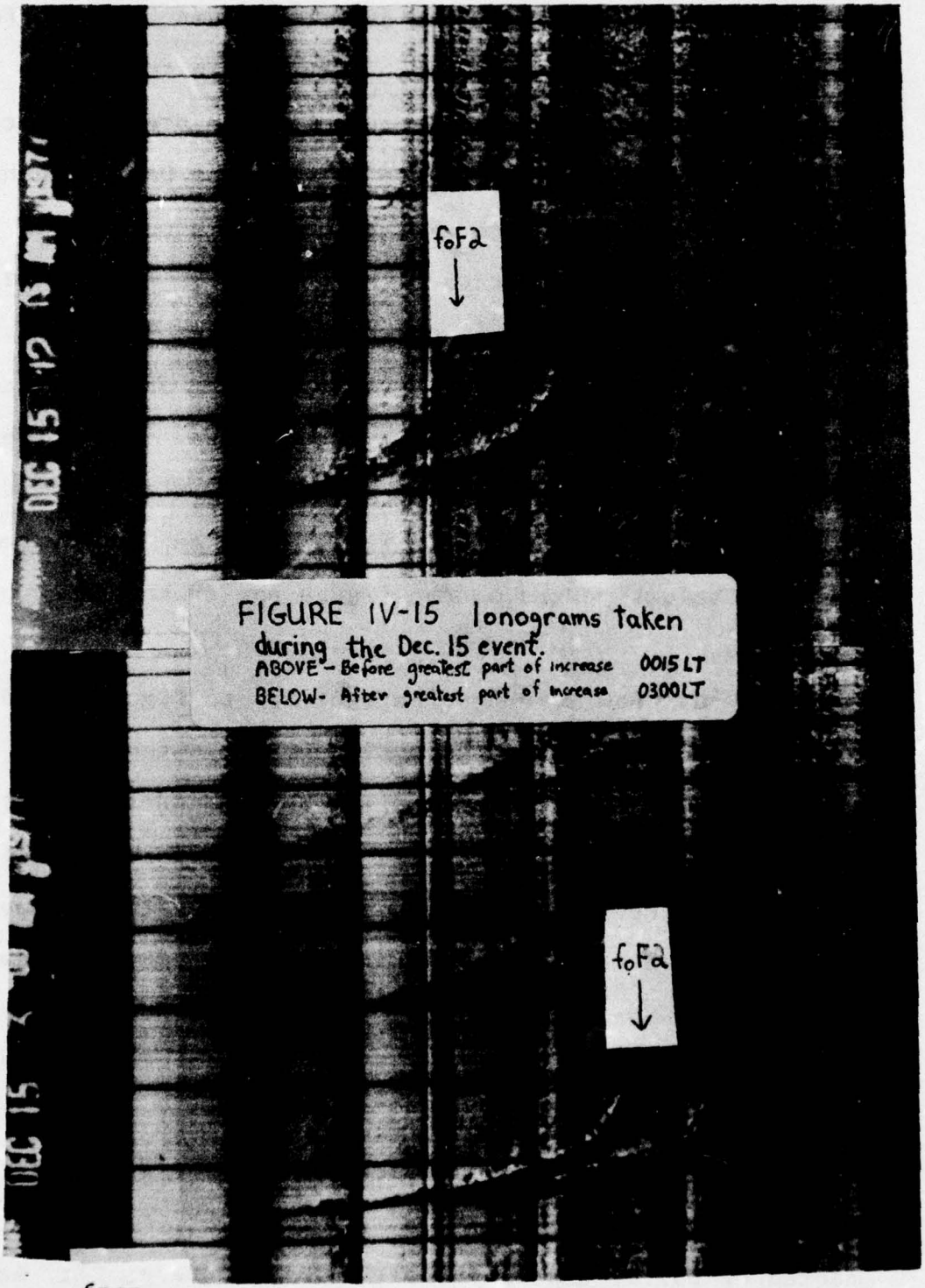

FIGURE IV-15 Ionograms taken during the Dec. 15 event.
ABOVE - Before greatest part of increase 0015 LT
BELOW - After greatest part of increase 0300 LT

semi-parabola used in the computer model gave a best yzero=213km at P_1 and 164km at P_2. One can see from the plots of these two profiles in figure IV-3, that the bottomside has filled in considerably, which seems to imply a downward flux of plasma.

On the night of December 8-9, no Ne(h) vs. latitude Isis II data were collected near the longitude of St. John's. We do, however, have the 71 degree west longitude pass previously mentioned. Nmax, N(700), and N(1000) vs. geographic latitude from this pass are plotted in figure IV-16. Slight changes were made at two points on the array where Nmax and hmax values were derived from ground based ionosonde data. Note the extremely sharp poleward trough edge. There is an unfortunate gap in the data between 51.68 degrees and 66.56 degrees. The computer model interpolation between these two points might exaggerate the actual plasma content in this latitude range.

Let us now discuss the December 15 data.

In figure IV-6 we can note that the beginning of the Nmax increase coincided (as on the case of December 9) with the greatest magnetic activity. A much larger Nmax increase did not begin, however, until about three hours later. The Nmax vs. UT plot for Wallop's Island looks similar to that for St. John's. Unlike the case of Dec. 9, when the increase at Maynard was far greater than that at St. Johns, on the 15th, the increase to the south (at Wallop's Island) is much

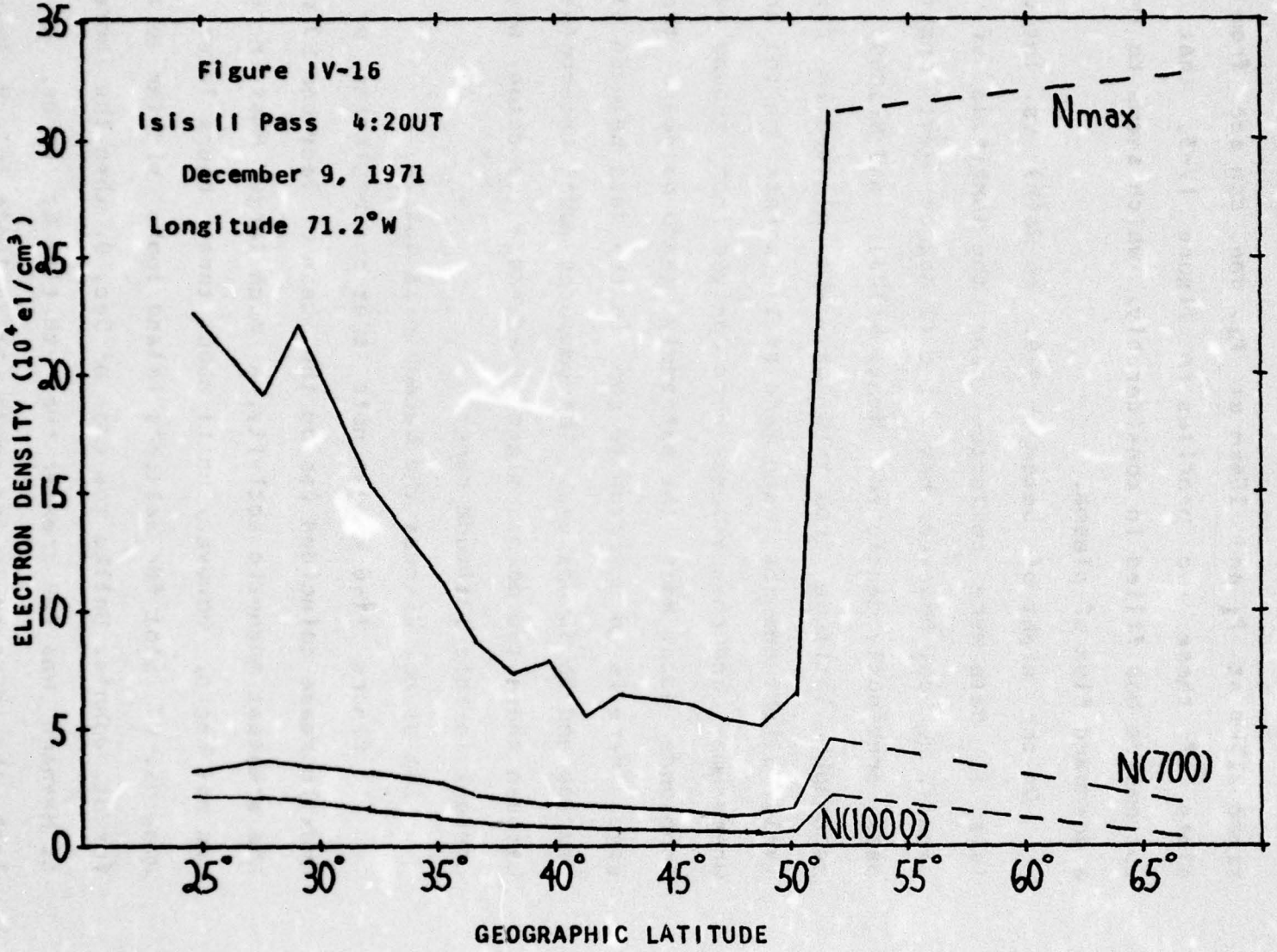
Figure IV-16
Isis II Pass 4:20UT
December 9, 1971
Longitude 71.2°W
Nmax
N(700)
N(1000)
ELECTRON DENSITY (10^4 el/cm^3)
GEOGRAPHIC LATITUDE
0
5
10
15
20
25
30
35
25°
30°
35°
40°
45°
50°
55°
60°
65°

less than that at St. John's. The increase at Wallop's Island occurs later than the increase at St. John's, but at about the same local time.

Profiles for the times 3:00 UT, 4:15 UT, and 6:45 UT obtained from World Data Center A are shown and indicated on the Nmax vs. UT plot for St. John's as P_1, P_2, and P_3. A least squares fit between the profile calculated from the St. Johns's ionogram by World Data Center A and the best fit semi-parabola used in the computer model gave yzero=219km at P_1, yzero=153km at P_2, and yzero=203km at P_3. Significant changes occurred on the bottomside during this event as these results indicate.

It is very fortunate that we have available Isis II data near the longitude of St. John's on December 15. Data from this 2:25 UT pass at 49 degrees west geographic longitude are plotted in figure IV-17. One change in this array was made, viz., Nmax and hmax obtained from St. John's ionograms were substituted for the topside values.

4.3.2 Computer Simulations of Slab Thickness Decreases for Dec. 9 and Dec. 15, 1971

4.3.2.1 Preliminary Considerations

As has been seen, the computer model we have developed takes as input data an Ne(h) vs. latitude array, and

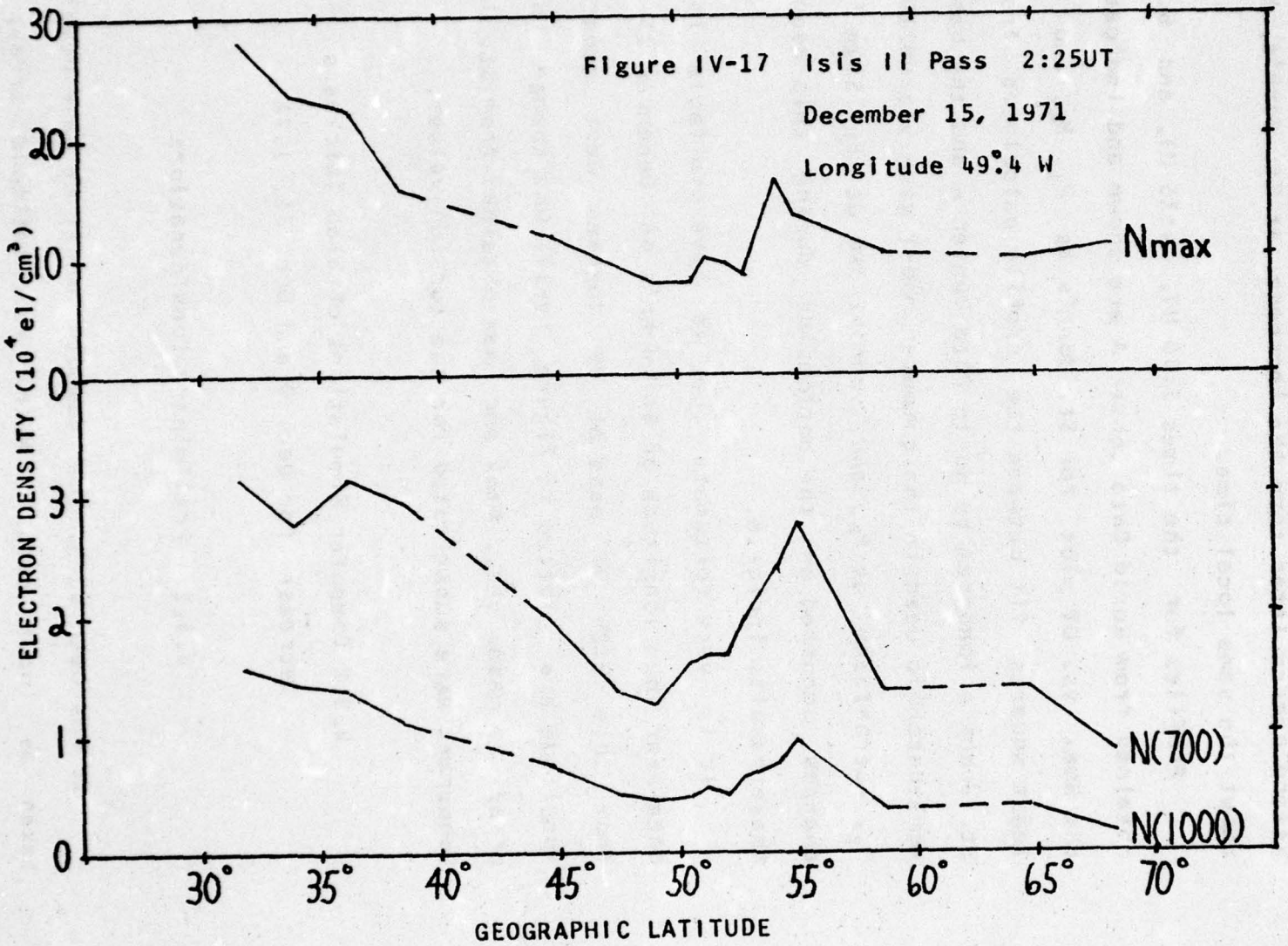
Figure IV-17 Isis II Pass 2:25UT
December 15, 1971
Longitude 49°.4 W
Nmax
N(700)
N(1000)
ELECTRON DENSITY (10^4 el/cm^3)
GEOGRAPHIC LATITUDE
30
20
10
0
3
2
1
0
30°
35°
40°
45°
50°
55°
60°
65°
70°

computes the Faraday rotation from the geostationary satellite to a given station. We wish to use this model to reproduce the effect observed on Dec. 9, and Dec. 15, i.e., constant Faraday Rotation accompanied by increasing peak density at St. John's.

Although we do have an Ne(h) vs. latitude array near the longitude of St. John's for Dec. 15, the array for Dec. 9 closest in longitude to St. John's is at 71.3 degrees west, too far to the west for us to expect to reproduce the St. John's and Goose Bay results very accurately. It is probably reasonable to assume, however, that a similar array would be found from a pass near St. John's. Therefore, it would be of great value for us to try to reproduce the observed slab thickness decrease which occurred on Dec. 9 as well as on Dec. 15.

We might ask, at this point, how well the total electron content of a vertical column at 420km height along the ray path calculated by our computer model, agrees with the actual equivalent vertical TEC observed at Goose Bay. In Table IV-VI is listed observed and calculated equivalent vertical TEC from Goose Bay and Hamilton, Mass. (Sagamore Hill Radio Observatory). Notice that the discrepancy between observed and calculated TEC is larger at Goose Bay than at Hamilton for both dates. This may be due to geometry effects not fully taken into consideration in our model. The computer simulation assumes that the satellite is on the

Table IV-VI

Calculated and Observed TEC

Date	Station	Equivalent Vertical TEC $\times 10^{12}$ el/cm^2 Observed TEC	Time of Observation	Calc. TEC	Time of Isis II pass
Dec. 9	Goose Bay	3.5	4:00 UT	2.43	4:20 UT
	(53°.3N, 60°.3W)	3.5	5:00 UT		
	Hamilton	4.7	4:00 UT	3.95	
	(42°.6N, 70°.8W)	4.7	5:00 UT		
Dec. 15	Goose Bay	4.4	2:00 UT	3.04	2:25 UT
	(53°.3N, 60°.3W)	4.3	3:00 UT		
	Hamilton	6.3	2:00 UT	5.54	
	(42°.6N, 70°.8W)	5.7	3:00 UT		

station's meridian. For ATS-3, stationed at 70°W, this is a good approximation for the Sagamore Hill case, but not for the Goose Bay ray path.

An additional factor contributing to the remaining discrepency between observed and calculated equivalent vertical TEC is found by remembering that the lowest height at which electron density is given by the Isis II topside sounder is often somewhat above hmax (see sec. 2.1.3.3). However, the density at this height, which is lower than Nmax, is taken in our model to be the peak density. This may represent a source of systematic error, subtracting a considerable amount of plasma around the F-2 peak in our model and lowering the calculated Faraday rotation.

Of course, we cannot expect perfect agreement between observed and calculated TEC for other reasons. The computer model reads in only five parameters to represent the entire ionosphere. The exospheric models are not perfect, either, extrapolating as they do from the very idealized conditions at 1000km all the way to the geostationary satellite. In addition, whenever the satellite pass is at a different longitude from the ray path to the geostationary satellite, different conditions are being sampled.

In spite of these sources of error, we can be confident that the semi-empirical computer model we have developed should enable us to reproduce, at least qualitatively, observed physical effects which occur on a large scale.

We will use this computer model in two ways to attempt to reproduce for Dec. 9 and Dec. 15, the observed anomalistic effect, i.e., constant TEC observed at Goose Bay coincident with an increase in peak density at St. John's. The changes which must be accounted for are shown in Table IV-VII and Table IV-VIII.

The first method which we will use involves a latitudinal shift of the entire Ne(h) vs. latitude array (as was done in Chapter 2). Shifting the poleward edge of the electron density trough over St. John's will clearly increase Nmax. We must discover the effect of such a shift on the Faraday rotation.

The second method is a vertical distortion of the Ne(h) vs. latitude array without a latitude shift of the array as a whole. It appears fairly likely that there are a large number of latitude dependent distortion schemes which will reproduce the desired effect. One such scheme will be presented which seems physically reasonable.

After using both methods, results from a certain combination of the two will also be presented.

4.3.2.2 Latitude Shift Method

The reader will recall that in Chapter 2, in order to examine the effect of a severe trough on the determination of an appropriate $\bar{M}$ factor, the feature of our computer

Table IV-VII

OBSERVED INCREASES - December 9

	4:20 UT	6:00 UT	% change
Nmax $x10^4$ el/cm^3	5.4 (Isis II)	7.1	+31
TEC $x10^{12}$ el/cm^2	3.5	3.4	-3

Table IV-VIII

OBSERVED INCREASES - December 15

	2:25 UT	6:45 UT	% change
Nmax $x10^4$ el/cm^3	9.1 (Isis II)	17.9	+97
TEC $x10^{12}$ el/cm^2	4.4	3.65	-17

model which allows us to shift the Ne(h) vs. latitude array an arbitrary number of degrees north or south was employed. With this technique available to us, we now attempt to reproduce the observed temporal behavior of Nmax and Ω on Dec. 9 and Dec. 15, 1971 by shifting latitudinal Ne(h) arrays southward. The results of shifting the Dec 9th array 5 times southward in one degree steps are shown in Table IV-IX. For yzero, we chose the value of 215km for all latitudes in the input array except the two northernmost points, which are north of the trough poleward edge. There a value of 165km was used. The motivation for these choices of yzero is apparent from remembering that yzero for P_1 in figure IV-3 was 213km and yzero for P_2 was 164km. If shifting the array south is to represent a temporal process, then yzero at St. John's must change from about 215km to about 165km as the poleward edge passes over St. John's.

One can see that in Table IV-IX, changing from a shift of -3 degrees to one of -5 degrees (which corresponds to moving the poleward edge of the trough over St. John's), gives a 395% increase in Nmax coincident with a 29% increase in Ω. While this Faraday rotation increase is very small compared to the Nmax increase, it is still significant, and inconsistent with observations. Furthermore, to reproduce the observations we must compare a zero degree shift with another shift, assumed to give the ionospheric densities at a later time. Examination of Table IV-IX shows that the

Table IV-IX

LATITUDE SHIFT RESULTS - December 9

yzero=165km north of poleward edge, yzero=215km elsewhere.

Shift	St. John's Nmax	Goose Bay Ω	TEC
	$x10^4$ el/cm^3	degrees	$x10^{12}$ el/cm^2
0	5.5	109	2.4
-1	5.3	127	2.9
-2	5.3	204	4.6
-3	6.3	277	6.2
-4	18.6	325	7.3
-5	31.2	357	8.0

Table IV-X

LATITUDE SHIFT RESULTS - December 9

yzero=230km north of poleward edge, yzero=120km in trough south to St. John's, yzero=215km from St. John's southward.

Shift	St. John's Nmax	Goose Bay Ω	TEC
	$x10^4$ el/cm^3	degrees	$x10^{12}$ el/cm^2
0	5.5	130	2.9
-1	5.3	140	3.2
-2	5.3	165	3.7
-3	6.3	219	4.9
-4	19.2	263	5.9
-5	31.2	291	6.5

desired effect has not been reproduced, since initially (as we shift one, two, three degrees south), Nmax does not increase while Ω does, contrary to the actual temporal sequence of events. In addition, comparing the zero degree shift with the -5 degree shift gives a 467% Nmax increase and a 228% Ω increase, completely at variance with the observed increases listed in Table IV-VII.

If we suppose that the change in yzero at the trough poleward edge is very sharp, taking yzero=230km north of it and 120km south of it as far as St. John's (with yzero=215km southward from St. John's), then we can reduce the Faraday rotation increase in changing from no shift to a -5 degree shift by about 50%. This is because although Nmax in the trough is very low, yzero is required to be very low there so that the vertical TEC is greater than it otherwise would be. Even with this artificial device we cannot reproduce the observations for we still have a 124% increase in Faraday rotation coupled with the 467% Nmax increase. The results for the shifts from 0 to -5 degrees using these values for yzero are listed in Table IV-X.

For the Dec. 15 case we initially tried yzero=203km north of the poleward edge, 153km south of the poleward edge to the latitude of St. John's and 222km from St. John's southward. As we shift southward, yzero above St. John's changes from 222km to 153km to 203km, which is the observed temporal behavior.

The results for shifts of zero to -6 degrees in one degree steps for Dec. 15 are shown in Table IV-XI. A shift of six degrees is necessary for the poleward edge to reach St. John's producing a 72% increase in Nmax. Faraday rotation increased by a much smaller percentage, 23%.

We now artificially distort the trough bottomside profiles north of St. John's by letting yzero equal 120km there instead of 153km. This decreases the Faraday rotation increase from the zero degree shift to the -6 degree shift to 17% (see Table IV-XII). A further distortion is obtained by keeping yzero=120km south of the poleward edge to St. John's and letting yzero=230km north of the poleward edge instead of 203km. Now the 72% Nmax increase from 0 degree shift to -6 degree shift is accompanied by a 7% Faraday rotation increase (see Table IV-XIII). A summary of these three sets of results is found in Table IV-XIV. Graphs of Faraday rotation and Nmax for the three calculations are shown in figure IV-18 for a wide range of latitude shifts. The best agreement to the observed effect on Dec. 15 (small TEC decrease coincident with Nmax increase) is found in the third calculation (7% Ω increase).

To get a feeling for the change in the latitudinal structure sampled by the ray path, two contour plots are drawn in figure IV-19, one for the zero degree shift and one for the -6 degree shift, for the results of the aforementioned third calculation. The ray path is drawn

Table IV-XI

LATITUDE SHIFT RESULTS -December 15

yzero=203km north of poleward edge, yzero=153km in trough south to St. John's, yzero=222km from St. John's southward.

Shift	St. John's Nmax $x10^4$ el/cm^3	Goose Bay Ω degrees	TEC $x10^{12}$ el/cm^2
0	8.8	160	3.6
-1	7.9	161	3.6
-2	7.8	160	3.6
-3	9.0	149	3.4
-4	9.6	144	3.2
-5	9.6	166	3.7
-6	15.1	172	3.9

Table IV-XII

LATITUDE SHIFT RESULTS - December 15

yzero=203km north of poleward edge, yzero=120km in trough south to St. John's, yzero=222km from St. John's southward.

Shift	St. John's Nmax $x10^4$ el/cm^3	Goose Bay Ω degrees	TEC $x10^{12}$ el/cm^2
0	8.8	160	3.6
-1	7.9	161	3.6
-2	7.8	161	3.6
-3	9.0	152	3.4
-4	9.6	152	3.4
-5	9.7	175	3.9
-6	15.1	187	4.2

Table IV-XIII

Latitude Shift Results - December 15

yzero=230km north of poleward edge, yzero=120km in trough south to St. John's, yzero=222km from St. John's southward.

Shift	St. John's Nmax $x10^4$ el/cm^3	Goose Bay Ω degrees	TEC $x10^{12}$ el/cm^2
0	8.8	160	3.6
-1	7.9	161	3.6
-2	7.8	160	3.6
-3	9.0	149	3.4
-4	9.6	144	3.2
-5	9.6	166	3.7
-6	15.1	172	3.9

Table IV-XIV

Summary of Changes in Nmax and Ω for Different yzeros

yzero north of poleward edge (km)	yzero in trough south to St. John's (km)	yzero from St. John's southward (km)	% changes Nmax	% changes Ω
203	153	222	72	25
203	120	222	72	17
230	120	222	72	7

Figure IV-18 Model Nmax and Ω for Dec. 15 using various yzeros for a wide range of latitude shifts

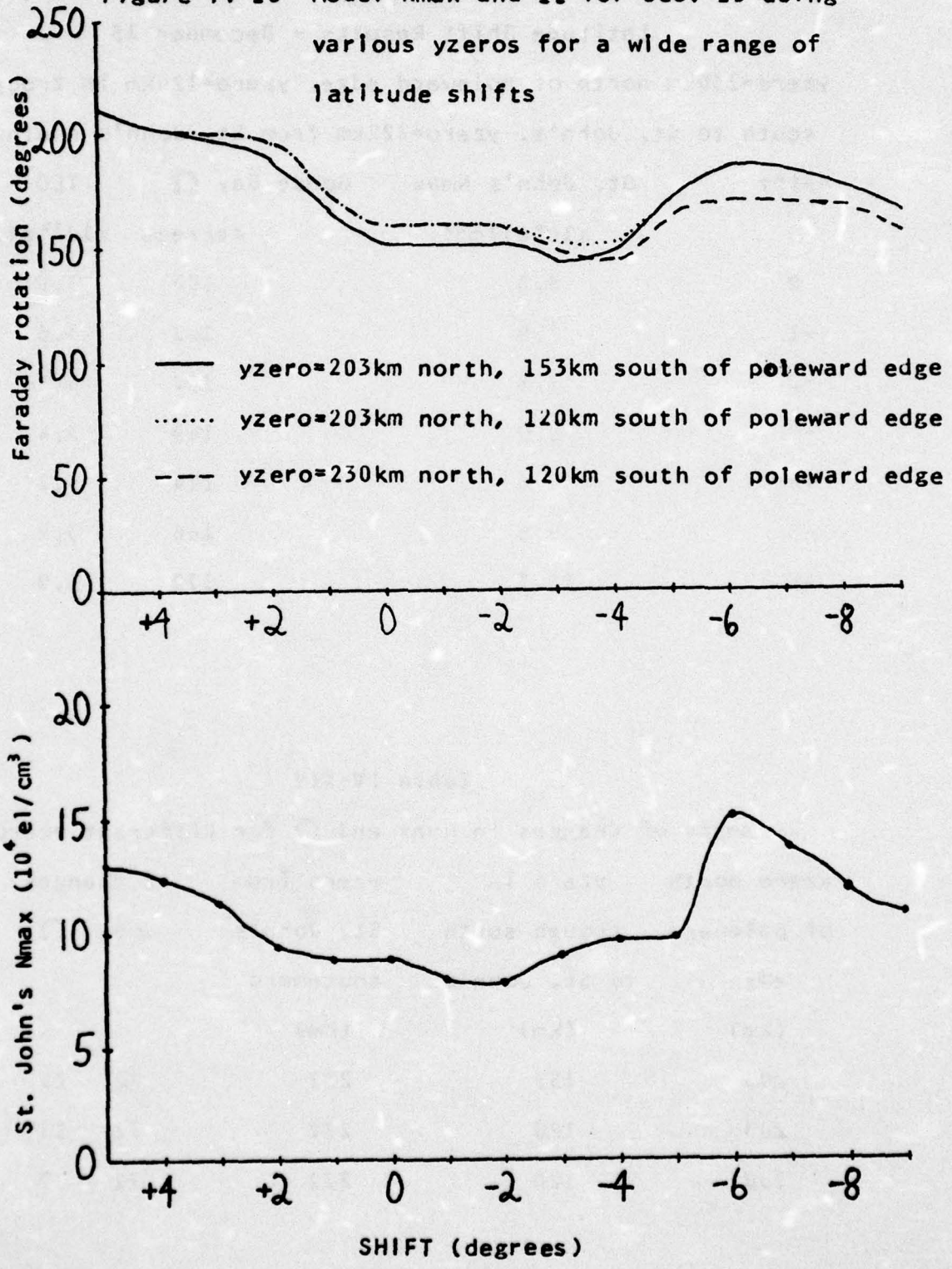

Figure IV-19

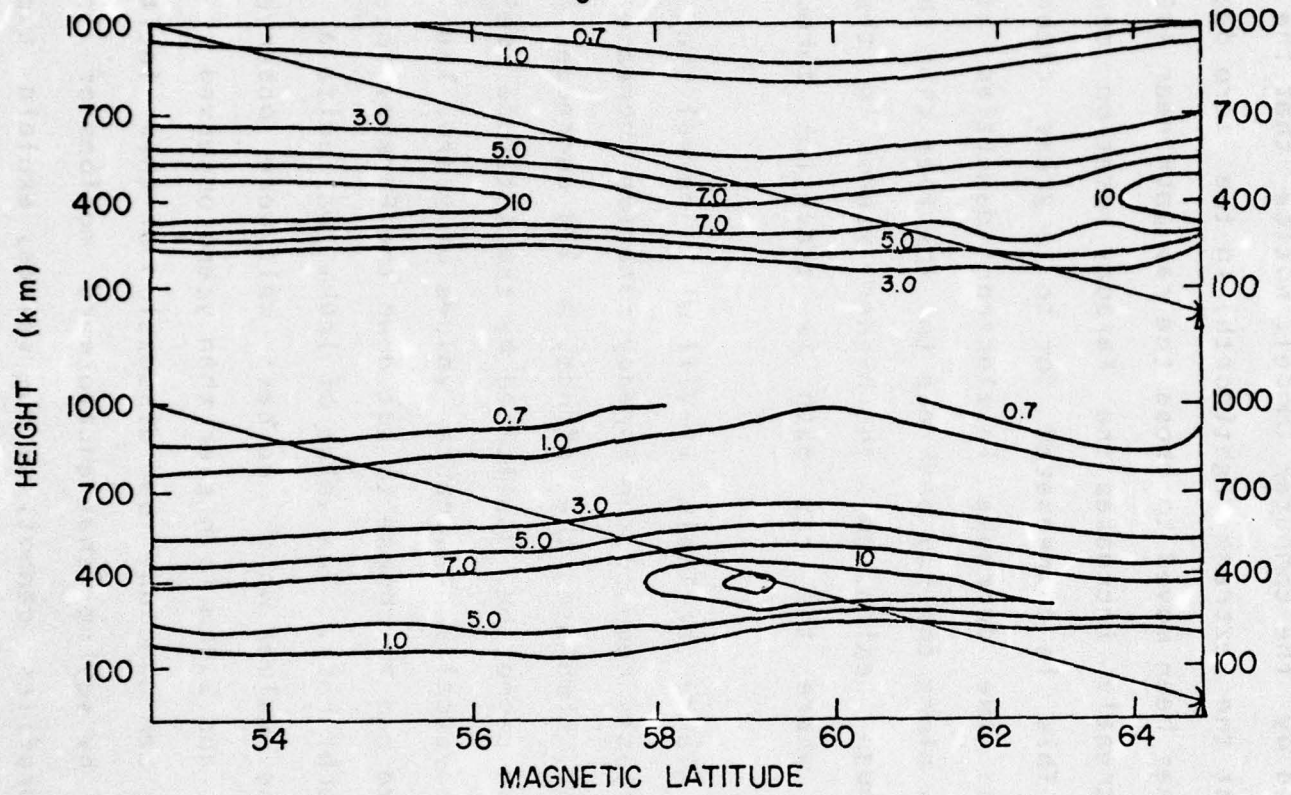

15 DECEMBER 1971

Electron Density Contours (10^4 el/cm^3) with Ray Path from Goose Bay to ATS-3

through the interpolated density profiles of Ne(h) vs. latitude from 0 km in height to 1000km in height, which were provided by the computer model. Notice that the poleward edge, at the extreme right(north) in the zero degree shift plot, has been moved to cross the ray path near 400km height which greatly increases the Faraday rotation contribution there. This is compensated for to a great extent by two factors: the decrease in electron densities at greater heights along the ray path due to the fact that this is now the trough region; and the higher yzeros in the poleward region where the ray path is traveling through lower heights.

A glance at Table IV-VIII will reveal that while we have greatly reduced the Faraday rotation increase, we still have not simulated the effect. A 17% decrease in Faraday rotation cannot be duplicated by the latitude shift method using physically reasonable values of yzero. The values of yzero we had to choose to cut down the Faraday rotation were quite arbitrary. The value of 120km was quite a bit lower than the values which we have said were observed at St. John's, and 230km is higher than yzero observed at 6:45 UT.

We can conclude our discussion of this latitude shift method by saying that equatorward motions of latitudinal Ne(h) profiles cannot, by themselves, explain the observed anomalistic effect, i.e., flat or decreasing TEC combined with an Nmax increase. This conclusion is strengthened by

examination of the succeeding Isis II passes on both Dec. 9 and Dec. 15 (compare figures IV-20 and IV-21 with figures IV-16 and IV-17). Although the succeeding passes are far to the west of the original ones, if any substantial motion of the ionization trough occurred, it should show up in the later passes. Examination shows that the poleward edge did not seem to change its position appreciably on Dec. 9, and on Dec. 15, it is impossible to tell where the poleward edge was at the later time (if it actually was present).

In spite of this negative conclusion, we note that appreciable decreases in slab thickness (TEC/Nmax) were reproduced on both Dec. 9 and Dec. 15. Even though TEC increased, the increase in Nmax was much greater.

In short, it is certainly possible that some latitudinal plasma motions occurred, as a simple drift model to be discussed presently suggests. These latitudinal motions are apparently not the primary cause of the phenomenon we are concerned with (flat TEC with increasing Nmax), however.

4.3.2.3 Vertical Drift Method

It seems reasonable to hypothesize that a vertical redistribution of plasma over a wide latitude range, increasing Nmax but depleting the electron density by appropriate amounts at certain other heights, will produce a

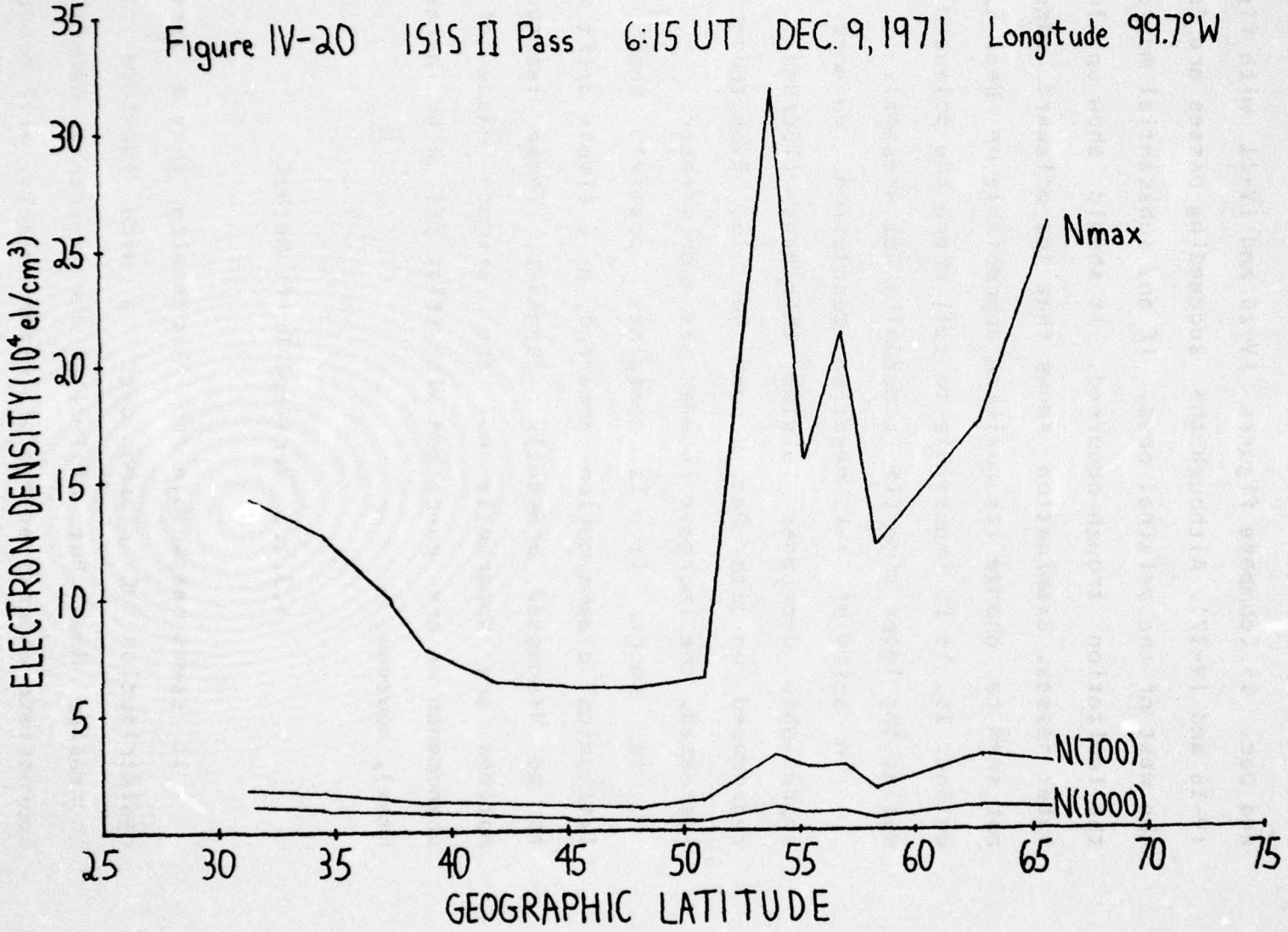
Figure IV-20 ISIS II Pass 6:15 UT DEC. 9, 1971 Longitude 99.7°W
ELECTRON DENSITY (10^4 el/cm^3)
35
30
25
20
15
10
5
Nmax
N(700)
N(1000)
25
30
35
40
45
50
55
60
65
70
75
GEOGRAPHIC LATITUDE

Figure IV-21 ISIS II Pass 4:20 UT DEC 15, 1971
Longitude 77.9°W

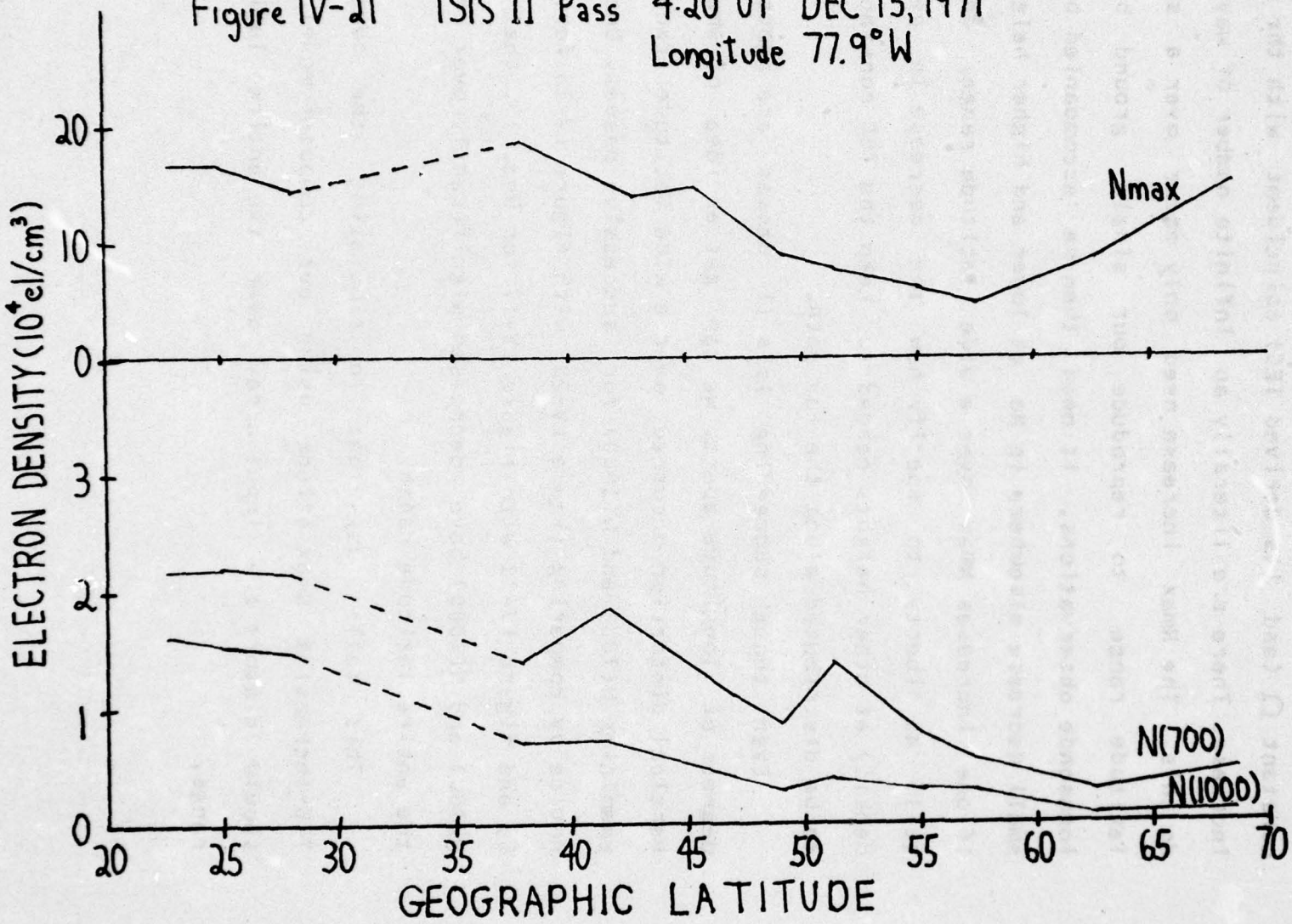

constant Ω (and its derived TEC) coincident with the Nmax increase. There are literally an infinite number of ways to do this. The Nmax increase need only occur over a small latitude range to reproduce our single ground based ionosonde observations. It need then be accompanied by a small decrease elsewhere in Ne at lower and higher heights. If one increases Nmax over a wide latitude range, one is still at liberty to specify how the decrease in plasma density at other heights needed to keep the TEC constant is to be distributed along the ray path.

Even though succeeding Isis II passes are about 30 degrees of longitude apart, we can get an idea of whether vertical distortion occurred over a wide latitude range by examining N(700) and N(1000) for successive passes. One can notice by comparing figure IV-20 with figure IV-16 for Dec. 9, and figure IV-21 with figure IV-17 for Dec. 15, that both N(700) and N(1000) have decreased significantly over nearly the entire latitude range.

This tells us, that in simulating the constant TEC-increasing Nmax effect using our computer model, we should distort the input array over the entire latitude range.

A simple model for "Magnetospheric Convection at Ionospheric Heights" has been offered by Mendillo (1973). In that analysis the vertical drift is expressed as follows:

$$Wvert = \frac{-E_{DD}\cos(\frac{\pi}{12}LT)}{B_{e,s}} \left(\frac{1+h/Re}{\cos\Lambda}\right)^3 \frac{\cos I}{\sqrt{1+3\sin^2\Lambda}} \quad (4.1)$$

In this formula:

E_{DD} is a uniform dawn to dusk magnetospheric electric field in the equatorial plane.

LT is the local time.

$B_{e,s}$ is the magnetic field at the Earth's surface at the equator.

h is the height.

Re is the Earth's radius.

Λ is the magnetic dipole latitude.

I is the magnetic dip angle.

We will use this equation to derive distortion factors as a function of latitude and height to be applied to the Ne(h) vs. latitude array in our computer model.

We will assume that E_{DD}, $B_{e,s}$, and local time are the same for the entire pass (the satellite covers about 45 degrees of latitude in 15 minutes). Then we can suppress the dependence on these quantities in (4.1) to obtain relative drift velocities as follows:

$$Wvert \propto \left(\frac{1+h/Re}{\cos\Lambda}\right)^3 \frac{\cos I}{\sqrt{1+3\sin^2\Lambda}} \quad (4.2)$$

We now must give an explanation of how wvert(h) and the

change in Ne(h) are related. While the actual relation is probably quite complicated, the following simple argument will be sufficient to provide some physical justification for the particular distortion method we chose for our computer simulation. The purpose of this vertical distortion exercize is to qualitatively discuss the large scale changes of ionospheric structure that must be primarily responsible for the observed effects. It is unfortunately beyond the scope of this thesis to attack the full time and spatial dependence of the modified ionospheric structure.

Consider an imaginary box in the ionosphere with cross-sectional area A and height Δh. For a downward drift, the fluxes in and out of the box are given by:

$$F_{in} = N_{top} V_{top}$$

$$F_{out} = N_{bot} V_{bot} \qquad (4.3)$$

Here we assume no horizontal drifting of plasma, and for further simplicity, no net production or recombination of free electrons in the box. Then we can write:

$$N_{box}(t+\Delta t)A\Delta h = N_{box}(t)A\Delta h + (N_{top} V_{top} - N_{bot} V_{bot})A\Delta t \qquad (4.4)$$

so that:

$$N_{box}(t+\Delta t) = N_{box}(t) + (N_{top} V_{top} - N_{bot} V_{bot})\Delta t/\Delta h \qquad (4.5)$$

Since this is not a large box, we can take

$$V_{top} = V_{bot} = Wvert \qquad (4.6)$$

Then:

$$N_{box}(t+\Delta t) = N_{box}(t) + (\Delta N_{box}/\Delta h)Wvert\Delta t \qquad (4.7)$$

Here $\Delta N_{box}/\Delta h$ should be an average value, i.e., the true value of $\Delta N/\Delta h$ at some time between t and $t+\Delta t$. Unfortunately, all we have available to us are the interpolated density arrays for the beginning of the effect we wish to simulate. Therefore we must use:

$$N(t+\Delta t) = N(t) + (\Delta N/\Delta h)_t W_{vert}\Delta t \qquad (4.8)$$

A more general expression for dN/dt is given by:

$$\frac{dN}{dt} = q - L + \vec{v}\cdot\vec{\nabla}N + N\vec{\nabla}\cdot\vec{v} \qquad (4.9)$$

This is the continuity equation (1.10) with a motion term added. Here we took q=L, and $\vec{\nabla}\cdot\vec{v}=0$, so (4.9) reduces to (4.8). This equation should be applied to N(1000), N(700) and Nmax.

It is clear why decreases occur at 700km and 1000km, i.e., $dN/dh < 0$. To see why Nmax increases, where $dN/dh = 0$, consider the following. We cannot apply (4.8) to Nmax. This is because $dN/dh = 0$ at hmax for any profile, and in particular, the semi-parabola we have modeled around the F-2 peak is such that:

$$N(hmax+\Delta h) = N(hmax-\Delta h) \qquad (4.10)$$

So that $\Delta N/\Delta h$ is zero at the peak. If our semi-parabolic model represented the correct distribution, we could not, according to (4.8), increase Nmax using vertical plasma drifts (because as much plasma would be entering the region of peak density as would be leaving it). The semi-parabola is only an approximation, of course. We know from experience

that generally during the nighttime:

$$N(hmax-\Delta h) < N(hmax+\Delta h)$$

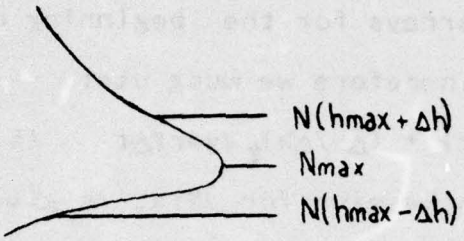

Figure IV-22

We have drawn a typical nighttime ionospheric profile schematically in figure IV-22 which demonstrates that Ne(h) normally falls off more rapidly below hmax (due to increased recombination rates) than it does above hmax (also see figures IV-25 and IV-26). Therefore, in reality $\Delta N/\Delta h$ is positive near the F-2 peak and according to (4.8), Nmax will increase as expected. This can also be easily seen from (4.4) with $N_{bot} < N_{top}$. Conversely, $\Delta N/\Delta h$ is negative at h=700km and h=1000km, so the electron density decreases there, as desired.

For the topside heights, we thus have:

$$N_{1000}(t+\Delta t) = N_{1000}(t) + (\Delta N/\Delta h)_{1000,t}\, Wvert(1000)\Delta t$$

$$N_{700}(t+\Delta t) = N_{700}(t) + (\Delta N/\Delta h)_{700,t}\, Wvert(700)\Delta t \qquad (4.11)$$

Since (4.2) does not give the absolute magnitude of Wvert, we replace $Wvert\Delta t$ in (4.11) by:

$$K \cdot w = Wvert\Delta t \qquad (4.12)$$

where from (4.1):

$$K = \frac{-E_{DD}\cos\left(\frac{\pi}{12}LT\right)\Delta t}{B_{e,s}} = K(E_{DD}, LT, B_{e,s}, \Delta t) \qquad (4.13)$$

Then equations (4.11) become:

$$N_{1000}(t+\Delta t) = N_{1000}(t) + (\Delta N/\Delta h)_{1000,t}\, K \cdot w(1000)$$
$$N_{700}(t+\Delta t) = N_{700}(t) + (\Delta N/\Delta h)_{700,t}\, K \cdot w(700) \qquad (4.14)$$

The equivalent formalism for Nmax would be an equation of the form:

$$Nmax(t+\Delta t) = Nmax(t) + (\Delta N/\Delta h)_{hmax,t} K \cdot W(hmax) \qquad (4.15)$$
$$Nmax(t+\Delta t) = Nmax(t)\left\{1 + \frac{(\Delta N/\Delta h)_{hmax,t} K \cdot W(hmax)}{Nmax(t)}\right\}$$

A convenient way to avoid the uncertainty of how to choose $\Delta N/\Delta h$ at hmax for each latitude is to assume that the normalized quantity $(\Delta N/\Delta h)_{hmax,t}/Nmax(t)$ (a profile shape parameter) does not change appreciably over the latitude range covered by the ray path in the F-region. The quantity may therefore be evaluated above St. John's where actual Nmax(t) and Nmax(t+Δt) observations are available. Thus:

$$\frac{K\cdot(\Delta N/\Delta h)_{hmax,t}}{Nmax(t)} = \left[\frac{Nmax(t+\Delta t) - Nmax(t)}{Nmax(t)}\,\frac{1}{w(hmax)}\right]_{St.John's} = C \qquad (4.16)$$

and equation (4.16) becomes, for all other latitudes:

$$Nmax(t+\Delta t) = Nmax(t)(1 + Cw(hmax)) \qquad (4.17)$$

We now have only one adjustable parameter for the distorted array, the constant K in (4.14). This constant is actually a function of magnetic and electric fields, and the time (from 4.13). We choose K in order to reproduce the observed flat TEC-increasing Nmax effect. After increasing Nmax to the desired value, we only need to decrease N(700) and N(1000) by sufficient amounts to keep the Faraday rotation constant. For the distorted array, yzero was found from available ionosonde data, while hmax was obtained by decreasing the hmax values in the original array by an average of 20km with the size of the decreases proportional to w. This was done because it was observed that hmax tended to drop during the effect.

On occasion, i.e., the extreme northern and southern ends of the array, use of equations (4.14) resulted in unreasonable values for N(700) and N(1000). For example, negative values for electron density, or N(700)<N(1000) might occur. At whatever latitudes this happened, the values at N(1000) and N(700) there were obtained by distorting the original array by the same percentage as was done for the nearest latitude point at which reasonable values were obtained. Unreasonably high values of Nmax also were obtained using (4.14) at the extreme poleward end of the array. These points are north of the ray path (except when shifted far south), so they will not contribute to Ω. In the input array, the northernmost reasonable value was used

for these points also.

Having discussed the approach used, let us now present the results of the computer model simulations of ionospheric vertical distortions. In Table IV-XV the reader will find Nmax, TEC, and Faraday rotation computed for both Hamilton and Goose Bay for the events of both December 9 and December 15, 1971. The value of K used in equation (4.14) for both dates is also shown.

Table IV-XV

Vertical Distortion Results

	STATION	Nmax(St. John's) (10^4 el/cm^3)	TEC (10^{13} el/cm^2)	Ω (deg)	K (meters)
Date Dec. 9, 1971					
Original	Hamilton		3.95	157	
Array-4:20 UT	Goose Bay	5.4	2.43	108	
Distorted	Hamilton		3.30	131	
Array-6:00 UT	Goose Bay	7.3	2.40	107	1.2×10^5
Date Dec. 15, 1971					
Original	Hamilton		5.54	219	
Array-2:25 UT	Goose Bay	8.7	3.04	135	
Distorted	Hamilton		6.81	270	
Array-6:45 UT	Goose Bay	18.7	3.04	135	1.12×10^5

The values of K we have used to reproduce the observed flat TEC-increasing Nmax effect can be used to find an approximate value for the dawn-dusk electric field. From (4.13) we arrive at:

$$E_{DD} = \frac{-K B_{es}}{\cos\left(\frac{\pi}{12} LT\right) \Delta t} \qquad (4.18)$$

where LT is in hours, E_{DD} is in volts/meter, B_{es} is in webers/meter^2=(volts)(sec)/meter^2, K is in meters, and Δt is

in seconds.

In (4.18) we use the times midway between the times of the original array and of the disturbed array shown in Table IV-XV for the local time, the time intervals shown in Table IV-XV for Δt, and the value of $.305 \times 10^{-5}$ wb/m^2 for B_{es}. The calculation gives $E_{\phi\phi}$=-.67mV/m for the Dec. 9 event, and $E_{\phi\phi}$=-.23mV/m for Dec. 15. We will discuss these numerical $E_{\phi\phi}$ values further in sec. 4.4 when we take up the question of the mechanism for the flat TEC-increasing Nmax effects.

The distorted arrays for Dec. 9 and Dec. 15 are graphed in figures IV-23 and IV-24. Direct comparison with figures IV-16 and IV-16 reveals the *type of distortions* that have been invoked. The dramatic decreases in N(1000) and N(700) are clearly evident, as are the increased Nmax values.

The distortion on Dec. 15 seems to be more severe, in that N(700) and N(1000) are reduced to values typically less than 10^3el/cm^3 for high latitudes where Nmax is multiplied by a factor of from 3 to 5. The reason for the larger distortion on the 15th is clear from Table IV-VIII. The large percentage increase in Nmax (97%) necessitated the greater compensating decreases in N(700) and N(1000).

Notice that even with this large distortion, the 17% decrease in TEC has not been reproduced. From Table IV-XV we see that this large distortion was accompanied by constant TEC (3.04×10^{18}el/cm^2). To produce a decrease in TEC, even greater distortions would be required. For December 9,

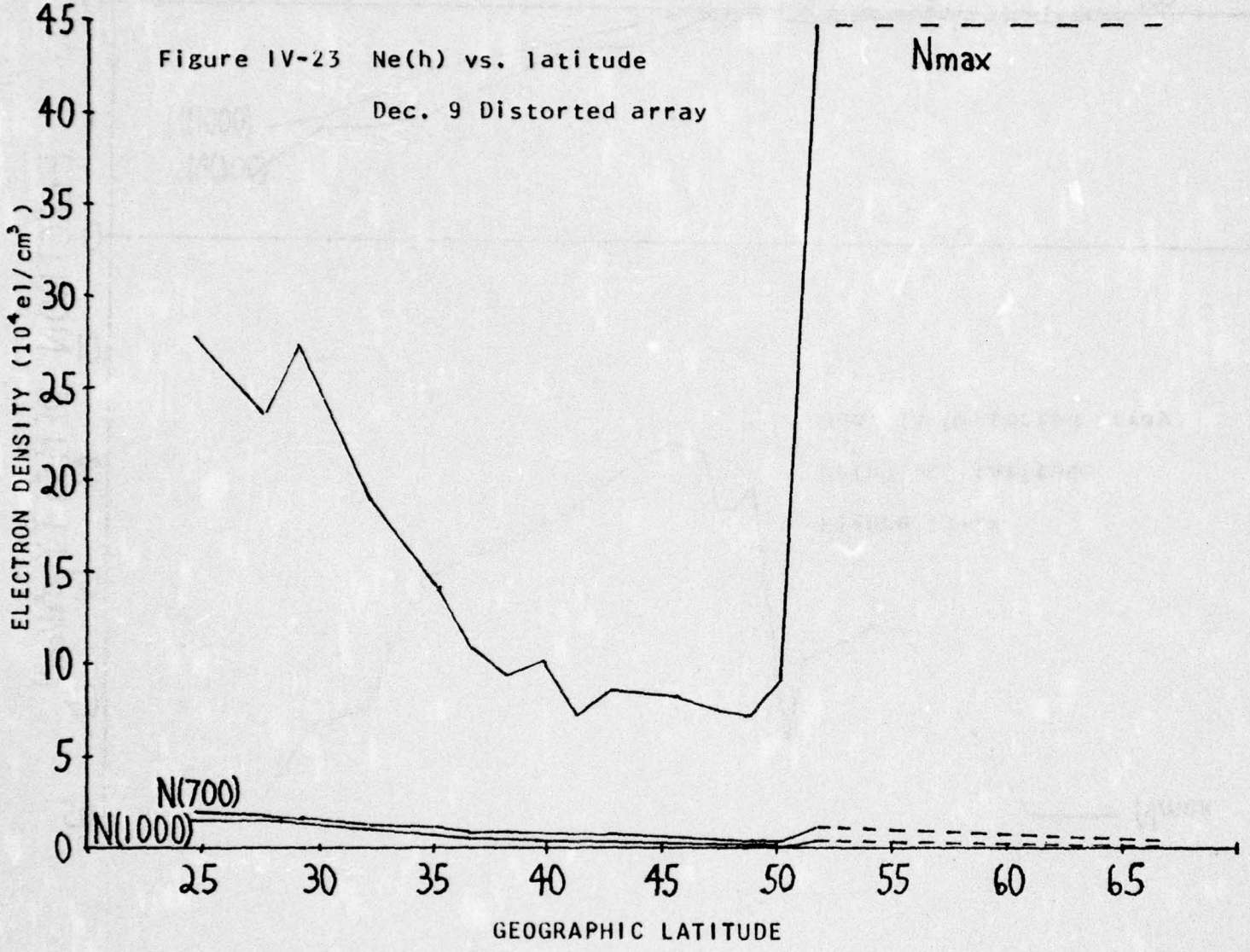

Figure IV-23 Ne(h) vs. latitude

Dec. 9 Distorted array

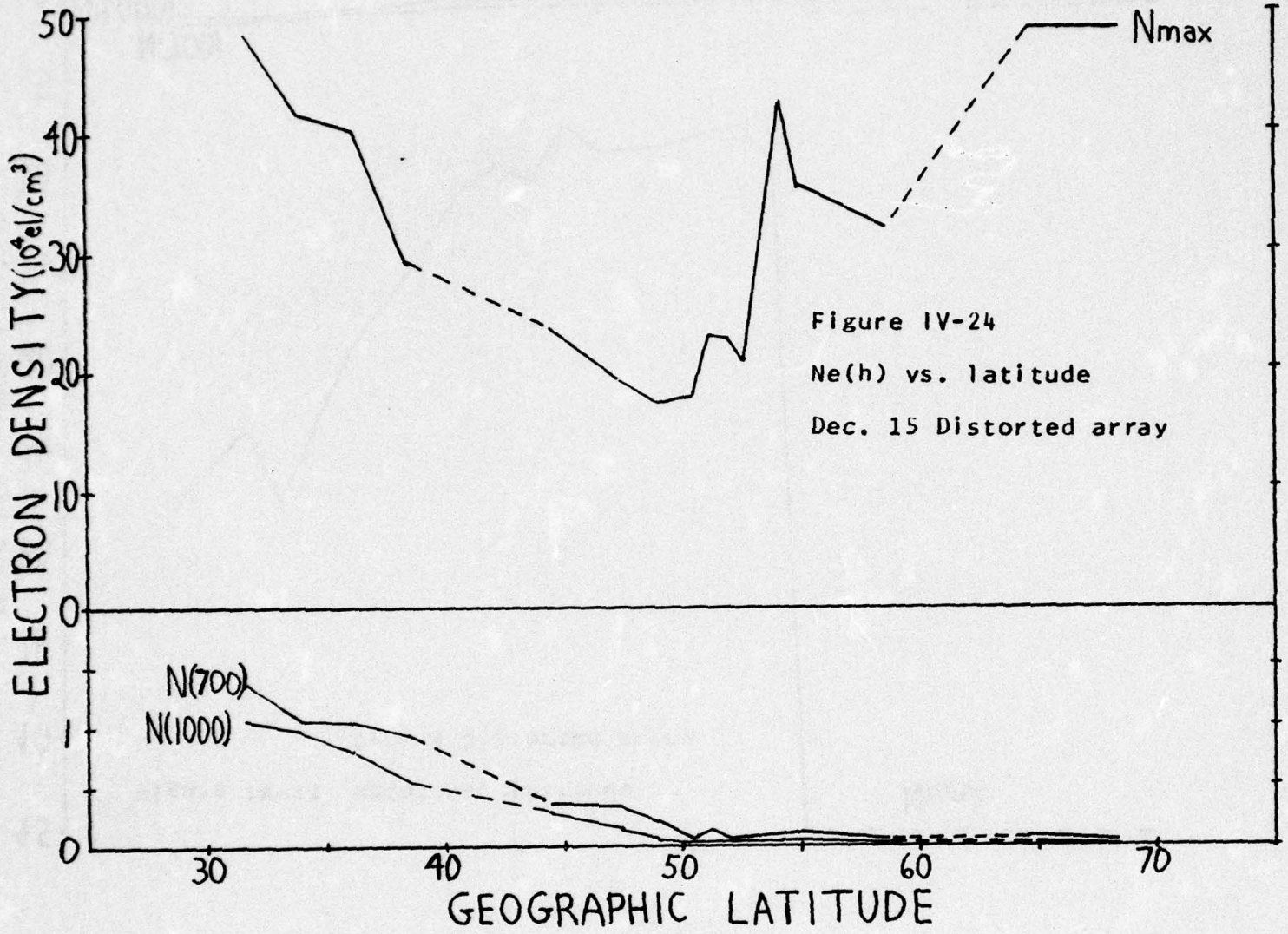

Figure IV-24

Ne(h) vs. latitude

Dec. 15 Distorted array

however, the observed changes have been reproduced in detail. The relatively small increase in Nmax evident in Table IV-VII (31%) can be accounted for by a smaller vertical distortion than in the December 15 case.

One effective method for demonstrating how these vertical distortions are capable of producing a flat TEC-increasing Nmax effect is to graph Ne(h) along the ray path up to 1000km both before and after the Nmax increase. This is done for Dec. 9 in figure IV-25, and for Dec. 15 in figure IV-26. The anomalous increase in the distorted array's value of Ne at about 170km height in figure IV-25 is due to the lower value of yzero at the highest array latitudes.

One can see from these figures that the large increase in electron concentrations around the F-2 peak and including the bottomside is compensated for by lower values of Ne for the distorted array from about 400km out to the satellite.

As previously noted (sec. 2.1.3.3), the computer model adds up the vertical TEC above each latitude in the interpolated array. This vertical TEC is directly added up to 1000km, and then extrapolated to 2000km using a scale height of 1000km, as explained in section 2.2.1. The vertical TEC up to 2000km can then be compared with the equivalent vertical TEC obtained from the Faraday rotation and the $\bar{M}$ factor at 420km height along the ray path.

In Table IV-XVI, changes in the vertical TEC up to

Figure IV-25

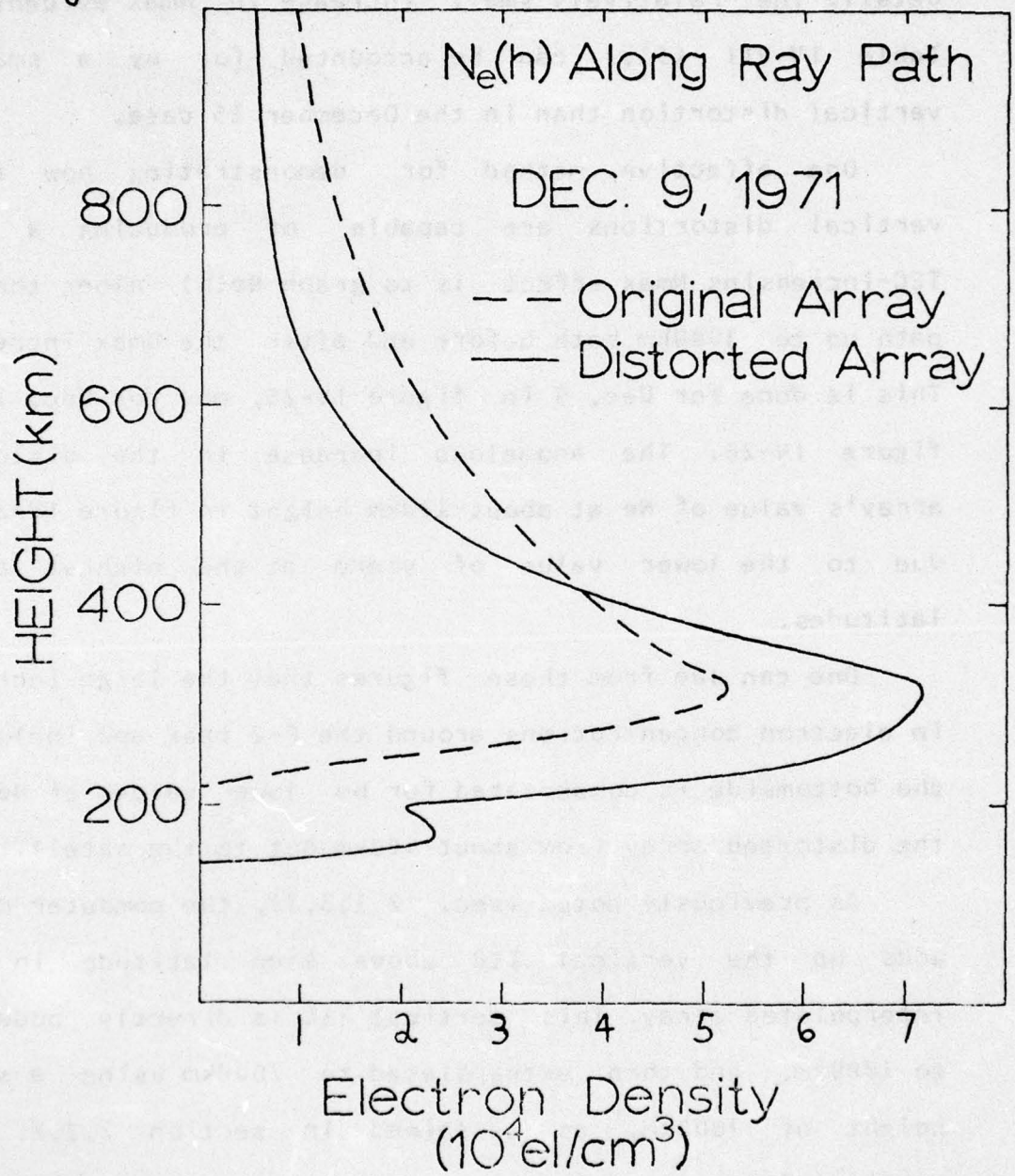
$N_e(h)$ Along Ray Path
DEC. 9, 1971
Original Array
Distorted Array
HEIGHT (km)
800
600
400
200
1
2
3
4
5
6
7
Electron Density
(10^4el/cm^3)

Figure IV-26

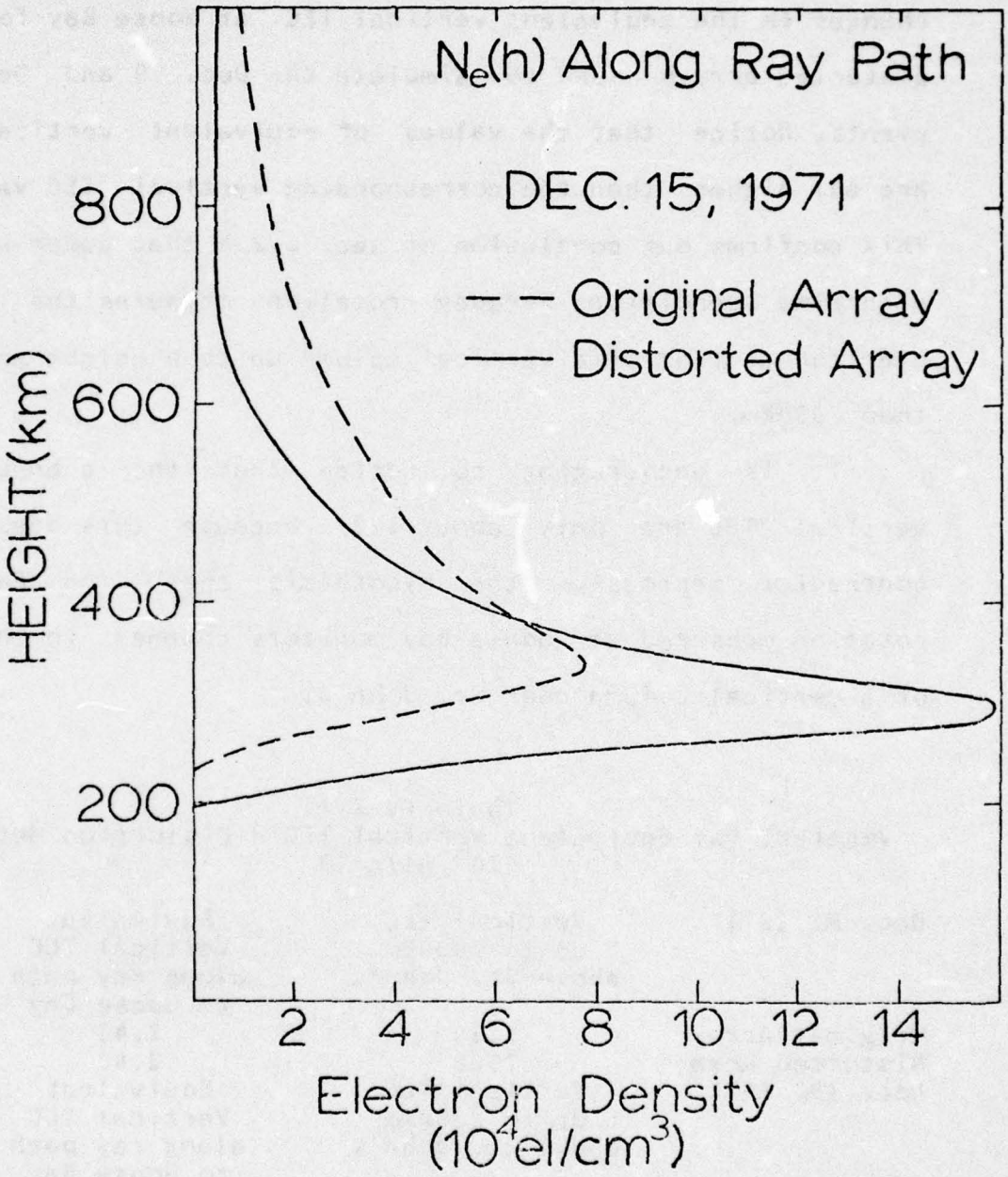
$N_e(h)$ Along Ray Path
DEC. 15, 1971
Original Array
Distorted Array
HEIGHT (km)
800
600
400
200
2
4
6
8
10
12
14
Electron Density
(10^4el/cm^3)

2000km above St. John's are compared with corresponding changes in the equivalent vertical TEC at Goose Bay for the distorted arrays used to simulate the Dec. 9 and Dec. 15 events. Notice that the values of equivalent vertical TEC are all higher than the corresponding vertical TEC values. This confirms our conclusion of sec. 2.2.4 that under winter nighttime conditions Faraday rotation measures the total electron content of a vertical column up to a height greater than 2000km.

It is encouraging to notice that the changes in vertical TEC are only about 12%, because this does not contradict seriously the hypothesis that the Faraday rotation measured at Goose Bay monitors changes in the TEC of a vertical column near St. John's.

Table IV-XVI
Vertical vs. Equivalent Vertical TEC - Distortion Method
(10^{18} el/cm^2)

Dec. 9, 1971	Vertical TEC up to 2000km above St. John's	Equivalent Vertical TEC along ray path to Goose Bay
Original Array	2.10	2.43
Distorted Array	1.86	2.40
Dec. 15, 1971	**Vertical TEC up to 2000km above St. John's**	**Equivalent Vertical TEC along ray path to Goose Bay**
Original Array	2.54	3.04
Distorted Array	2.86	3.04

Comparison of Table IV-XV with figures IV-3 and IV-6 reveals that an increase in TEC at Hamilton has been

reproduced for Dec. 15. This effect increased electron densities at lower latitudes. The F-2 peak height is at approximately 39 degrees geographic latitude along the ray path from Hamilton, a latitude apparently inside the plasmasphere for both Dec. 9th and 15th. One might initially propose that substantial dumping of plasma from the magnetic tubes of force occurred on the 9th but not on the 15th as this would explain the TEC increase observed from Hamilton on the 9th, which we were not able to reproduce using our vertical distortion technique.

4.3.2.4 Shift and Distort Results

As pointed out by Mendillo (1973), theory predicts vertical, longitudinal, and latitudinal drifts due to a dawn-dusk electric field. While we have not been able to investigate east-west drifts, we have looked at both vertical and latitudinal motions. One might ask whether a combination of vertical and latitudinal drifts could account for the observed flat TEC-increasing Nmax effect.

To investigate this question we have utilized the latitude shift capability of the computer model in combination with the distorted arrays plotted in figures IV-23 and IV-24. Results are shown in Table IV-XVII for 0 degree to -3 degree shifts on Dec. 9 and 0 to -6 degree shifts on Dec. 15. One should compare the results for the

Table IV-XVII

SHIFT AND DISTORT RESULTS

Date	Description	Station	Ω (degrees)	Model Nmax 420-km point (10^4 el/cm^3)
Dec. 9	Original Array	Hamilton	157	7.2
		Goose Bay	108	5.4
	Distorted Array	Hamilton	131	8.9
	Shift = 0	Goose Bay	107	7.3
	Distorted Array	Hamilton	107	9.7
	Shift =-1	Goose Bay	155	7.1
	Distorted Array	Hamilton	100	7.8
	Shift =-2	Goose Bay	247	7.3
	Distorted Array	Hamilton	102	8.6
	Shift =-3	Goose Bay	322	8.8

Table IV-XVII (continued)

Date	Description	Station	Ω (degrees)	Model Nmax 420-km point (10^4 el/cm^3)
Dec. 15	Original Array	Hamilton	219	15.3
		Goose Bay	135	8.7
	Distorted Array	Hamilton	270	28.3
	Shift = 0	Goose Bay	135	18.7
	Distorted Array	Hamilton	264	27.2
	Shift =-1	Goose Bay	167	17.4
	Distorted Array	Hamilton	248	26.2
	Shift =-2	Goose Bay	151	16.2
	Distorted Array	Hamilton	232	25.4
	Shift =-3	Goose Bay	119	19.5
	Distorted Array	Hamilton	213	24.6
	Shift =-4	Goose Bay	194	22.8
	Distorted Array	Hamilton	207	23.9
	Shift =-5	Goose Bay	275	24.0
	Distorted Array	Hamilton	186	19.5
	Shift =-6	Goose Bay	323	38.5

original array with the distorted array from Goose Bay for each shift.

For December 9 southward shifting greatly increases the Faraday rotation at Goose Bay, and is thus inconsistent with the observed effect. On December 15, the -3 degree shift gave a 12% decrease in Faraday rotation. This compares well with the observed 17% decrease (see Table IV-VIII and figure IV-6). Remember that with the vertical distortion method alone, a decrease in Ω could not be realistically achieved. These results imply that a combination of latitude shift and vertical distortion were at work on Dec. 15 but only vertical distortion on December 9.

One might try to contend that to reach a -3 degree shift, one first has to pass through the -1 and -2 degree shifts, where increases in Ω occurred. However, if the original array represents the beginning of the event, and the distorted array shifted 3 degrees southward represents the peak of the effect, the intermediate stages are represented by <u>smaller</u> distortions than that of the distorted array. In other words, it is important to realize that the shift results presented in Table IV-XVII do not represent a temporal sequence, but only a number of possible final stages of the two events.

Intermediate stages with smaller distortions just mentioned have not been investigated, as this question opens up a whole new level of complexity in the calculations. A

computer program which automatically distorts input arrays as a function of time could be developed to investigate this question further.

Ω and Nmax obtained from the computer model for Hamilton and Wallop's Island, respectively, are also given in Table IV-XVII. These results should be compared with figures IV-3 and IV-6. Notice that the increase in Ω at Hamilton has been reproduced on Dec. 15 using shifts of -1, -2, or -3 degrees. This agrees with the conclusion that a combination of vertical distortion and latitudinal motions occurred on Dec. 15. An increase in Ω at Hamilton is not obtained, however, on Dec. 9. This is not a cause for concern, however, since we have already concluded that a southward shift of the electron density vs. latitude array did not occur on Dec. 9.

We might conclude this section by remarking that although model results seem to indicate that a combination of latitude shift and vertical drift occurred on December 15, further studies are needed to model the temporal evolution of the event on that night.

4.3.3 Conclusions

Computer model studies were undertaken in an attempt to simulate the flat TEC-increasing Nmax effect which occurred during the nights of Dec. 8-9 and Dec. 14-15, 1971. These

studies indicate that an equatorward shift of the Ne(h) pattern existing before the effect cannot by itself account for the observations on either night. A vertical distortion, which is essentially TEC preserving, can, by itself, be responsible for the effect on Dec. 9, and can produce a flat TEC combined with an increase in Nmax on Dec. 15. A combination of latitude shift and vertical distortion can reproduce the observed decrease in TEC on Dec. 15, but cannot reproduce the observations on Dec. 9.

4.4 Mechanism for the Slab Thickness Decreases

It is clear that the vertical distortions of the winter nighttime ionosphere we have observed near L=4 are substorm related. On all five nights depicted in figures IV-1 to IV-6, substorms were observed at Narssarssuaq, the nearest of the eleven geomagnetic observatories whose records are combined in the AE index. For the case of Dec. 9 (figure IV-3), the beginning of the distortion of the ionosphere above St. John's is coincident with the substorm which occurred at 4 UT at Narssarssuaq. In the other four cases a substorm was observed at Narssarssuaq earlier in the course of the night, while the ionosphere above St. John's was still decaying. There could have been an immediate response to the substorm which was masked by the underlying decay. This possibility is sketched schematically in figure IV-27.

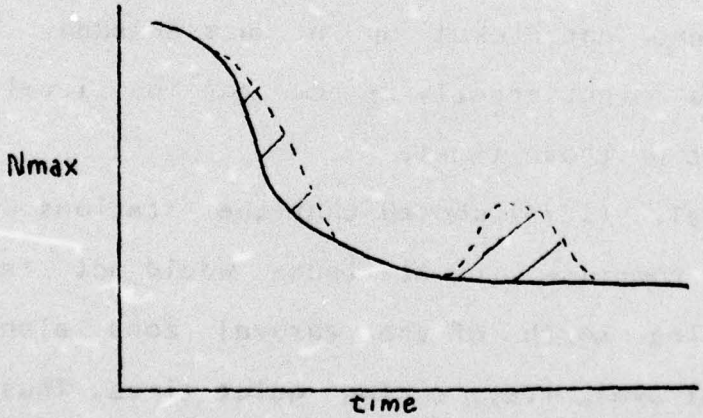

figure IV-27
The areas shaded are the same.

In figure IV-27, possible responses of the ionosphere to substorms occurring earlier during the night (while the ionosphere is still decaying) and near midnight (when the

ionospheric densities have reached a state of stable equilibrium) are depicted. Clearly, the increased concentration near midnight would appear as a "bump" while that occurring earlier would not. From this kind of argument it becomes apparent that immediate response by the ionosphere near St. John's to the substorms observed at Narssarssuaq could have occurred, even though the appearance of such a response would not be obvious in the data.

It is true, however, that on four of the five nights the greatest part of the increases in St. John's peak density occurred a few hours after the substorms occurred at Narssarssuaq, at times when the ionosphere would be expected to reach a stable level of ionization during magnetically quiet conditions. The magnetic conditions were not quiet, however, on those nights, so one might speculate that substorms might have occurred near St. John's and near midnight which were not picked up at Narssarssuaq. Even small disturbances might greatly affect the low levels of ionization present at those times.

Akasofu et. al. (1973) showed that the stations whose magnetic records comprise the AE index would not record substorms occurring north of the auroral zone along a contracted auroral oval, i.e., during quiet times. Thus, if a substorm occurred during relatively quiet times, its associated enhanced dawn to dusk electric field might cause ionospheric distortions without a magnetic disturbance being

recorded at Narssarssuaq, or other AE stations. One may also argue that the 11 magnetic stations whose records comprise the AE index do not adequately cover all longitudes, so that a substorm occurring near the longitude of St. John's might not be detected at Narssarssuaq, 8.6 degrees of magnetic longitude to the east. Allen (1975) has confirmed that this might be a possibility, although Allen and Kroehl (1973) concluded that the 11 stations provide adequate longitudinal coverage to pick up most substorms. In short, there is certainly no evidence for the contention that all substorms which affect the ionosphere near L=4 are reflected in the AE index. We therefore can contend that the distortions which occurred on all five nights were associated with magnetic disturbances.

The mechanism by which a substorm affects the ionosphere near L=4 is the enhanced convection electric field associated with it. This enhanced dawn-dusk electric field has radial and tangential components which map along magnetic lines of force from the equatorial plane to the ionosphere. The radial component causes east-west drifts, while the tangential component produces both vertical and north-south drifts. While we have not been able to investigate possible effects of east-west drifts on ionospheric density profiles, we have shown that both vertical and north-south drifts are important in producing some of the observed effects.

There are fields other than that due to convection which do contribute to the total electric field in the ionosphere. These are the corotation electric field and the dynamo electric field. In a review paper dealing with these various electric fields, Mozer (1973) concluded that, on the average, the ionospheric electric field near L=4 is primarily of magnetospheric origin whether the plasmasphere is equatorward or poleward of L=4. Under magnetically disturbed conditions, the convection electric field is greatly enhanced. Table IV-XVIII, reproduced from (Carpenter, 1970), shows how the dawn-dusk electric field is enhanced during a moderate magnetic storm period.

Table IV-XVIII

from (Carpenter, 1970)

	Moderate Magnetic Storm Period			Conditions of prolonged quiet
	Peak Values during substorms	Typical values between substorms	Average level	mV/m
	mV/m	mV/m	mV/m	
Dusk*	1-4	~0.4-0.6	~1	~0.1
Midnight†	0.5-2	0.05-0.1	~0.2-0.3	$\lesssim$0.1

*based on statistics of the position of the plasma bulge.

†based on tracking of whistler paths.

From the computations in the previous chapter we derived values of 0.67mV/m for the December 9th event and 0.23mV/m for the December 15th event. The 0.67 value is in agreement with the peak values at midnight during substorms in Table IV-XVIII, and of course a substorm was observed at the commencement of the increase in Nmax on December 9. The 0.23mV/m result for December 15 is greater than typical values between substorms in the table, and fits well into the average level for a magnetic storm period near midnight in that table. This seems to support our contention that the Nmax increases we have observed are due to substorm related enhancements of the convection electric field.

One final comment should be made concerning figure IV-27, which has already shed light on the relation between substorms and nighttime Nmax increases. This figure also is most relevant to the question of why the nighttime Nmax increase effect is primarily a winter phenomenon. Only during the winter months is Nmax relatively flat for many hours during undisturbed nighttime conditions, at which times a "bump" in Nmax would be obvious in the data. For the same reason, most of the bumps observed during October, February and March necessarily fall into the group we classified as "low bumps," while during December, for instance, large bumps can occur with much greater frequency.

REFERENCES

Akasofu, S.-I., Polar and Magnetospheric Substorms, Reidel Publishing Co. (1968)

Akasofu, S.-I., et. al., Auroral substorms and the interplanetary magnetic field, Jour. Geophys. Res., 78, 7490 (1973)

Allen, J.H., Private communication (1975)

Allen, J.H. and Kroehl, H.W., Spatial and temporal distributions of magnetic effects of auroral electrojets as derived from AE indices, Jour. Geophys. Res., 80, 3667 (1975)

Angerami, J.J. and Carpenter D.L., Whistler studies of the plasmapause in the magnetosphere 2. Electron density and total tube electron content near the knee in magnetospheric ionization, Jour. Geophys. Res., 71, 711 (1966)

Angerami J.J. and Thomas J.O., Studies of planetary atmospheres, 1. The distribution of electrons and ions in the earth's exosphere, Jour. Geophys. Res., 69, 4537 (1964)

Axford, W.I. and Hines, C.O., Can. Jour. Physics, 39, 1433 (1961)

Brace, L.H. et. al., Deformation of the night side plasmasphere and ionosphere during the August, 1972 geomagnetic storm, Jour. Geophys. Res., 79, 5211 (1974)

Brace, L.H., Reddy, B.M., and Mayr, H.G., Global behavior of the ionosphere at 1000km altitude, Jour. Geophys. Res., 72, 265 (1967)

Bradley, P.A. and Dudeney, J.R., A simple model of the vertical distribution of electron concentration in the ionosphere, J. Atmos. Terr. Phys., 35, 2131 (1973)

Brice, N.M., Bulk motion of the magnetosphere, Jour. Geophys. Res., 72, 5193 (1967)

Carpenter, D.L., Whistler evidence of a "knee" in the magnetospheric ionization density profile," Jour. Geophys. Res., 68, 1675 (1963)

Carpenter, D.L., Whistler studies of the plasmapause in the magnetosphere 1. Temporal variations in the position of the knee and some evidence on plasma motions near the knee, Jour. Geophys. Res., 71, 693 (1966)

Carpenter, D.L., Whistler evidence of the dynamic behavior of the duskside bulge in the plasmasphere, Jour. Geophys. Res., 75, 3837 (1970)

Chapman, S., The absorption and dissociative or ionizing effect of monochromatic radiation in an atmosphere on rotating earth, Proc. Phys. Soc., 43, 26 (1931)

Davies, K., Ionospheric radio propagation, National Bureau of Standards Monograph 80 (1965)

Eviatar, A., Lenchek, A.M., and Singer S.F., Distribution of density in an ion-exosphere of a non-rotating planet, Phys. Fluids, 7, 1775 (1964)

Gold, T., Motions in the magnetosphere of the earth, Jour. Geophys. Res., 64, 1219 (1959)

Grebowsky, J.M., Chen, A.J., and Taylor Jr., H.A., High latitude troughs and the polar cap boundary, Jour. Geophys. Res., 81, 690 (1976)

Hawkins, G.S., and Klobuchar, J.A., Seasonal and diurnal variations in the total electron content of the ionosphere at invariant latitude 54 degrees, AFCRL Tech. Report-74-0234 (1974)

Heikkila, W.J., The aurora, EOS, Trans. AGU, 54, 764 (1973)

Hosseinieh, H.H., The effects of troughs on measurements of ionospheric total electron content, Master's thesis, Boston University (1975)

Klobuchar, J.A., and Allen, R.S., A first order prediction model of total-electron-content group path delay for a midlatitude ionosphere, AFCRL Tech. Report-70-0403 (1970)

Mendillo, M., Magnetospheric convection at ionospheric heights, AFCRL Tech. Report-73-0358 (1973)

Mendillo M. and Klobuchar, J.A., An atlas of the midlatitude F-region response to geomagnetic storms, AFCRL Tech. Report 74-0065 (1974)

Mozer, F.S., Electric fields and plasma convection in the plasmasphere, Rev. Geophys. and Space Phys., 11, 755, (1973)

Nishida, A., Formation of plasmapause, or magnetospheric

plasma knee, by the combined action of magnetospheric convection and plasma escape from the tail, Jour. Geophys. Res., 71, 5069 (1966)

Papagiannis, M.D., Space Physics and Space Astronomy, Gordon and Breach Science Pub. Ltd. (1972)

Papagiannis, M.D., Hosseinieh, H.H., and Mendillo, M., Changes in the ionospheric profile and the Faraday M with Kp, Planet. Space Sci., 23, 197 (1975)

Parker, E.N., Dynamic properties of the magnetosphere, in Physics of the Magnetosphere, R.L. Carovillano, ed. (1968)

Pike, C.P., Akasofu, S.-I., and Wagner, R.A., An ionospheric substorm model, in Defense meteorological satellite program auroral-ionospheric interpretation guide, Pike, C.P., editor, AFCRL Tech. Report-75-0191 (1975)

Prasad, S.S., Ionic composition and temperature over Arecibo 2, Jour. Geophys. Res., 75, 1911 (1970)

Rishbeth, H., and Garriott, O.K., Introduction to ionospheric physics, Academic Press, Inc. (1969)

Shimazaki, T., J. Radio Res. Labs., Japan, 2, 85 (1955)

Taylor, H.A. et. al., Thermal ions in the exosphere; evidence of solar and geomagnetic control, Jour. Geophys. Res., 73, 5521 (1968)

Titheridge, J.E., Determination of ionospheric electron content from the Faraday rotation of geostationary

satellite signals, Planet. Space Sci., 20, 353 (1972)

Tulunay, Y. and Sayers, J., Characteristics of the mid-latitude trough as determined by the electron density experiment on Ariel III, J. Atmos. Terr. Phys., 33, 1737 (1971)

Wright, J.W., and McDuffie, R.E., J. Radio Res. Labs., Japan, 7, 409 (1960)